Effects of temperature on gold single crystal electrochemistry

Thesis submitted in accordance with the requirements
of the University of Liverpool for
the degree of Doctor of Philosophy by

Lena Reichenbach

September 2018

Abstract

While most industrial processes that include metal deposition use elevated temperatures, the majority of scientific investigations are done at room temperature. Thus, an electrochemical study of the effect of the temperature on the metal deposition was seen as necessary. For a basic study, the underpotential deposition (UPD) was chosen to be investigated as a controlled amount of metal can be deposited.
The copper underpotential deposition (Cu-UPD) on Au(111) in sulphuric acid was chosen due to being a well-known model system. As the sulphate anion strongly influences the UPD process, perchloric acid was also studied to investigate the dependence on the strength of the adsorbing anion. To see whether or not the temperature dependence was only due to the metal deposition, the copper-free electrolytes were also investigated.
For the metal-free electrolytes, only cyclic voltammetry was used. For the Cu-UPD the study used both cyclic voltammetry and chronoamperometry. The temperature range for the study was between 10°C and 55°C.
It was found that the increase of the kinetic energy due to the increasing temperature affects the speed of the processes. Moreover, it affects the stability of the formed phases, especially for mobile adlayers. Additionally, alloying was seen for the Cu-UPD on Au(111) in perchloric acid.

Acknowledgements

First and foremost, I'd like to thank my main supervisor Yvonne Gründer for her mentoring and support. It would have been very hard to produce this work otherwise. Also, I'd like to thank Chris Lucas for his help and support.
To Josh, Nick and Graeme, thank you guys for the discussions, feedback, general support and just generally being there. I am glad for you guys starting at the same time, it was really great to have a group like ours. Lisa and Jack, also thanks for the support and discussions. You were just as much part of the group, even though you started later. Really, I appreciate having you people there, even just for talking over coffee. To Angeline, thanks for all the feedback and discussion. I'm kinda sorry to be finishing up when you've just started in the group.
Most of all, thanks to my family. Without their unwavering and unconditional support as well as their absolute belief in me I would have never been able to achieve all that I did.

Contents

List of Figures v

List of Tables xiii

List of Acronyms xv

1. Introduction 1

1.1. Electrochemistry 1

1.1.1. Cyclic Voltammetry 7

1.1.2. Chronoamperometry 9

1.2. Influence of the temperature 15

1.3. Investigated systems 18

1.4. Au(111) 19

1.4.1. Au(111) in sulphuric acid 22

1.4.2. Cu-UPD on Au(111) in sulphuric acid 24

1.4.3. Au(111) in perchloric acid 40

1.4.4. Cu-UPD on Au(111) in perchloric acid 41

2. Methodology 47

2.1. Au(111) in sulphuric acid 49

2.2. Cu-UPD on Au(111) in sulphuric acid 50

2.3. Au(111) in perchloric acid 51

2.4. Cu-UPD on Au(111) in perchloric acid 52

3. Au(111) in 0.1 M sulphuric acid 53

3.1. Experimental results 53

3.2. Discussion 61

3.2.1. Reconstruction lifting 61

3.2.2. ST/ST' 62

3.2.3. SA,SAD1 to SAD3 64

3.2.4. SD,SDD1 and SDD2 66

3.3. Summary 67

4. Copper underpotential deposition on Au(111) in 0.1 M sulphuric acid 69

4.1. Experimental results 69

4.1.1. Cyclic voltammetry 70

4.1.2. Chronoamperometry 76

4.2. Analysis & discussion 79

4.2.1. Cyclic voltammetry 79

4.2.2. Chronoamperometry 89

4.3. Summary 99

5. Au(111) in 0.1 M perchloric acid 101

5.1. Experimental results 101

5.2. Discussion 106

5.2.1. PA1,PA2 and PD1 to PD3 106

5.2.2. B/B' 110

5.2.3. D/D' 111

5.3. Summary 112

6. Copper underpotential deposition on Au(111) in 0.1 M perchloric acid 113

6.1. Experimental results 113

6.1.1. Cyclic voltammetry 114

6.1.2. Chronoamperometry 118

6.2. Analysis & discussion 122

6.2.1. Cyclic voltammetry 122

6.2.2. Chronoamperometry 126

6.3. Summary 140

7. Conclusion 141

7.1. Future Outlook 143

References 144

A. Appendix **151**

A.1. Python script for fitting with Avrami equation 151

A.1.1. params.py 160

List of Figures

1.1. A schematic of an electrochemical cell 2
1.2. Graphical representation of the electrochemical interface. 4
1.3. Basic form of the change in potential with time for one cycle in cyclic voltammetry. 7
1.4. CV of Au(111) in 0.1 M sulphuric acid at a scan rate of 10 mV/s at 20°C. The arrows indicate the direction of the potential scan. . 8
1.5. Basic form of the change in potential with time for a chronoamperometric transient. 10
1.6. Visualization of the impinging of two nuclei N1 and N2 on each other, with the overlap area in green. 13
1.7. Current-time response according to the Avrami equation (Eq. 1.3) for the different values of m which represent different growth modes (1: instantaneous nucleation with either on-dimensional growth or two-dimensional growth and surface diffusion, 2: instantaneous nucleation and two-dimensional growth, 3: progressive nucleation and two-dimensional growth). 15
1.8. Series of cyclic-voltammetry profiles for the deposition and stripping of Cu-UPD on Pt(111) in aqueous 0.05 M H_2SO_4 + 5 mM $CuSO_4 \cdot 5\ H_2O$ recorded at seven different T values in the 273-333 K range (ΔT=10 K); s=5 mVs^{-1} and A=0.0431 cm^2. The annotations C_I, C_{II}, A_I, and A_{II} stand for two cathodic and two anodic peaks. The inset presents a series of cyclic-voltammetry profiles for Pt(111) in aqueous 0.05 M H_2SO_4 solution recorded at seven different T values in the 273-333 K range (ΔT=10 K) immediately following the Cu-UPD deposition-stripping experiments; s=50 mVs^{-1} and A=0.0431 cm^2. Reprinted with permission from reference 13. Copyright 2009 American Chemical Society. 16

1.9. Series of cyclic voltammograms for UPD of Ag on Pt(111) in 0.1 M H_2SO_4 + 1 mM Ag_2SO_4 solution at 273 ≤ T ≤ 333 K with an interval of 10 K; s=5 mVs^{-1}. Arrows indicate changes in the CV profiles associated with T increase. Reprinted with permission from reference 14. Copyright 2002 American Chemical Society. 17

1.10. Gold unit cell with (111) plane. 20

1.11. Simplified model of the reconstructed (left) and unreconstructed (right) Au(111) surface. 20

1.12. Schematic of the herringbone superstructure of the Au(111) reconstruction. Each area has the $(22 \times \sqrt{3})$ structure, with domain walls separating them. 20

1.13. CV for Au(111) in 0.1 M sulphuric acid at 10 mV/s. Reprinted from reference 35, Copyright 2000, with permission from Elsevier. 23

1.14. (a) CV at 1 mV/s and (b) electrochemically retrieved copper coverage (normalized charge due to Cu-UPD) of the Cu-UPD on Au(111) in 0.05 M sulphuric acid 1 mM copper sulphate. Reprinted from reference 53, Copyright 1994, with permission from Elsevier. . . . 26

1.15. Interfacial structure of the coadsorbed copper and sulphate $(\sqrt{3} \times \sqrt{3})$R30° layer on Au(111) formed in step II. (a) Top view. (b) Side view. 26

1.16. Equivalent coverages calculated from the faradaic charge (red), the sulphate species (black) and of the total deposited copper(blue) for 0.1 M sulphuric acid 10 mM copper sulphate. For the UPD I region, a charge-neutral coadsorption process of copper and sulphate with $T\Delta_R S_{coad} = 7kJ/mol$ was assumed, with the total copper coverage derived from the sum of the faradaic coverage as well as the sulphate coverage. The copper coverage in the UPD II region was assumed to be from faradaic copper deposition. For the sulphate coverage, a charge-neutral substitution of bisulphate with oxygen species was assumed (dashed black line). Reprinted with permission from reference 57. Copyright 2016 American Chemical Society. 30

1.17. CVs of the Cu-UPD on Au(111) in 0.05 M sulphuric acid 1 mM copper sulphate with a scan rate of 5 mV/s depending on the step density. The surface orientations for (a-e) are as given in the figures, (f) has a misscut<0.5° but was taken after five oxidation-reduction cycles up to 1.5 V_{SCE} with a scan rate of 50 mV/s. Reprinted from reference 54, Copyright 1995, with permission from Elsevier. . . . 33

1.18. CVs of the Cu-UPD on Au(111) in 0.05 M sulphuric acid 1 mM copper sulphate with a scan rate of 5 mV/s depending on added halides. (a) dashed: no addition, solid: +0.1 mM potassium chloride, (b) +0.1 mM potassium bromide, (c) +0.1 mM potassium iodide. Reprinted from reference 63, Copyright 1994, with permission from Elsevier. 34

1.19. CVs of the Cu-UPD on Au(111) in 0.05 M sulphuric acid 1 mM copper sulphate with a scan rate of 1 mV/s depending on the chloride concentration (solid: 0 M, dotted: $5 \cdot 10^{-6}$ M, dashed: $5 \cdot 10^{-5}$ M). Reprinted by permission from Springer Nature Customer Service Centre GmbH: Springer Nature Journal of Chemical Sciences reference 48, copyright 2009. 35

1.20. Transients of Au(111) in 0.05 M sulphuric acid 1 mM copper sulphate for the first (A, A') and second (B, B') stage of the Cu-UPD with the potential steps (E vs SCE) indicated in the figures. Reprinted from reference 53, Copyright 1994, with permission from Elsevier. 37

1.21. Transients of Au(111) in 0.05 M sulphuric acid 1 mM copper sulphate at different surface defects for the deposition (B,left) and dissolution (B',right) of the second stage of the Cu-UPD with the potential steps (E vs SCE) indicated in the figures. The surfaces have different step densities expressed through the surface orientation or have been modified by oxidation-reduction cycles (ORC). Reprinted from reference 54, Copyright 1995, with permission from Elsevier. 38

1.22. Transients of the whole Cu-UPD process on Au(111) and polycrystalline gold in 0.1 M sulphuric acid 10 mM copper sulphate. Potential step:-50 mV_{SSE} to -445 mV_{SSE}. Republished with permission of Electrochemical Society, from reference 55; permission conveyed through Copyright Clearance Center, Inc.. 39

1.23. CVs in the double-layer region on Au(111) at 5 mV/s in 0.1 M perchloric acid at 1°C. Solid line after 6 cycles at 50 mV/s between -0.3 V_{SCE} and 1.4 V_{SCE}, the surface has an increased defect density due to going into the oxidation region. Dashed line after 6 cycles at 50 mV/s between -0.3 V_{SCE} and 0.8 V_{SCE}. Reprinted from reference 72, Copyright 1991, with permission from Elsevier. . . . 41

1.24. CVs of the Cu-UPD on Au(111) in 0.1 M perchloric acid 10 mM copper perchlorate with x M hydrochloric acid added and a scan rate of 2 mV/s. Reprinted from reference 74, Copyright 1995, with permission from Elsevier. 42

1.25. CVs on Au(111) in 0.1 M perchloric acid (dashed line), 0.1 M perchloric acid 5 mM copper perchlorate (solid line) and 0.05 M sulphuric acid 5 mM copper sulphate (dotted line) with a scan rate of 10 mV/s. Reprinted from reference 37, Copyright 1998, with permission from Elsevier. 46

2.1. Schematical representation of the experimental setup 47

3.1. CVs of the Au(111) single crystal in 0.1 M sulphuric acid at 20°C and 40°C for 10 mV/s with labelling for peaks 54

3.2. CVs of Au(111) in 0.1 M sulphuric acid at scan rates of 50 mV/s, 20 mV/s, 10 mV/s and 5 mV/s for (a) 10°C, (b) 20°C, (c) 30°C, (d) 40°C and (e) 50°C. The cyclic voltammograms (CVs) for 20 mV/s, 10 mV/s and 5 mV/s have the current density j scaled for convenience by a factor of 2.5, 5 and 10, respectively. 55

3.3. CVs of Au(111) in 0.1 M sulphuric acid at 10°C, 20°C, 30°C, 40°C and 50°C for (a) 50 mV/s, (b) 20 mV/s, (c) 10 mV/s and (d) 5 mV/s. The current density of the 50°C CVs are scaled by a factor of 0.4 for easier comparison. 56

3.4. Change of the peak positions with the scan rate ν at different temperatures for (a) SAD1, (b) SAD2, (c) SAD3, (d) SDD1 and (e) SDD2. 57

3.5. Change of the peak positions with the scan rate ν at different temperatures for (a) SA, (b) SD, (c) ST and (d) ST'. 58

3.6. Change of the peak positions with the temperature at different scan rates for (a) SAD1, (b) SAD2, (c) SAD3, (d) SDD1 and (e) SDD2. 59

3.7. Change of the peak positions with the temperature at different scan rates for (a) SA, (b) SD, (c) ST and (d) ST'. 60

4.1. CV of the Au(111) single crystal in 0.1 M sulphuric acid 1 mM copper sulphate at 20°C for 5 mV/s with labelling for the peaks. . 70

4.2. CVs of Au(111) in 0.1 M sulphuric acid 1 mM copper sulphate at scan rates of 50 mV/s, 20 mV/s, 10 mV/s and 5 mV/s for (a) 10°C, (b) 20°C, (c) 25°C, (d) 30°C, (e) 35°C, (f) 40°C, (g) 45°C, (h) 50°C and (i) 55°C. The CVs for 20 mV/s, 10 mV/s and 5 mV/s have the current density j scaled for convenience by a factor of 2.5, 5 and 10, respectively. 72

4.3. CVs of Au(111) in 0.1 M sulphuric acid 1 mM copper sulphate at 10°C, 20°C, 25°C, 30°C, 35°C, 40°C, 45°C, 50°C and 55°C for (j) 50 mV/s, (k) 20 mV/s, (l) 10 mV/s and (m) 5 mV/s. 72

4.4. Change of the peak positions with the scan rate ν at different temperatures for (a) A, (b) A', (c) B and (d) B'. 73

4.5. Change of the peak positions with the temperatures at different scan rates for (a) A, (b) A', (c) B and (d) B'. 74

4.6. Change with cycling for the CV of Au(111) in 0.1 M sulphuric acid 1 mM copper sulphate at room temperature (24.5°C) for (a) the first five cycles and (b) every five cycles. 74

4.7. Transients of Au(111) in 0.1 M sulphuric acid 1 mM copper sulphate at 20°C for (a) B', (b) A', (c) B and (d) A. 77

4.8. Transients for Au(111) in 0.1 M sulphuric acid 1 mM copper sulphate with fixed starting potential at (a) 10°C, (b) 20°C, (c) 30°C, (d) 40°C and (e) 50°C. 78

4.9. Change of (a) the peak potential and (b) the peak current density with $\nu^{\frac{1}{2}}$ at different temperatures for peak A'. 81
4.10. Change of (a) the peak position and (b) the peak current density with $\nu^{\frac{1}{2}}$ at different temperatures for peak B. 86
4.11. Change of (a) the peak position and (b) the peak current density with $\nu^{\frac{1}{2}}$ at different temperatures for peak B'. 88
4.12. Fits for the transients of Au(111) in 0.1 M sulphuric acid 1 mM copper sulphate at 20°C for (a),(b) B and (c) A. 91
4.13. Plot of the rate constants (a) k_1, (b) k_2 and (c) k_3 over the potential for the fit the temperature dependent transients of the Cu-UPD on Au(111) in 0.1 M sulphuric acid. 95
4.14. Plot of the coverages of (a) function 1, (b) function 2, (c) function 3 and (d) the overall coverage over the potential for the fit of the temperature dependent transients of the Cu-UPD on Au(111) in 0.1 M sulphuric acid. The coverages were not corrected for sulphate coadsorption. 96

5.1. CVs with labelled peaks for (a) 5 mV/s at 20°C and 40°C and (b) 50 mV/s at 20°C 102
5.2. CVs of Au(111) in 0.1 M perchloric acid at scan rates of 50 mV/s, 20 mV/s, 10 mV/s and 5 mV/s for (a) 10°C, (b) 20°C, (c) 30°C, (d) 40°C and (e) 50°C. For the lower scan rates, the current density j has been scaled. 103
5.3. CVs of Au(111) in 0.1 M perchloric acid at 10°C, 20°C, 30°C, 40°C and 50°C for (a) 50 mV/s, (b) 20 mV/s, (c) 10 mV/s and (d) 5 mV/s. 104
5.4. Change of the peak positions with scan rate ν at different temperatures for (a) PA1, (b) PA2, (c) PD1 and (d) PD3 (PD2 included for 40°C). 105
5.5. Change of the peak positions with the temperature at different scan rates for (a) PA1, (b) PA2, (c) PD1 and (d) PD3 106

6.1. CV of the Au(111) single crystal in 0.1 M perchloric acid 1 mM copper perchlorate at 20°C and 50°C for 5 mV/s with labelling for the peaks. 114

6.2. CVs of Au(111) in 0.1 M perchloric acid 1 mM copper perchlorate at scan rates of 50 mV/s, 20 mV/s, 10 mV/s and 5 mV/s for (a) 10°C, (b) 20°C, (c) 30°C, (d) 40°C and (e) 50°C. The CVs for 20 mV/s, 10 mV/s and 5 mV/s have the current density j scaled for convenience by a factor of 2.5, 5 and 10, respectively. 115
6.3. CVs of Au(111) in 0.1 M perchloric acid 1 mM copper perchlorate at 10°C, 20°C, 30°C, 40°C and 50°C for (a) 50 mV/s, (b) 20 mV/s, (c) 10 mV/s and (d) 5 mV/s. 116
6.4. Change of the peak positions with the scan rate ν at different temperatures for (a) peak S1 and S1b, (b) peak S2 and (c) peak A. 117
6.5. Change of the peak positions with the temperatures at different scan rates for (a) peak S1 and S1b, (b) peak S2 and (c) peak A. . 117
6.6. Transients for Au(111) in 0.1 M perchloric acid 1 mM copper perchlorate with a fixed starting potential of 0.6 V at (a) 10°C, (b) 20°C, (c) 30°C, (d) 40°C and (e) 50°C. 119
6.7. Transients for Au(111) in 0.1 M perchloric acid 1 mM copper perchlorate for 180 mV→600 mV at (a) 10°C and (b) 50°C. The alloying potential as well as the holding time at that potential are indicated for each transient. 121
6.8. Fit parameters for the transients of Au(111) in 0.1 M perchloric acid 1 mM copper perchlorate for 180 mV→600 mV at 10°C: (a) the charge density q and (b) the rate constant k against the alloying potential E_A for different holding times at the same. The baseline is at 180 mV. 128
6.9. Fit parameters for the transients of Au(111) in 0.1 M perchloric acid 1 mM copper perchlorate for 180 mV→600 mV at 50°C: (a) the charge density q and (b) the rate constant k against the alloying potential E_A for different holding times at the same. The baseline is at 180 mV. 128
6.10. Plot of the number of electrons per surface atom $n_{e^-,a}$ of (a) function 1, (b) function 2, (c) function 3, (d) function 4, (e) function 5 and (f) the overall number of electrons per surface atom over the potential at different temperatures for the fit of the transients in Fig. 6.6 of the Cu-UPD on Au(111) in 0.1 M perchloric acid. 131

6.11. Plot of the time constant τ at (a) 300 mV, (b) 250 mV, (c) 200 mV, (d) 150 mV, (e) 100 mV, (f) 50 mV and (g) 0 mV over the temperature at different end potentials for the fit of the transients in Fig. 6.6 of the Cu-UPD on Au(111) in 0.1 M perchloric acid. . . . 132
6.12. Plot of the number of electrons per surface atom $n_{e^-,a}$ at (a) 10°C, (b) 20°C, (c) 30°C, (d) 40°C and (e) 50°C over the potential for the fit of the transients in Fig. 6.6 of the Cu-UPD on Au(111) in 0.1 M perchloric acid. 133
6.13. Plot of the time constants τ at (a) 10°C, (b) 20°C, (c) 30°C, (d) 40°C and (e) 50°C over the potential for the fit of the transients in Fig. 6.6 of the Cu-UPD on Au(111) in 0.1 M perchloric acid. . . . 134

List of Tables

1.1. Comparison of the peak separation in the CVs with different electrolyte concentrations at room temperature. 36

4.1. χ^2_{red} for the linear fits of the peak potential and peak current density for peak A' shown in Fig. 4.9. 82
4.2. χ^2_{red} for the linear fits of the peak potential and peak current density for peak B shown in Fig. 4.10. 86
4.3. χ^2_{red} for the linear fits of the peak potential and peak current density for peak B' shown in Fig. 4.11. 89
4.4. Parameters for the fits of the transients of Au(111) in 0.1 M sulphuric acid 1 mM copper sulphate shown in Fig. 4.12. 92

6.1. χ^2_{red} for the fits of the alloying investigation transients at 10°C (Fig. 6.7a) ordered by previous potential history. 128
6.2. χ^2_{red} for the fits of the alloying investigation transients at 50°C (Fig. 6.7b) ordered by previous potential history. 128
6.3. Offset in µAcm^{-2} for the fit of the transients in Fig. 6.6 of the Cu-UPD on Au(111) in 0.1 M perchloric acid. 135
6.4. χ^2_{red} for the fit of the transients in Fig. 6.6 of the Cu-UPD on Au(111) in 0.1 M perchloric acid. 135

List of Acronyms

CV	cyclic voltammogram
UPD	underpotential deposition
HER	hydrogen evolution reaction
OCP	open circuit potential
Cu-UPD	copper underpotential deposition
UHV	ultra-high vacuum
ECQM	electrochemical quartz crystal microbalance
SEIRAS	surface-enhanced infrared absorption spectroscopy
pzc	point of zero charge
STM	scanning tunneling microscopy
XRD	x-ray diffraction
LEED	low-energy electron diffraction
RHEED	reflection high-energy electron diffraction
AES	Auger electron spectroscopy
EXAFS	extended x-ray absorption fine structure
ML	monolayer
AFM	atomic force microscopy
XANES	x-ray absorption near structure

1. Introduction

In the industry, electrodeposition is often performed at elevated temperatures since this results in an increased conductivity as well as decreased anode and cathode polarization.[1] While there are many fundamental studies at room temperature, there are to my best knowledge few systematic studies of the temperature dependence of the UPD, which is a subset of the metal deposition. Therefore, it would be good to study the effect of temperature, as conclusions from room temperature systems might be flawed. Furthermore, other applications in which the structure of a deposited layer might also be of consequence, for example electrocatalysis, do not have to be restricted to room temperature, and again the knowledge of the temperature influence might prove valuable.

1.1. Electrochemistry

Electrochemistry is the study of chemical reactions that involve the transfer of electric charge.[2,3] As such, a part of the field is the study of reactions that take place at the electrode when a current flows through an electrochemical cell. To conduct investigations of the influence of electricity on reactions, an electrochemical cell is used, which contains the electrolyte as well as the electrodes (see Fig. 1.1). Usually, three electrodes are used for a measurement: a working electrode, on which the reactions take place, a counter electrode to apply the potential difference as well as to measure the current and a reference electrode to accurately measure the change in potential in the working electrode.[3] All of the electrodes are connected through the electrolyte solution. The interface between electrode and electrolyte represents a change in the type of the conduction of the charge.[2,3] In the solution, the charge is transported by the ions, which is called ionic conduction.[2,3] The electrode, however, uses electronic conduction.[2,3]
The potential E of the working electrode at equilibrium is governed by both the

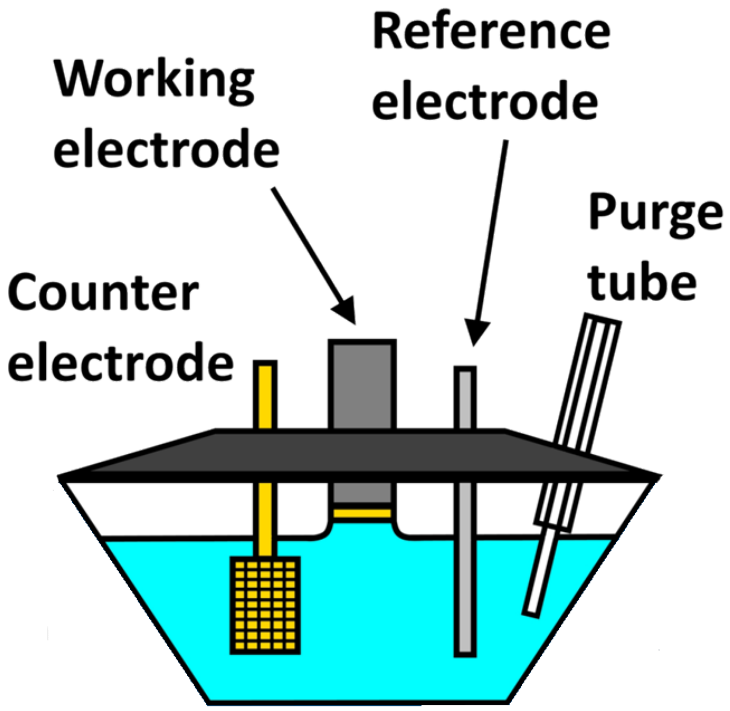

Figure 1.1.: A schematic of an electrochemical cell

standard potential E^0 of the reaction as well as the activity of the reactants at equilibrium.[3–5] This relationship is expressed by the Nernst equation:

$$E = E^0 + \frac{RT}{nF} ln \frac{a_{Ox}}{a_{Red}} \tag{1.1}$$

with F the Faraday's constant, n the number of electrons, R the universal gas constant and T the temperature.[3–5] The activity of the reactants are denoted by a_{Ox} for the oxidized and a_{Red} for the reduced reactant. If the activity coefficients are at unity, the surface concentrations of the reactants can be used.[4] At the equilibrium, no current flows through the cell, however if the potential is changed, the concentrations of the reactants have to be adjusted to the new concentrations according to the Nernst equation and a current has to flow through the electrode/-solution interface at which the reaction takes place.[5]

For electrochemical reactions, the driving force is the gradient of the electrochemical potential $\bar{\mu}$.[3] Here, $\bar{\mu}_i = \mu_i + z_i F \phi$, with z_i being the charge number of species i, ϕ being the inner potential of the phase and μ_i being the chemical potential.[3,6]

The inner potential ϕ is the work required for the transportation of a unit point charge inside the phase from a point at infinite distance, while the chemical potential μ_i is the work required to add a molecule of the species to the system at constant temperature and pressure.[6] As such, the electrochemical potential is the work required to add a charged species to the system, which requires work to be done against the inner potential of the phase.[6] However, it has to be kept in mind that the chemical interaction represented by μ_i cannot be separated from the electrical interaction represented by $z_i F\phi$ due to the interaction of the charge with the molecules in the phase.[3]

Furthermore, the difference ${}^{\alpha}\Delta^{\beta}\phi$ between the inner potential of two phases α and β cannot be measured, because the inner potential cannot be measured directly.[3] However, the change in the potential difference between two phases, $\delta({}^{\alpha}\Delta^{\beta}\phi)$, can be measured, but not without creating at least one more interface.[3] This is because another interface is required to close the circuit. In an electrochemical cell containing only the working electrode, the counter electrode and the electrolyte, which is the minimum requirement for an electrochemical measurement, the change in potential δE, would look as following:[3] $\delta E = E_j - E_{j=0} = \delta({}^{W}\Delta^{S}\phi) + jR_s + \delta({}^{S}\Delta^{C}\phi)$. Hereby, W references the working electrode, C the counter electrode and S the electrolyte solution, with jR_S being the potential drop across the solution due to the solution resistance.[3]

This potential drop is usually compensated separately, so if $\delta({}^{C}\Delta^{S}\phi)$ can be discounted, the measured change in potential would be $\delta({}^{W}\Delta^{S}\phi)$, the change in the potential difference between the working electrode and the electrolyte.[3] To make the contribution of the counter electrode negligible, either a highly reversible counter electrode is needed, or one that is much larger than the working electrode.[3,5] The later option is because the change in potential is proportional to the current density, and the total current flowing through both electrodes always being the same.[3] Thus, if one has a much larger volume, the current density it experiences is much smaller.[3]

A three electrode setup can be considered to have two circuits: one between the working and counter electrode, through which a current flows, and one between the working and reference electrode, with practically no current.[3,5,6] With the reference electrode potential being considered constant, the measured change in potential between the reference and the working electrode would be equal to the

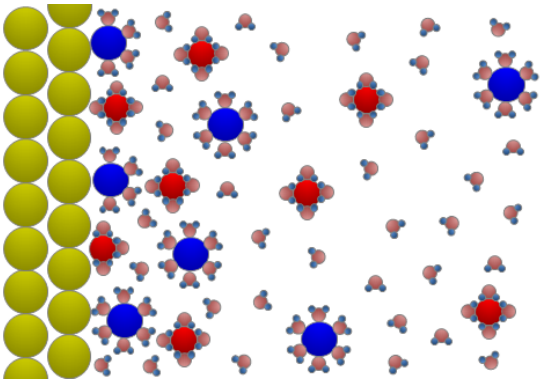

Figure 1.2.: Graphical representation of the electrochemical interface.

change in potential of the working electrode.[3,5,6] As said before, the reference electrode is used to have an accurate measure of the working electrode potential, and it thus needs to have a stable and reproducible potential.[3,6] It is usually placed near the working electrode to reduce the potential drop across the solution, although care has to be taken to reduce the risk of contamination.[3,5,6] Moreover, the exact chemical composition of the reference electrode as well as the chemical composition of the electrolyte has to be considered to avoid complications due to incompatibility, i.e. formation of an insoluble salt in the reference electrode due to ions from the electrolyte.[3]

The electrochemical processes taking place are dependent on the composition of the electrolyte as well as the electrodes. It is usually preferable to choose the electrodes in such a way that only the working electrode and the electrolyte impact the system.[5] For example, ion exchange of the reference electrode with the electrolyte can be problematic if it introduces a contamination in the electrolyte.[3] Also, the electrolyte can be purged with an inert gas like argon or nitrogen to eliminate oxygen. Electrochemical processes take place in the electrical double-layer, which is the interface between the electrode and the electrolyte and a region where the chemical and electrical potential is different from both the electrode and the electrolyte (see Fig. 1.2).[2] While the reason of adsorption and desorption taking place directly at the electrode are simply because the ions would be adsorbed on the electrode itself, the reason for the reactions taking place near it is because charge can only be transferred over a very short distance from the electrode and thus the physical proximity is a necessity.[3] The electrical double-layer also acts like a capacitor, though the double-layer capacitance can change depending on

the applied potential.[3,5,6] The working electrode also has a surface charge due to this, with the point of zero charge (pzc) being the potential where the surface charge of the electrode is zero.[5] The current measured in response to a change in the applied potential is composed of the faradaic current due to electrochemical processes at the electrode and the double-layer charging current, which is due to the double-layer capacitance.[5]

The electrode processes are divided into anodic processes, where the species is oxidised, and cathodic processes, where the species is reduced.[5] While adsorption might not include electron transfer, anodic processes would also include adsorption of anions or desorption of cations, while cathodic processes would include cation adsorption or anion desorption. This is due to the surface charge of the working electrode, which attracts anions at a positive surface charge and cations at a negative surface charge.[5] Adsorbed species can of course act as reactants and contribute to the current in that way. However, adsorption of ions also produces a current due to charge being transported to the interface and thus necessitating a charging current as the adsorbed ions act like part of a capacitor.[2,3] Adsorption of neutral species is possible, but usually takes place when there is no competition from ions.[5] Another factor influencing the reactions is mass transport, as the reactions take place at the interface and thus need the surface concentration, which can differ from the bulk concentrations.[3,5,6] There are three modes of mass transport: diffusion, which is due to a concentration gradient, migration due to a potential gradient and convection due to mechanical forces.[3,5] Convection most often is applied through stirring of the electrolyte. Migration is due to the ionic conduction in the electrolyte, but is negligible if the ionic strength in the solution is sufficiently high.[3,5] Diffusion will take place if there is a difference in the bulk and surface concentrations and is the usual mode of mass transport if the other two are avoided.

Adsorption is usually divided into non-specific adsorption, which is only due to electrostatic forces and where the ions remain fully solvated.[2] Specifically adsorbing anions, on the other hand, lose part of their solvation shell to form a chemical bond with the electrode surface.[2] Thus, whether an ion is specifically adsorbed depends on how strongly solvated it is.[2] The extend of the adsorption is usually expressed through the surface coverage θ, which is the fraction of the surface covered by the adsorbate.[5] Adsorbed species can also form an ordered

adlayer on the electrode surface.[5] Deposition is when the neutral product of the electrochemical reaction forms a layer on the surface, for example metal deposition would refer to a metal cation being reduced and forming a layer on the electrode surface.[3] As previously mentioned, a specific case of metal deposition is the UPD, which is the deposition of usually one monolayer of metal at potentials positive of the Nernst potential, which is the equilibrium potential of the bulk deposition.[3,6,7] This is due to the interactions of the deposited metal with the substrate being stronger than the interaction between atoms of the deposited metal, thus making the deposition on the substrate energetically favourable even at higher potentials.[3,6,7] Usually, only one monolayer is formed since the UPD depends on the interaction with the substrate, which grow weaker if there is already a layer deposited, however more than one can be deposited in case of very strong interactions.[6] Furthermore, the UPD shift, which is the difference in the potential of the bulk deposition and the UPD, is independent of the bulk concentrations in simple systems.[6] This is due to the UPD still following the Nernst equation, with the earlier onset being due to the change in standard potential because of the difference in interaction with the substrate. Therefore, both have the same dependence on the bulk concentration.[6] However, the coadsorption of other ions may lead to deviations of this.[6]

Chemical reversibility of a reaction requires the product to be stable.[4] For electrochemical reversibility, it is additionally required that the electrochemical surface processes are in equilibrium.[5] This means the surface concentrations are in accordance with the Nernst equation for the applied potential and requires the charge transfer to be fast compared to the mass transport.[3,5,6] It is also dependent on the time scale of the experiment.[3] Otherwise, the reaction is termed irreversible and the surface concentrations are not at their equilibrium values.[5] Furthermore, the mass transport introduces a limiting current, as it influences the surface concentration of the reactant.[3,6] Since the current depends on the amount of charge flowing through the electrode and thus the amount of reactant at the surface as well as the electron transfer rate, the maximum current flowing is limited by the amount of reactant that can be transported to the surface.[3] As such, whether the reaction is controlled by the charge transfer or the mass transport affects the reactions and the resulting dependence of the current on the potential.[5] The control depends on which is slower, as this is the rate-determining

step.[5] There also exists a region of mixed control if both the charge transfer and the mass transport have similar rate constants.[5]

1.1.1. Cyclic Voltammetry

Cyclic voltammetry is a electrochemical technique which correlates a current response to a change in applied potential. The potential is varied consistently over time according to the scan rate ν, as shown in Fig. 1.3.[3,5] The scan rate ν is also the slope of the potential waveform shown in Fig. 1.3. The resulting plot of the current I or the current density j versus the potential E is called a CV. Fig. 1.4 shows an example of such a plot. As the potential is related to the measurement time by the scan rate ν, the measured current is also a function of time.[3,5] The part of the CV in which the potential is increasing is referred to as the anodic or positive going part, while it is called cathodic or negative going for decreasing potential. These also correspond to the possible electrochemical processes, with anodic processes seen during the anodic part of the CV and cathodic processes during the cathodic part. An increased current response over a certain potential region is called a peak, f.e. in Fig. 1.4 at 500 mV positive going, which would be called an anodic peak.
A CV, as a plot of the current density j versus the potential E, actually shows the change in potential difference between the working electrode and the electrolyte solution $\delta({}^{W}\Delta^{S}\phi)$, as long as the technical considerations mentioned in the previous section are fulfilled.[3] Also, since the double-layer acts as a capacitor, a

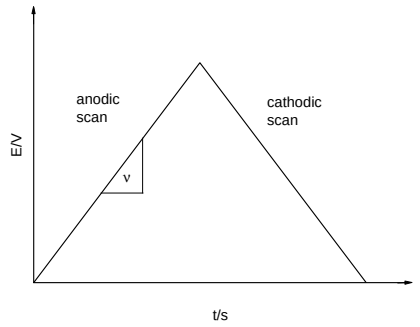

Figure 1.3.: Basic form of the change in potential with time for one cycle in cyclic voltammetry.

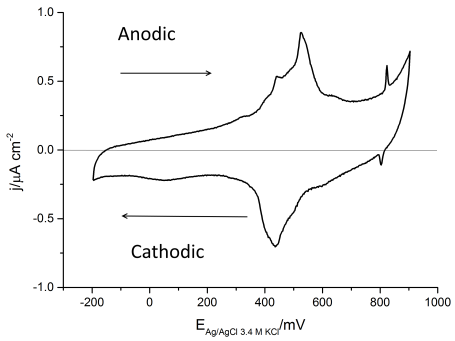

Figure 1.4.: CV of Au(111) in 0.1 M sulphuric acid at a scan rate of 10 mV/s at 20°C. The arrows indicate the direction of the potential scan.

double-layer charging current density $j_{DL} = C_{DL} \times \nu$ contributes to the overall measured current density.[3,5] This double-layer charging current rises with the scan rate and forms a baseline for the CV.[3,5] Since the faradaic current is proportional to $\sqrt{\nu}$, the influence of the double-layer charging current increases with increasing scan rate, and can even distort a CV at high scan rates.[5] The distortion increases if the double-layer capacitance C_{DL} varies over the potential, which means a changing baseline.[5] A correction can be made by assuming that the baseline can be measured in a solution without the reacting species, but that requires the reacting species to not influence the double-layer capacitance for the assumption to be correct, which is not necessarily realistic.[5]

For the electrode reactions, including adsorption and metal deposition, the current is either due to electron transfer or, for adsorption, also due to a change in the capacitance.[2,3,5] Additionally, both the rate constant and the mass transport influence the measured current density, as already explained in the previous section.[3,5,6] For an electrochemical reaction with the reactant remaining in solution, the peaks are due to the concentration gradient as well as the charge transfer, with a hysteresis between cathodic and anodic peaks due to diffusion.[4,5] The current can also become diffusion limited if the surface concentration reaches zero.[5,6] For cyclic voltammetry, the reversibility also depends on the scan rate, as the rate of the mass transport also depends on the scan rate.[5] Thus, an increase in the scan rate can change the regime from reversible to quasi-reversible or irreversible.[5] As such, the scan rate also has a strong influence on the CV, with the peak current increasing with the scan rate due to an increasing concentration

gradient.[5]
Another effect of the scan rate that should be considered is if the speed of the process is slow compared to the scan rate, which means the process is kinetically limited. As the scan rate is the change in potential with time, it is a representation of the measurement time. Therefore, if the time measured at one potential is less than the time needed for the process to be completed at that potential, the process is considered to be slow compared to the scan rate. If the process is diffusion-controlled, this is called diffusion limitation, which was already mentioned previously. Whilst most electron transfer is fast and thus not likely to become the reason for a kinetic limitation, adsorption and metal deposition include steps which can also become rate-controlling and kinetically limiting. Kinetic limitations result in a shift of the peak potential to higher potential for anodic peaks or lower potential for cathodic peaks with increasing scan rate. Furthermore, the peaks broaden with increasing scan rate.
Adsorption can also lead to sharp peaks due to adlayer ordering, or several peaks due to adsorption at different surface sites.[2] Sharp adlayer ordering peaks can be an indication of a first-order phase transition.[2] Similarly, metal deposition can show several peaks for either adsorption at different surface sites or due to a change in the structure of the deposited adlayer.[6] Furthermore, several processes can happen in the same potential range, which complicates the CV and can lead among others to overlap between peaks.[6]
Due to the different influences on the CV, the uncertain baseline as well as possible simultaneous processes, it is not an ideal method to estimate the charge density or kinetics of a process.[5] However, it can determine the potential range for different processes, involvement of coupled reactions as well as being used for recognising adsorption or metal deposition, among others.[5]

1.1.2. Chronoamperometry

For a chronoamperometric transient, the potential is stepped from a starting potential E_s at times t=0 to an end potential E_e (see Fig. 1.5), with the current being measured as a function of the potential.[3,5,6] As such, the current is measured over time while the system relaxes to the new equilibrium state.[5,6] Since this includes a change of the surface concentration of the reactants, the current varies

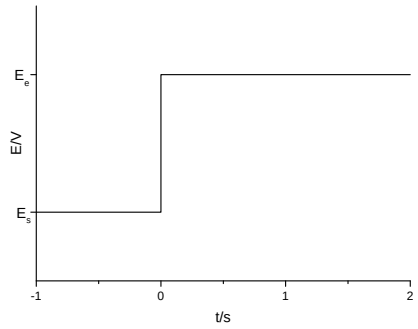

Figure 1.5.: Basic form of the change in potential with time for a chronoamperometric transient.

over time, in most cases decreasing.[6] However, the current at t=0 cannot be measured due to, for one, the rise-time of the potentiostat.[5] While the potential step is supposed to be instantaneous, the limitation of instrumentation leads to a small time necessary to complete the step.[5] Furthermore, the double-layer charging after a change in the potential also induces a sharp current spike after the potential step, which can't be separated from the current due to the electrochemical reactions.[5,6] As such, there is a limitation on the ability to measure very fast reaction, which can be masked due to the double-layer charging current.
While chronoamperometric transients are a good method for obtaining kinetic parameters as well as the charge of a process, the kinetics need to be extracted.[5] As such, they need to be fitted with an appropriate model.[5] While there might be some indications about the type of process visible from the transients, and several models can be tested against each other, previous knowledge of the mechanism of the process is generally needed to select an appropriate model.[5]
Appendix A shows the Python program used in this work for the fitting of the chronoamperometric transients. It employs the least squares method, which minimizes the square of the residuals. To show the goodness-of-fit, χ^2_{red} is used:

$$\chi^2_{red} = \frac{1}{\nu_F} \sum_i \frac{(y_i - y_{T,i})^2}{\sigma_i^2} \tag{1.2}$$

Here, ν_F is the degree of freedom, y_i the measured value for the peak position or the peak current density, $y_{T,i}$ the calculated value for the same and σ_i^2 the

variance for that value. A value of one would show a good agreement with the model as well as that the difference between the model and the fit falls within the error variance. A value below one still indicates a good fit, but also that the errors are larger than needed for the fit to fall within the error variance. Value above one either indicate that the data disagrees with the model or that the error variance was underestimated.

Electrocrystallisation

Electrocrystallisation is a term for electrode processes which involve the formation of a solid phase, for example through metal deposition on the electrode.[5] The generally involved steps in the process are diffusion of the ion to the electrode surface, electron transfer, total or partial stripping of the solvation shell, surface diffusion of the adspecies, the formation of critical nuclei from the adspecies as well further incorporation of adspecies at lattice sites for the growth of the adlayer.[5] For the deposition of an adspecies on a single crystal surface, the deposition can be assumed to be due to heterogeneous nucleation.[5] The nuclei are unstable before reaching a critical size, with the necessary energy supplied by thermal fluctuations of the system.[5,8–10] The formation of nuclei on a foreign surface generally takes place at active sites, which are energetically favourable.[5,10] As the adspecies is totally or partially stripped of the solvation shell, sites with larger coordination number, for example step edges and or other surface defects, are energetically favourable.[5] The charge transfer in the electrochemical environment is favoured on surface sites, so that nucleation at defects involves surface diffusion to the active sites.[5]
For the nucleation at active sites, the number density of nuclei N(t) would depend on the number of active sites N_0:

$$N(t) = N_0(1 - e^{-At})$$

Here, A is the first-order rate constant of the nucleation.[5] There are two limiting cases, one being a large At and thus a fast formation of nuclei, with the other being a small At, which leads to a dependence of the number of nuclei on the time.[5] The first case is called instantaneous nucleation, with $N(t) = N_0$, while the second is a progressive nucleation, with $N(t) = N_0 At$.[5]

For the formation of monolayers, the height of the new phase is limited to the height of the adspecies.[5] Thus, the growth of the monolayer is only in two directions, and thus it is a two-dimensional electrocrystallisation.[5] The nuclei can be assumed to be discs of height h and radius r.[5] Assuming the rate determining step to be the incorporation of adspecies at the edge of the nuclei leads to the following growth current per nuclei:[5]

$$i = nFk2\pi rh$$

Here, k represents the rate of incorporation.[5] The charge for the formation of a disc-shaped nuclei is:[5]

$$Q(r) = \frac{\pi r^2 hnF\rho}{M}$$

With M being the molecular weight and ρ the density of the deposit.[5] If the radius is given in regard to the surface area so that $\pi r^2 = 1$ for the full monolayer, the charge density of the full monolayer would thus be $q_{ML} = \frac{hnF\rho}{M}$.[5] The derivative of Q(r) can be used to find the time dependence of the growth current for one nucleus:[5]

$$i(r,t) = \frac{2\pi r(t)hnF\rho}{M} \cdot \frac{dr(t)}{dt}$$

Comparing the two expressions for the growth current of one nucleus gives a rate of radial expansion of $\frac{dr(t)}{dt} = \frac{Mk}{\rho}$, which means $r(t) = \frac{Mk}{\rho}t$.[5] Therefore, the growth current for one nucleus depending on the time is as following:[5]

$$i(t) = \frac{2\pi hnFk^2M}{\rho}t$$

It is also possible that there is one-dimensional growth, for example growth at steps. The general expression for the current into the surface area S_N would be:[11]

$$i = nFkS_N$$

The time dependence of the current for two-dimensional nucleation comes from the changing amount of incorporation sites for the adspecies with time due to a change in the circumference of the nucleus. As the one-dimensional growth by

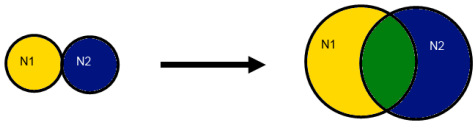

Figure 1.6.: Visualization of the impinging of two nuclei N1 and N2 on each other, with the overlap area in green.

its nature does not change the number of incorporation sites as long as growth is unobstructed, the current stays constant. The charge for a monolayer would stay the same as for two-dimensional growth, as the fully formed monolayer covers the whole crystal surface independent of the growth mode.
For the growth of the whole phases, the growth of all nuclei has to be considered. Also, the interaction between the nuclei has to be considered, with nuclei possibly impinging on each other. For the growth of crystalline phases, which includes the growth of solid metal monolayers, impinging nuclei usually adhere to each other, which means growth stops at the point of contact of the impinging nuclei while continuing otherwise (see Fig. 1.6).[10] This overlap has to be considered in the growth calculations, as otherwise the overlapping area would be counted two times. For this overlap problem, Avrami et al.[8–10] introduced the concept of extended parameters, which are the parameters if no impingement was taking place. So, for the growth current, the extended current density for all nuclei would be the growth current of one nucleus multiplied by the number density of nuclei:

$$j_{ex} = i(t)N(t)$$

The growth current thus depend on the type of nucleation. For instantaneous nucleation and two-dimensional growth, it would be:[5]

$$j_{ex,i2D} = \frac{2\pi hnFk^2MN_0}{\rho}t$$

Progressive nucleation and two dimensional growth would have the following extended current density:[5]

$$j_{ex,p2D} = \frac{2\pi hnFk^2MAN_0}{\rho}t^2$$

One-dimensional growth with instantaneous nucleation would be:[11]

$$j_{ex,i1D} = nFkN_0S_N$$

For the normalised extended area S_{ex} covered by the deposited phase, the Avrami theorem $S = 1 - e^{-S_{ex}}$ gives the relation to the normalised area S.[5,8–10] The extended charge density q_{ex} can be related both to the extended current density j_{ex} and the total charge density for one monolayer q_{ML}:[5]

$$q_{ex} = \int_0^t j_{ex}dt = S_{ex}q_{ML}$$

Therefore, $j_{ex} = q_{ML}\frac{dS_{ex}}{dt}$ and $j = q_{ML}\frac{dS}{dt}$ and with the relation of S and S_{ex} through the Avrami theorem:[5]

$$j = j_{ex}e^{-S_{ex}} = j_{ex}e^{\frac{q_{ex}}{q_{ML}}}$$

For instantaneous nucleation and two-dimensional growth, the current density is thus:[5]

$$j_{i2D} = \frac{2\pi hnFk^2MN_0}{\rho}t \cdot e^{-\frac{\pi k^2M^2N_0}{\rho^2t^2}}$$

Similarly, for progressive nucleation and two-dimensional growth the following current density would apply:[5]

$$j_{p2D} = \frac{\pi hnFk^2MN_0A}{\rho}t^2 \cdot e^{-\frac{\pi k^2M^2N_0A}{3\rho^2t^3}}$$

Instantaneous nucleation and one-dimensional growth leads to:

$$j_{i1D} = nFkN_0S_Ne^{-\frac{kN_0S_NM}{h\rho}t}$$

A general expression for the current density can be found with

$$j_g(t) = q_g \cdot m_g \cdot k_g \cdot t^{(m_g-1)} \cdot e^{(-k_g \cdot t^{m_g})} \tag{1.3}$$

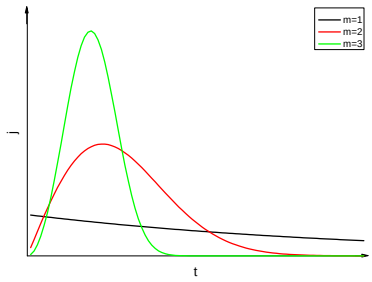

Figure 1.7.: Current-time response according to the Avrami equation (Eq. 1.3) for the different values of m which represent different growth modes (1: instantaneous nucleation with either on-dimensional growth or two-dimensional growth and surface diffusion, 2: instantaneous nucleation and two-dimensional growth, 3: progressive nucleation and two-dimensional growth).

which will be called the Avrami equation. Here, k_g represents the rate constant of the process, and q_g is the current density related to that process, with m_g giving the type of process. For instantaneous nucleation and two-dimensional growth $m_g = 2$, with $k_g = \frac{\pi N_0 M^2 k^2}{\rho^2}$ and $q_g = q_{ML} = \frac{hnF\rho}{M}$. Progressive nucleation and two-dimensional growth would be indicated by $m_g = 3$, with $k_g = \frac{\pi A N_0 M^2 k^2}{3\rho^2}$ and $q_g = q_{ML} = \frac{hnF\rho}{M}$. From the previous equations, $m_g = 1$ can represent instantaneous nucleation and one-dimensional growth with $k_g = \frac{N_0 M k S_N}{h\rho}$. It can also represent instantaneous nucleation and two-dimensional growth combined with surface diffusion.[12] When considering the power of the time as well as the equations of k_g, it is clear that the unit of k_g depends on the process and is s^{-m_g}. The corresponding time constant would be $\tau_g = k_g^{-\frac{1}{m_g}}$.
Fig. 1.7 shows an example the shape of the current transients for the different nucleation and growth behaviours according to the Avrami equation (Eq. 1.3). Of note is the characteristic current peak obtained for m=2 and m=3, which is generally considered a sign for a nucleation and two-dimensional growth process.

1.2. Influence of the temperature

Since the temperature, along with pressure and concentration is one of the factors that modifies the Gibbs energy driving chemical reaction, an influence of the

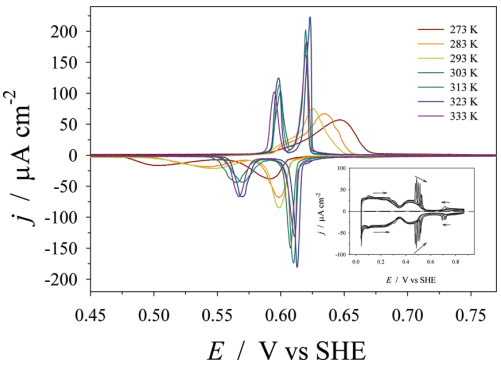

Figure 1.8.: Series of cyclic-voltammetry profiles for the deposition and stripping of Cu-UPD on Pt(111) in aqueous 0.05 M H_2SO_4 + 5 mM $CuSO_4 \cdot 5\ H_2O$ recorded at seven different T values in the 273-333 K range (ΔT=10 K); s=5 mVs^{-1} and A=0.0431 cm^2. The annotations C_I, C_{II}, A_I, and A_{II} stand for two cathodic and two anodic peaks. The inset presents a series of cyclic-voltammetry profiles for Pt(111) in aqueous 0.05 M H_2SO_4 solution recorded at seven different T values in the 273-333 K range (ΔT=10 K) immediately following the Cu-UPD deposition-stripping experiments; s=50 mVs^{-1} and A=0.0431 cm^2. Reprinted with permission from reference 13. Copyright 2009 American Chemical Society.

temperature on electrochemical reactions and thus on electrodeposition would be expected.[13] One of the expected effects of the temperature is that an increased temperature increases the thermal energy of the particles in the system, and thus decreases the degree of order.[13] The increased thermal energy means an increase in the internal energy of the system. For the particles in the system, this also translates into an increase in the kinetic energy. This leads to an increase in the mobility of the particles, as well as an increase in vibrational and rotational energy if the particles are molecules. The increased mobility would be the reason for the decreased degree of order of the system with increasing temperature.
Jerkiewicz et al.[13] studied the effect of temperature on the Cu-UPD on Pt(111) in sulphuric acid, while Radovic-Hrapovic et al.[14] looked at silver on Pt(111) in sulphuric acid. The temperature range for both was between 0°C and 60°C. Both studies found an influence of the temperature on the peak potential and peak current density, with the influence on the charge density being different between the two deposited metals. The peak potential displacement was found to only take place at low temperatures below 25°C, with a shift of the potential while the temperature increased (see Fig. 1.8 and Fig. 1.9). Both also found that the

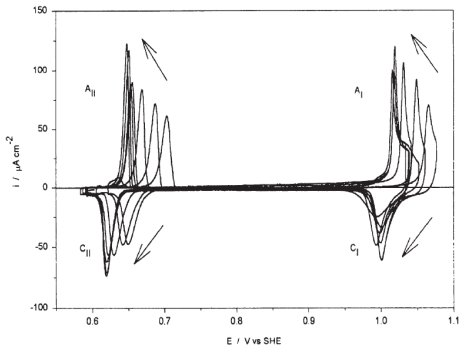

Figure 1.9.: Series of cyclic voltammograms for UPD of Ag on Pt(111) in 0.1 M H_2SO_4 + 1 mM Ag_2SO_4 solution at $273 \leq T \leq 333$ K with an interval of 10 K; s=5 mVs^{-1}. Arrows indicate changes in the CV profiles associated with T increase. Reprinted with permission from reference 14. Copyright 2002 American Chemical Society.

change with temperature depends on the temperature range, with differing trends above and below 25°C.[13,14]

For the silver UPD, the charge density redistribution with varying temperature was found to be an effect of the interaction of the two deposited Ag-monolayers, with a temperature dependent phase transition taking place.[14] As the Cu-UPD shows a strong dependence on the temperature, an influence of the temperature on the surface structure or even disordering of the phase with increasing temperature is possible.[13] Furthermore, Jerkiewicz et al.[13] found that for Pt(111) in sulphuric acid, the long-range ordering of the sulphate adlayer is inhibited at high temperatures. Therefore, the amount of the ordered sulphate adlayer formed decreases with increasing temperature.[13] The sharpening of the peaks in the CV for the Cu-UPD found by Jerkiewicz et al.[13] with increasing temperature suggests a synergetic effect of the adsorbed species, as the increased disorder which would be expected with an increase in temperature would lead to broader peaks in the CV (see Fig. 1.8).

The only study of the temperature dependence of the Cu-UPD on Au(111) is by Gründer et al.,[15] with the study being in sulphuric acid and in the presence of bromide anions. It also explored the UPD of silver on Au(111), with both UPD processes being studied at low (6°C) and high (38°C) temperature.[15] The primary findings of the paper in regards to the Cu-UPD were an improvement of the degree of ordering in the Cu-UPD layer with increasing temperature, and a

decreased ordering with decreasing temperature.[15]
A previous study by Lucas et al.[16] in a temperature range between 2°C and 46°C had shown that a change in temperature had only negligible effects on the structure and phase transition of the bromide adlayer on Au(001) in potassium hydroxide and on Pt(111) in perchloric acid. The only influence of the temperature was on the surface mobility of the bromide, thus influencing the kinetics of the ordering.[16] Following that, it was assumed that the bromide adlayer was uninfluenced by the temperature, and thus the temperature influence was only on the copper adatoms.[15] The temperature effect on the ordering was attributed to an increased surface mobility of the copper adatoms at elevated temperatures.[15] Furthermore, for the UPD of silver it was found that at low temperatures the adlayer was disordered due to a decreased mobility of the adspecies.[15] Therefore, the principal effect of the temperature was assumed to be the control of the mass transport of the metal adatoms.[15] Since bromide is a strongly adsorbing anion, and as such has a strong effect on the Cu-UPD, the temperature dependent study in this work is an extension of that study, to find out if the temperature effect differentiates when weakly adsorbing anions are used.

1.3. Investigated systems

The Cu-UPD on gold had been chosen because it is a standard system to test the influence of different factors on the UPD process, as it is well understood and extensively studied.[17,18] One factor that greatly influences the structure of the copper UPD-layer is how strongly adsorbing the anion in the electrolyte is.[7] Especially chloride anions, a strongly adsorbing anion with a high affinity for copper, can induce a structural change in the copper layer even at trace concentrations.[17,19] This can be extended to bromide and iodide, which show a similar behaviour to chloride, with the Cu-halide and halide-halide interactions dominating instead of the Cu-Au interactions as is the case with more weakly adsorbing anions.[17] The strength of the specific adsorbtion of anions follows the order $F^- < ClO_4^- < SO_4^{2-} < Cl^- < Br^- < I^-$, with an increasing strength of solvation leading to a decreasing strength of adsorption.[19] The effect of anions on a metal surface can also be seen by looking at the anion adlayers on a metal electrode, where adsorbed anions have a strong influence in the surface structure.[20]

The effect of the anions also depends on the structure of the anion adlayer. Ordered adlayers have a strong influence on the surface morphology and the dynamic behaviour of the metal atoms, while disordered adlayers have a weak influence for weakly adsorbing anions and low surface concentration.[20] However, at high surface concentrations, they can have a noticeable influence and even change the mass transport mechanism of the metal atoms.[20]
For the Cu-UPD on Au(111), Shi et al.[18] show that the anions coadsorb with the copper and form a mixed layer, with the structure of the layer depending on the nature of the anion. Also, the anions affect the rate and the energetics of the copper deposition.[18] Generally, the structure of the copper deposit seems to depend on the relative strength of the Cu_{UPD}-substrate, Cu_{UPD}-anion and substrate-anion interactions in regards to each other.[7]
As the effect of more weakly adsorbing anions than bromide is of interest, sulphuric acid and perchloric acid have been chosen as electrolytes. The Cu-UPD on Au(111) in sulphuric acid is often used as a model system since it has been extensively studied.[17,18] Perchloric acid was chosen as it is one of the most weakly adsorbing electrolytes and thus the influence of the perchlorate on the UPD is less than it is in sulphuric acid. Furthermore, the temperature dependence of Au(111) in sulphuric acid and perchloric acid were included to isolate the effect of the temperature on the anions.

1.4. Au(111)

The (111) face of gold (see Fig. 1.10) is a widely used and studied surface, and is often used in sulphuric acid as a model system. There are two surface structures: the (1×1) structure of the bulk and a reconstruction (see Fig. 1.11). A surface reconstruction is a rearrangement of the surface atoms compared to the bulk due to the termination of the bulk structure.[21] It includes a lateral displacement of the surface atoms and results in a change of the surface symmetry.[7,21] The driving force is to reduce the surface energy, as the bulk structure is energetically unfavourable due to the surface atoms being exposed to a different environment.[21]
The reconstruction of Au(111) slightly compresses the surface structure, so that the reconstructed surface has more gold atoms than the unreconstructed surface.[7,21]

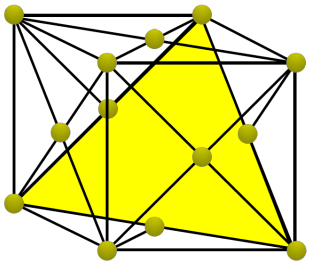

Figure 1.10.: Gold unit cell with (111) plane.

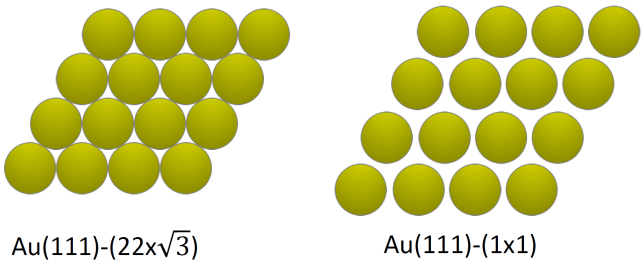

Figure 1.11.: Simplified model of the reconstructed (left) and unreconstructed (right) Au(111) surface.

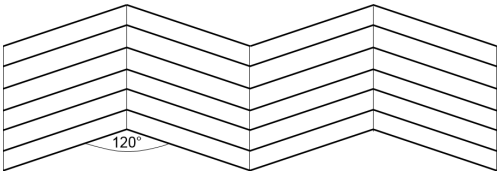

Figure 1.12.: Schematic of the herringbone superstructure of the Au(111) reconstruction. Each area has the $(22 \times \sqrt{3})$ structure, with domain walls separating them.

The reconstruction domains are generally accepted to have a $(22 \times \sqrt{3})$ structure.[7,21–23] Additionally, there is a so called chevron or herringbone superstructure that is the long-range ordering of the reconstructed domains.[7,22–24] These domains of the reconstruction can have one of three orientations due to the threefold symmetry of the surface.[21,24] The chevron structure is formed by reconstructed domains of two out of the three orientations that are rotated 120° in respect to each other and separated by discommensuration lines (see Fig. 1.12).[23–25] This reduces the surface stress in all three directions of the Au(111) surface.[22,26] Since the chevron structure is formed due to surface stress and surface defects also release surface stress, the reconstruction is altered around defects.[22–24,26,27] Thus, for surfaces with high defect density, the reconstruction can be irregular, poorly ordered or even completely absent.[22,26,28] The availability of surface defects furthermore also influences the kinetics of the reconstruction, with monoatomic islands serving as nucleation centres for the reconstruction.[21] Monoatomic islands are formed from the excess gold surface atoms if the reconstruction is lifted, roughening the surface in the process.[21]

At room temperature, the reconstruction is the thermodynamically stable form at neutral charge, although it can be lifted through adsorption of adspecies and an energy barrier exists for forming the reconstruction again at room temperature.[21] The activation barrier is due to the transition involving bond-breaking between surface atoms and lateral diffusion of the same.[21] Reconstruction lifting from adsorption is likely due to the adsorbate providing a bulk-like environment to the surface layer, as the difference in the surface structure is not large enough to make the adsorption sterically more favourable on the (1×1) surface.[21] The $(1 \times 1) \leftrightarrow (22 \times \sqrt{3})$ transition takes place around the pzc, with the exact potentials depending on the adspecies.[21]

The reconstruction itself is stable up to 590°C in ultra-high vacuum (UHV) with a contraction of the unit cell with increasing temperature.[25] However, for the range between 0°C and 50°C, the effect of the temperature on the crystal surface structure itself should be negligible.

In an electrochemical environment, applying a potential negative of the pzc can be used to reduce the activation barrier of the reconstruction to allow reconstruction at room temperature after it was lifted.[21] This so called potential-induced reconstruction differs from the thermal reconstruction formed by heating the

crystal in that it is less well-ordered.[21,28] While in the thermal reconstruction the domains of the reconstruction on one Au(111) terrace are aligned in one direction, the potential-induced reconstruction has smaller domains and also has different orientations on the same terrace.[21,28] The higher defect density of the surface after reconstruction lifting could also be partly responsible for the less ordered potential-induced reconstruction.

1.4.1. Au(111) in sulphuric acid

In sulphuric acid, there are three different surface structures of phases in the double-layer region, depending on the potential. One is the reconstructed Au(111) surface with minimal sulphate adsorption, then the Au(111)-(1×1) region with adsorbed sulphate and a mobile overlayer of sulphate anions and last but not least the ordered $(\sqrt{3} \times \sqrt{7})$ sulphate adlayer on Au(111)-(1×1).[20,29–35] The reconstruction is as described in Sec. 1.4, with the lifting of the reconstruction due to specific adsorption of sulphate anions.[21,35]
The adsorbed species on Au(111) is controversial,[20] with Shi et al.[32,36] postulating sulphate as the adsorbed species based on findings with supporting perchloric acid electrolyte and Uchida et al.[37] finding bisulphate as the adsorbed species. Additionally, it has been found that bisulphate dissociates when adsorbed on Au(111)[38] and that the ordering does not take place in sodium sulphate solution.[30] Furthermore, as coadsorbed water has been found to play a role in the ordered sulphate adlayer and the sulphate species adsorption,[20,37,39] the exact nature of the adsorbed species might not be as simple as either sulphate or bisulphate. While the exact nature of the adspecies is not known, it will be referred to as simply sulphate for ease of use.
The ordering of the sulphate adlayer proceeds via a nucleation and 2D surface diffusion-controlled growth process with a fast adsorption of a small amount of sulphate prior to it.[29] The phase transition is fast and completely reversible.[30] The size of the ordered sulphate adlayer domains depends on the size of the Au(111) terraces, with large adlayer domains on large terraces.[29] However, even small terraces show patches of the ordered adlayer.[29] The regions between neighbouring domains are strongly disordered, which leads to an increased number of defects in the adlayer with decreasing domain size.[29] As such, the sulphate adlayer as a

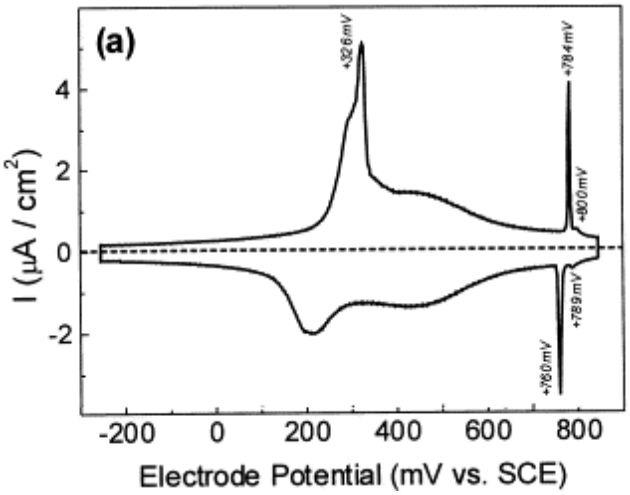

Figure 1.13.: CV for Au(111) in 0.1 M sulphuric acid at 10 mV/s. Reprinted from reference 35, Copyright 2000, with permission from Elsevier.

whole would seem increasingly disordered with decreasing domain size, leading to a smaller charge for the nucleation process overall.[29] Additionally, the rate of nucleation increases with decreasing domain size.[29] While the ordered sulphate structure is known to be $(\sqrt{3} \times \sqrt{7})$, it has been proposed that coadsorbed water is incorporated into the structure, with several possible structures. Since this is not focus of this work, the reader is referred to the review by Magnussen[20] for further details. While there might have been work done in this area since the publishing of the review, it should nevertheless provide a good starting point for the interested reader. Since the used investigative methods in this work cannot obtain any information on coadsorbed water, the exact structure for the coadsorbed water is not relevant to this work. The sulphate coverage is also subject to debate, with reported values of 0.4,[30] 0.33[37] and 0.2.[31,36] The coverage of 0.2 was based on results with supporting perchloric acid, which, although said to not or only weakly specifically adsorb, has been found to affect the adsorption of sulphate.[37] Thus, the sulphate coverage is more likely in the range of 0.3-0.4.

Fig. 1.13 shows an example CV from the literature. In the CV, the order-disorder transition of the sulphate adlayer is represented by a pair of spikes around 0.8 $V_{Ag/AgCl}$ which are shifted slightly in respect to each other.[20,29,30,33,35] The charge of the spikes depends on the charge of the nucleation process, while the potential depends on the nucleation rate. A faster nucleation leads to a shift

towards lower potentials. Thus, smaller $\sqrt{3} \times \sqrt{7}$ domains lead to the spikes being smaller and shifted negatively.[29] As the spikes are quite sensitive to the surface structure, they are one indicator that can be used to determine the surface quality.[33,39]

On well-ordered Au(111), the unordered sulphate adsorption and desorption should be between approximately 300 $mV_{Ag/AgCl}$ and 840 $mV_{Ag/AgCl}$, manifesting as a broad peak in the CV.[32,39]

The thermal reconstruction lifting is seen in the CV as a positive-going peak at 380 $mV_{Ag/AgCl}$ for the thermal reconstruction, with the peak becoming smaller and shifted to lower potentials with increasing defect density.[33] Therefore, the less well-ordered potential-induced reconstruction show the reconstruction lifting peak at more negative potentials with a lower height compared to the thermal reconstruction.[28] A CV with potential-induced reconstruction for 0.05 M sulphuric acid show the reconstruction lifting peak around 320 $mV_{Ag/AgCl}$.[29] With the sensitivity of the reconstruction lifting to the defect density, especially the height of the reconstruction lifting peak, it can also be used to determine the surface quality.[33]

1.4.2. Cu-UPD on Au(111) in sulphuric acid

The UPD of copper on Au(111) in sulphuric acid is considered a well-understood model system ideal for investigating the effect of different variables on the UPD process.[17,18] It has been characterized extensively by many experimental methods, including coulometry,[18,36,40–43] scanning tunneling microscopy (STM),[42,44–48] in-situ x-ray scattering,[49] x-ray diffraction (XRD),[50,51] electrochemical quartz crystal microbalance (ECQM),[37] surface-enhanced infrared absorption spectroscopy (SEIRAS),[52] low-energy electron diffraction (LEED),[43] Auger electron spectroscopy,[43] chronoamperometry,[52–55] extended x-ray absorption fine structure (EXAFS),[56] microcalorimetry[57] and cyclic voltammetry.[43,54] Additionally, theoretical modelling has also been used to better understand the system.[43,58–62]

Cu-UPD

The Cu-UPD on Au(111) is due to the strong interaction between the copper adatoms and the surface gold atoms. However, copper also shows a strong coad-

sorption with sulphate, which influences the structure of the copper layer as well as the kinetics and energetics of the process.[18,43,47,49] Due to this, the Cu-UPD on Au(111) in sulphuric acid proceeds in several stages, each with a distinct structure.[17,18,37,43,47,53,58–61] The steps are as following:[17,43,47,58–60]

I) Coadsorption of copper and the sulphate species as a random lattice gas at potentials below the pure sulphate adsorption. Is visible in the CV as the broad shoulder of peak A at higher potentials in Fig. 1.14.[17,47,58,59]

II) A first-order order-disorder phase transition to an ordered coadsorbed ($\sqrt{3} \times \sqrt{3}$)R30° layer (structure see Fig. 1.15).[49] The copper forms a honeycomb structure with a coverage of 2/3 monolayer (ML), while the sulphate is adsorbed in the centre with a coverage of 1/3 ML.[49] The corresponding peak in the CV is peak A in Fig. 1.14.[53]

III) A second-order phase transition to the full Cu-(1x1) monolayer.[43] The copper monolayer is covered with a sulphate adlayer with a ($\sqrt{3} \times \sqrt{7}$)R19.1° structure, the same as for ordered sulphate on Cu(111) and Au(111).[44] In the CV, it corresponds to peak B in Fig. 1.14.[53]

The distinct coverages for each step can also be seen in Fig. 1.14, which shows distinct steps corresponding to the potential of the peaks for step II and III. While some information about the relation between the CV peaks and the steps has been given here, the cyclic voltammetry will be presented in more detail later.

The theoretical charge for the deposition of a full monolayer of copper on Au(111) is 0.44 $mCcm^{-2}$ for an ideal Cu(1x1) monolayer assuming a charge transfer of 2 electrons for each copper adatom.[62] Experimentally, there were two different charge values found using coulometry: one at 0.44 $mCcm^{-2}$[17,42] with a ratio of 2:1 for the first and second Cu-UPD stage, and one at 0.36 $mCcm^{-2}$.[17,40,41,43] However, the measurement criteria used for the two values were different, with the lower value not including the charge from the random adsorption.[17] Since the higher value matches the theoretically expected value, the random adsorption region should be included to gain an accurate charge.

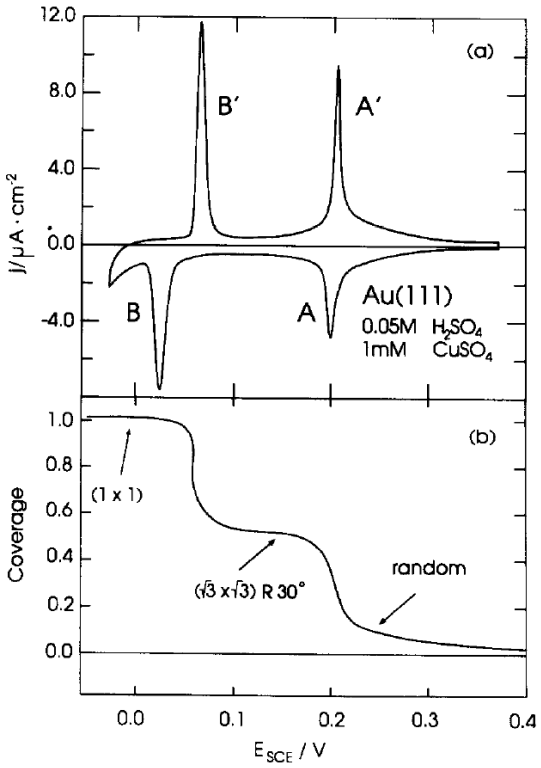

Figure 1.14.: (a) CV at 1 mV/s and (b) electrochemically retrieved copper coverage (normalized charge due to Cu-UPD) of the Cu-UPD on Au(111) in 0.05 M sulphuric acid 1 mM copper sulphate. Reprinted from reference 53, Copyright 1994, with permission from Elsevier.

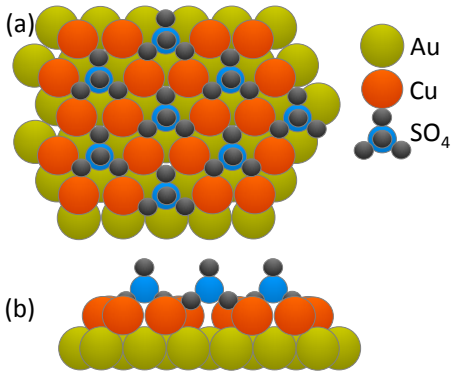

Figure 1.15.: Interfacial structure of the coadsorbed copper and sulphate ($\sqrt{3} \times \sqrt{3}$)R30° layer on Au(111) formed in step II. (a) Top view. (b) Side view.

Structure and processes of the first Cu-UPD stage

Steps I and II are generally taken as the first stage of the Cu-UPD process. The structure of the first ordered adlayer had at first been contested, as STM and atomic force microscopy (AFM) results of the copper coverage disagreed with those from other experimental methods and structure calculations.[17,18,40,42,45,46,49] Magnussen et al.,[45,46] as well as Hachiya et al.,[42] used STM imaged a $(\sqrt{3}\times\sqrt{3})$R30° structure with a coverage of 1/3 ML. The STM maxima that lead to the coverage were assumed to be the copper layer. Magnussen et al.[45,46] also found a (5x5) structure which was shown to be due to chloride contamination.[46,49] Shi et al.[18,40] found a copper coverage of 2/3 ML for the first ordered layer through the integration of CVs as well as coulometry. Hachiya et al.[42] assumed that the difference between the charge-derived coverage and the STM images was due to anion adsorption or desorption. On the other hand, Shi et al.[18,40] postulated that the imaged maxima in STM and AFM were sulphate instead of copper. This was shown by Toney et al.[49] using x-ray scattering, where they found a $(\sqrt{3}\times\sqrt{3})$R30° structure with a copper coverage of 2/3 ML in-situ. It had been assumed that the sulphate could not be imaged in STM since it was assumed to be weakly bound and thus conduct poorly.[49,62] However, due to the coadsorption with copper a strong bond between the adsorbates enabled the flow of the tunnelling current.[49,62]

Fig. 1.15 shows the accepted structure of the first ordered adlayer, which was confirmed by both experimental methods and theoretical modelling.[47,49,56,58–60] The copper forms a honeycomb lattice on the Au(111) surface with the sulphate adsorbed above the plane of the copper atoms in the centre of the honeycomb rings.[47,49,56] Both adsorbed species are situated in or above threefold hollow sites on the Au(111) surface.[47,49,56] Three oxygen atoms of the sulphate are chemically bonded to copper atoms, while the S-O bond of the last oxygen is perpendicular to the crystal plane.[47,49,56] Chabala et al.[50] found the copper residing in atop position instead, but admitted that due to using potentiodynamic measurements, the copper might still switch to the threefold hollow sites during equilibration.

For the formation of the ordered layer, Vasiljevic et al.[47] found a random nucleation of the $(\sqrt{3}\times\sqrt{3})$R30° structure and subsequent growth of the domains. Domain formation was also found by Hachiya et al.[42] Nakamura et al.[51] pos-

tulated that for the formation of the first Cu-UPD structure, the copper first coordinates on the adsorbed anion layer. The copper complex then changes its orientation with decreasing potential, leading to the discharge and adsorption of the copper on the surface and the change to the $(\sqrt{3}\times\sqrt{3})$R30° structure.[51] They also found the honeycomb copper phase to have semiconductor or isolator properties due to a large Cu-Cu distance in the honeycomb layer.[51] This comes from the copper adlayer being commensurate with the Au(111) surface while the copper diameter is smaller than that of gold.

Structure and processes of the second Cu-UPD stage

The second Cu-UPD stage is the formation of a full pseudomorphic Cu-(1x1) monolayer.[17,18,40,43,47,50,51,56] Here the copper atoms occupy the threefold hollow sites of the Au(111) surface by replacing the sulphate previously in that position.[17,18,40,43,47,50,51,56] The domain boundaries of the $(\sqrt{3}\times\sqrt{3})$R30° layer or surface defects serve as starting nucleation sites for the phase transition.[47,54] Furthermore, an ordered sulphate layer was found on top of the copper monolayer.[18,40,44,47,56,57] Vasiljevic et al.[47] found it to have a $p(2\times2)$ structure while Lee et al.[56] found indication of a $(\sqrt{3}\times\sqrt{3})$R30° structure instead. Madry et al.[44] found a $(\sqrt{3}\times\sqrt{7})$R19.1° sulphate structure on the Cu(1x1) monolayer, as it is on Au(111) and Cu(111). However, the deposition of a second copper layer proceed similar to the first monolayer, which includes the formation of a $(\sqrt{3}\times\sqrt{3})$R30° copper and sulphate structure for a copper coverage of 5/3 ML.[44] The isolation of the sulphate structure on one monolayer of copper is said to be difficult due to the sulphate ordering at lower potential compared to the copper monolayer formation.[44] It is most likely that Lee et al.[56] had a copper coverage of 5/3 ML instead of 1 ML.

Adsorbed species and coverage

There are differing opinions on whether the adsorbed anion species is sulphate or bisulphate. In the first stage of the Cu-UPD, copper and the sulphate species coadsorb, and the two have opposite charges and thus opposing signs of the related adsorption current.[18,40,53,57] The influence of the sulphate adsorption on the measurement techniques depend on whether there are two differing adsorption

processes or one coadsorption process which includes both species, with the literature suggesting it to be the later.[18,57] As such, the species and thus the charge of the sulphate species is needed to correct the observed charge density for the sulphate adsorption to gain the accurate charge density for the copper deposition. Since the coadsorption is only in the first Cu-UPD stage, the second Cu-UPD stage does not need a correction, as the faradaic charge is equal to the copper deposition.[57]

Whilst the dominant species in the bulk solution is easily determined through the pH, it is not given that the same species is the one adsorbed on the electrode surface. Several people assumed sulphate as the adsorbed species,[18,36,40,41,43] with a vacuum calculation by Xu et al.[62] also giving sulphate as the species. However, several experiments found evidence suggesting bisulphate as the species: Nakamura et al.[51] looked at the S-O bond length using XRD, Lee et al.[56] used EXAFS parameters and Uchida et al.[37] found the equivalent mass in ECQM to not be realistic for sulphate. However, all of these assumed adsorption of only one species of anions. Frittmann et al.[57] used microcalorimetry to determine the anion coverage per charge for the first Cu-UPD stage by comparing the faradaic charge to the molar Peltier heat for each process. From this, a coverage of 0.44 ML of monovalent anions in 0.1 M sulphuric acid was calculated for that stage, with the value depending slightly on the electrolyte concentration.[57] Comparison of the known coverage θ of $\theta_{sulphate} = \frac{1}{3}\ ML$ gave a coverage of $\theta_{HSO_4^-} = 0.22\ ML$ and $\theta_{SO_4^{2-}} = 0.11\ ML$, giving adsorption of both species with bisulphate being the dominant one.[57] Again, for conveniences sake, although both species are adsorbed, the adsorbed species will be generally referred to as sulphate. It is not clear, however, if the H^+ stays localized or is shared, especially as there is evidence that the sulphate still interacts with the surrounding water.[51,57] Fig. 1.16 shows the earlier mentioned correction of the copper coverage due to coadsorption with sulphate.[57]

As for the charge of the adsorbed species, there is a general consensus that the sulphate keeps its ionic character, with at most a partial neutralization.[18,41,43,57] However, for the most part the studies assumed the adsorption of only sulphate, with no bisulphate adsorption. Thus, it is also possible that the partial neutralization was simply due to both sulphate and bisulphate being adsorbed. Considering that the experimental methods do not probe one specific anion, having both

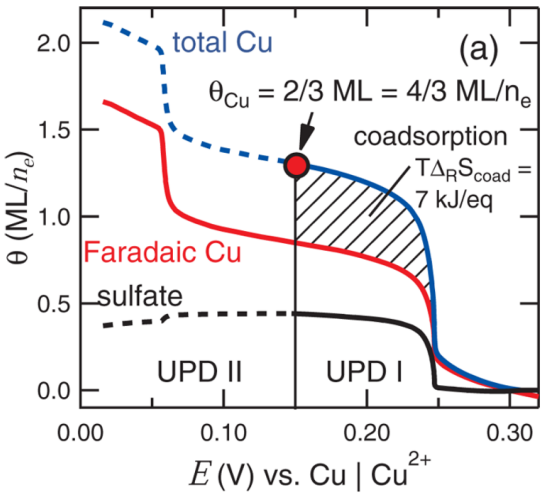

Figure 1.16.: Equivalent coverages calculated from the faradaic charge (red), the sulphate species (black) and of the total deposited copper(blue) for 0.1 M sulphuric acid 10 mM copper sulphate. For the UPD I region, a charge-neutral coadsorption process of copper and sulphate with $T\Delta_R S_{coad} = 7kJ/mol$ was assumed, with the total copper coverage derived from the sum of the faradaic coverage as well as the sulphate coverage. The copper coverage in the UPD II region was assumed to be from faradaic copper deposition. For the sulphate coverage, a charge-neutral substitution of bisulphate with oxygen species was assumed (dashed black line). Reprinted with permission from reference 57. Copyright 2016 American Chemical Society.

species adsorbed would lead to a lower charge than an adsorption of only sulphate. For the adsorbed copper, the charge is subject to debate. While x-ray absorption near structure (XANES) results[56] indicate an oxidation state of approximately +I or at the very least retaining a residual charge, chronocoulometry[40,41] suggests a near full charge transfer. Most likely, the adsorbed copper forms a polar bond with the gold surface, which is stabilized by the adsorbed sulphate.[17,18,40,41,49]

Kinetics

The second deposition stage of the Cu-UPD process as well as the dissolution stages can be described as a two-dimensional instantaneous nucleation and growth process with a constant growth rate coupled with a Langmuir-type adsorption/desorption process, with the two processes occurring at different sites.[52–55] The Langmuir-type process for the second deposition stage as well as the dissolution processes has been attributed to surface defects by Hoelzle et al.,[53] as the ratio of the nucleation process to the adsorption/desorption process increases in favour of the adsorption/desorption on crystals with higher surface defect densities. In particular, Hoelzle et al.[54] found a strong dependence for the second deposition stage as well as the associated dissolution on the step density. For the dissolution of the honeycomb phase, Ataka et al.[52] has proposed that the Langmuir-type desorption process is not related to defects but rather to the phase transition in the adlayer. They found that instead of being parallel, there was an initial Langmuir-type process with a subsequent nucleation and growth process.[52] Their combination of chronoamperometry and time-resolved SEIRAS showed a desorption of 1/3 ML of copper and sulphate each in the first step, with the remaining 1/3 ML copper being desorbed in the second step.[52] Thus, they assigned the codesorption of the copper and sulphate, along with the phase transition, to the Langmuir-type process, while the nucleation and growth process would desorb the remaining copper.[52] Both Hoelzle et al.[53,54] and Ataka et al.[52] show a Langmuir-type process with a nucleation and growth process, though there is disagreement whether it is parallel or subsequent. Hoelzle et al.[53] did find the adsorption/desorption process to be significantly faster than the nucleation and growth process, whilst the equation used by Ataka et al.[52] for fitting the processes does not incorporate a time-delay for the nucleation and growth process. As such whether they are parallel or subsequent seems to be mostly depending

on the interpretation of the Langmuir-type process being much faster than the nucleation and growth process. The main difference would be the interpretation of the origin of the two processes, but the experimental evidence presented by Hoelzle et al.[53,54] for the effect of the surface defects does, to my best knowledge, only cover the second deposition stage as well as the associated dissolution, whilst Ataka et al.[52] investigated the dissolution of the honeycomb phase. Thus, though they show the same general behaviour, it is certainly possible that the different stages have different origins of the processes. However, it also has to be remembered that there is no evidence to tell whether or not the kinetics of the dissolution of the honeycomb phase are affected by surface defects. The kinetics of the first deposition stage have, to the best of my knowledge, not yet been described. Garfias-Garcia et al.[55] found a progressive nucleation and growth in addition the Langmuir-type process and the instantaneous nucleation and growth when looking at the formation of a full Cu-(1x1) monolayer from a clean Au(111) surface. Whilst the kinetics for the first deposition stage had not been defined, Hoelzle et al.[53] did not find any of the current maxima characteristic for nucleation and growth processes, though the process could not be described by a simple adsorption process, either. It could be that one process is not sufficient as description due to the first Cu-UPD stage including both the random adsorption as well as the ordering in the honeycomb structure. However, an added second adsorption process for the formation of the full copper monolayer from clean Au(111) might also be a possibility instead of a second nucleation and growth process, and would be more in keeping with the findings of Hoelzle et al.[53] Garfias-Garcia et al.[55] furthermore found that the kinetics on polycrystalline gold were similar to Au(111), but slower and with a change in the contribution of each process.

Cyclic voltammetry

Fig. 1.17(a) shows a CV on a well-ordered Au(111) surface.[54] The two stages of the Cu-UPD translate to two pairs of well-defined, sharp peaks.[17,42,47,53,62] The first, higher potential pair of peaks has a broad shoulder at more positive potentials, corresponding to the random coadsorption before the phase transition, the first step of the Cu-UPD.[17,47,58,59] The second deposition peak splits in two on high quality surfaces, with the higher potential peak associated with nucleation at

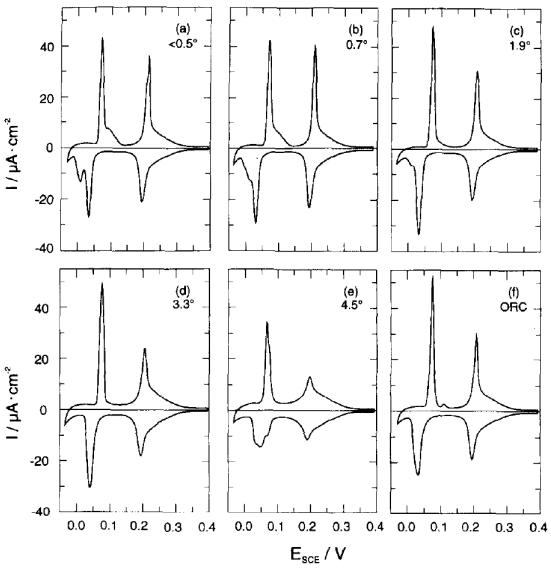

Figure 1.17.: CVs of the Cu-UPD on Au(111) in 0.05 M sulphuric acid 1 mM copper sulphate with a scan rate of 5 mV/s depending on the step density. The surface orientations for (a-e) are as given in the figures, (f) has a misscut<0.5° but was taken after five oxidation-reduction cycles up to 1.5 V_{SCE} with a scan rate of 50 mV/s. Reprinted from reference 54, Copyright 1995, with permission from Elsevier.

surface defects and the lower potential one with nucleation at (111) terraces.[42,54] In that case, the corresponding dissolution peak also gains a shoulder at more positive potentials corresponding to the lower potential deposition peak.[54] Furthermore, Fig. 1.17 shows that with higher step density or with the introduction of defects due to oxidation, the peak splitting is reduced or vanishes completely.[54] It also shows some effect of the step density on the first set of peaks. Also, Ataka et al.[52] found that for their Au(111) film electrode, the first set of peaks was broader and weaker, which they attributed to the island structure of the Au(111) film. As such, there is a strong dependence of the CV on the crystal surface, especially on the amount of defects due to the different nucleation processes on defects and terraces.[53,54]

The maximum peak current density shows a strong dependence on the scan rate ν, with a proportionality to ν for $\nu < 5\ mV/s$ and $\nu^{\frac{1}{2}}$ for $\nu > 5\ mV/s$.[17,42,53] This is due to slow desorption processes, which is also seen in the asymmetry of the CV.[17,42,53,57] The rather large asymmetry of the second peak pair comes from the strong stabilization of the $(\sqrt{3} \times \sqrt{3})$R30° structure due to the coadsorption

and ensuing interaction between copper and sulphate.[37] Therefore, a rather large overpotential is required for the removal of the sulphate.[37]
Due to the strong dependence of the Cu-UPD process on the anion, the electrolyte composition has a strong influence on the resulting CV. For example, the pH[54] as well as contaminations,[17,46,48,63] especially traces of more strongly adsorbing anions like chloride, affect the characteristics of the CV. Fig. 1.18 and 1.19 show the effect of different concentrations of halides on the CV of Au(111) in sulphuric acid. As for example chloride can change the structure of the adlayer and is more strongly bound to copper than sulphate, and thus can replace sulphate even if only a trace amount of chloride is in the electrolyte, the peaks which depend on the structure of the adlayer would change.[46,49]

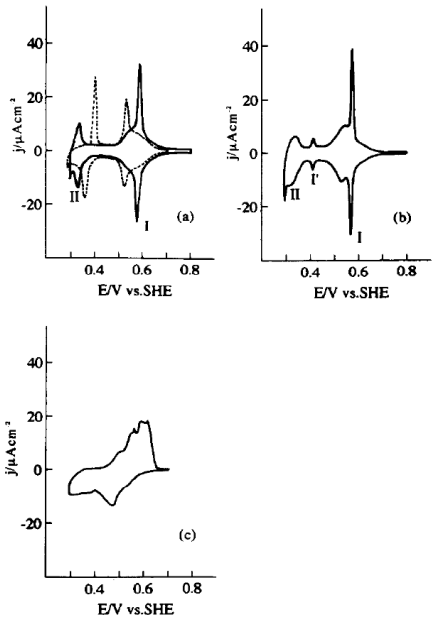

Figure 1.18.: CVs of the Cu-UPD on Au(111) in 0.05 M sulphuric acid 1 mM copper sulphate with a scan rate of 5 mV/s depending on added halides. (a) dashed: no addition, solid: +0.1 mM potassium chloride, (b) +0.1 mM potassium bromide, (c) +0.1 mM potassium iodide. Reprinted from reference 63, Copyright 1994, with permission from Elsevier.

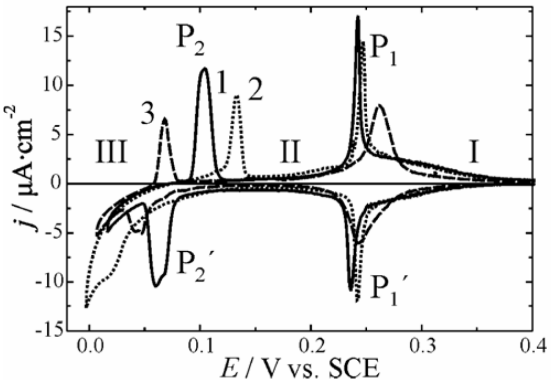

Figure 1.19.: CVs of the Cu-UPD on Au(111) in 0.05 M sulphuric acid 1 mM copper sulphate with a scan rate of 1 mV/s depending on the chloride concentration (solid: 0 M, dotted: $5 \cdot 10^{-6}$ M, dashed: $5 \cdot 10^{-5}$ M). Reprinted by permission from Springer Nature Customer Service Centre GmbH: Springer Nature Journal of Chemical Sciences reference 48, copyright 2009.

Since the sulphate has a strong influence on the Cu-UPD, it would be interesting to know the influence of the electrolyte concentration on the CV. While to the best of our knowledge no systematic study of the effect of the concentration on the CV has been published, comparison between different works can still give information about the concentration dependence. Tab. 1.1 shows the electrolyte, the pH as well as the peak separation for the deposition and dissolution peaks for several works. It has been shown by Frittmann et al.[57] that there is a dependence on the pH of the electrolyte, therefore this has to be accounted for as well when comparing different electrolyte composition. Furthermore, the ionic strength of the electrolyte has to be considered in addition to the sulphate concentration.
Shi et al.[40,41] and Zhang et al.[43] both work at low sulphate concentrations, but the use of perchloric acid as an inert electrolyte by Shi et al.[40,41] results in an ionic strength comparable to using 0.1 M sulphuric acid. While the difference in the scan rates ν has to also be considered, the values at different scan rates from this work show a maximum error of around 10 mV. For similar ionic strength and similar pH, there is a small difference in the peak separation, while the features of the CV stay similar, as also found by Zhang et al.[43] Comparing the CVs at different pH by Frittmann et al.,[57] there is a hysteresis of the second set of peaks with increasing pH, which changes the values of the peak separation for deposition

Table 1.1.: Comparison of the peak separation in the CVs with different electrolyte concentrations at room temperature.

Reference	Electrolyte	Peak separation deposition	Peak separation dissolution	ν in mV/s	pH
Shi et al.[40]	0.1 M $HClO_4$, 1 mM K_2SO_4, 5 mM $Cu(ClO_4)_2$	160 mV	120 mV	5	1
Shi et al.[41]	0.1 M $HClO_4$, 5 mM K_2SO_4, 1 mM $Cu(ClO_4)_2$	160 mV	120 mV	5	1
Hoelzle et al.[53]	0.05 M H_2SO_4, 1 mM $CuSO_4$	165 mV	135 mV	1	1.3
Zhang et al.[43]	0.1 mM H_2SO_4, 1 mM $CuSO_4$	120 mV	100 mV	2	4
Frittmann et al.[57]	0.1 M H_2SO_4, 10 mM $CuSO_4$	240 mV	160 mV	50	1
Frittmann et al.[57]	0.1 M K_2SO_4, 1 mM H_2SO_4 10 mM $CuSO_4$	260 mV	130 mV	50	4
This work	0.1 M H_2SO_4, 1 mM $CuSO_4$	180 mV	144 mV	5	1
This work	0.1 M H_2SO_4, 1 mM $CuSO_4$	192 mV	148 mV	50	1

and dissolution. The average peak separation however is very similar at both pH 1 and 4. The lower peak separation Zhang et al.[43] found is thus more likely due to the much lower ionic strength compared to the other works. For the copper concentration, Shi et al.[40,41] little difference in their CVs, though it was also coupled with a change in the sulphate concentration.

Altogether, it seems the sulphate concentration in the range presented in Tab. 1.1 does not influence the CV strongly, while both the pH and the ionic strength have stronger influence. However, since the comparison is between different works, it is only a very rough estimate, as there is a strong dependence of the CV on the used surface, as shown earlier. Since different works use different electrodes, the surface thus also affects the CV, which means the conclusions from this comparison are not as reliable as a systematic study using only one electrode.

Chronoamperometry

Chronoamperometry can be used to obtain the kinetics of a reaction at a certain potential by stepping the potential from a starting potential to the end potential. The obtained current transients depend on the processes that take place due to the potential step, so the choice of start and end potential influences the obtained information.

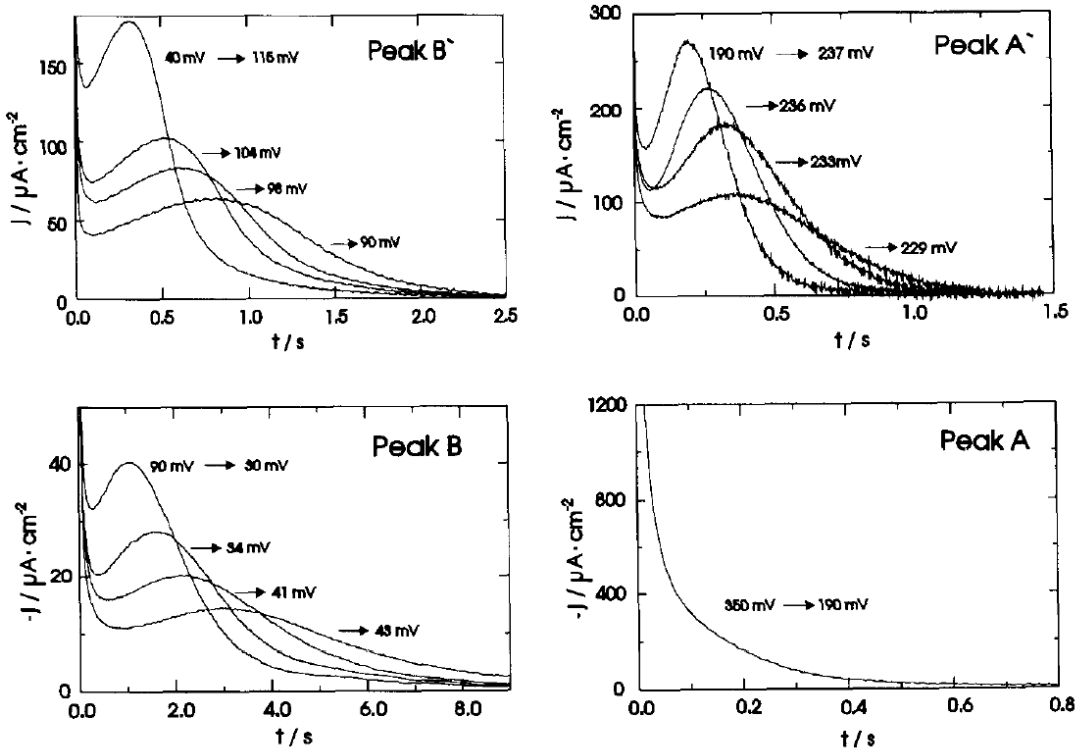

Figure 1.20.: Transients of Au(111) in 0.05 M sulphuric acid 1 mM copper sulphate for the first (A, A') and second (B, B') stage of the Cu-UPD with the potential steps (E vs SCE) indicated in the figures. Reprinted from reference 53, Copyright 1994, with permission from Elsevier.

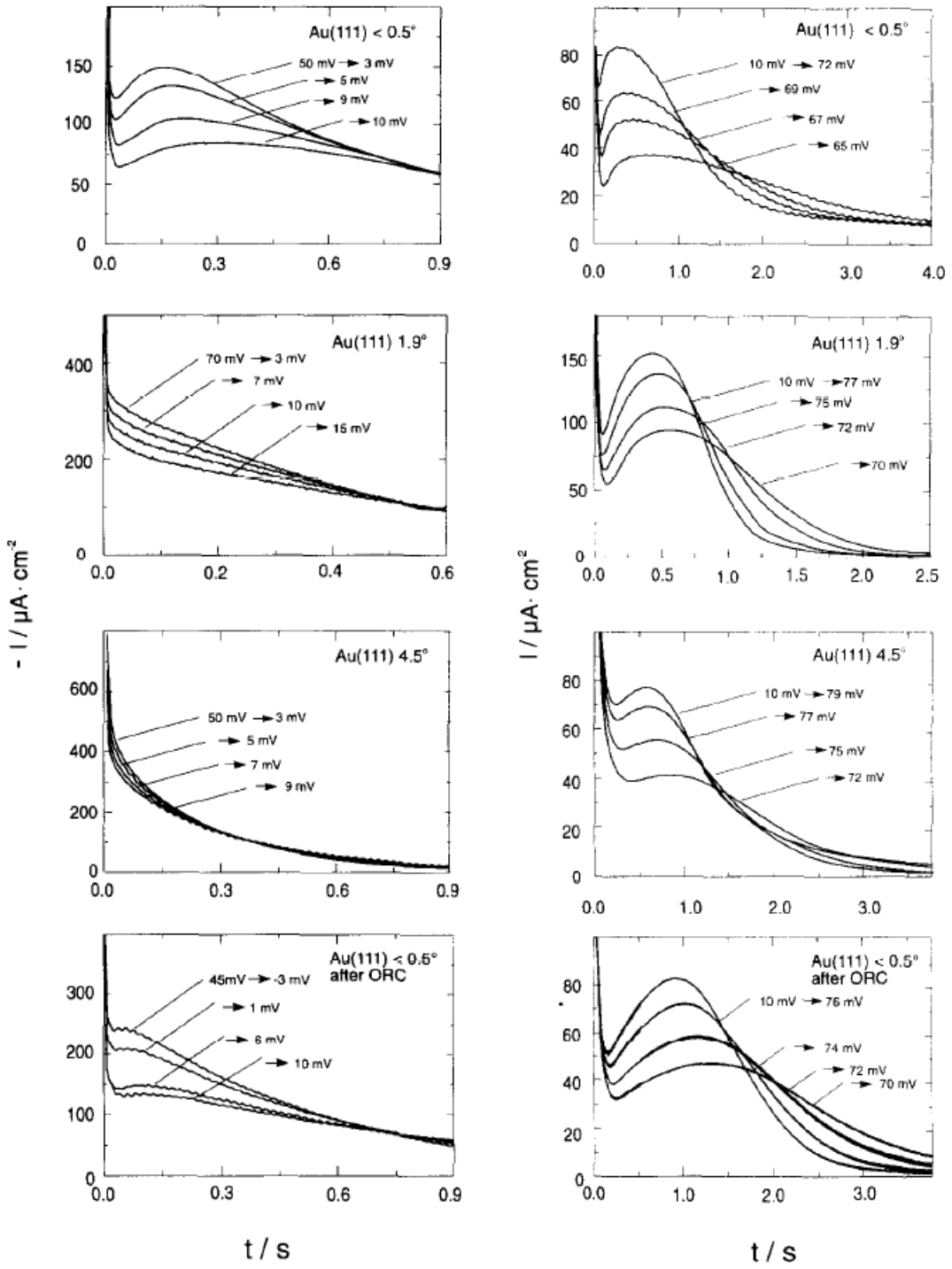

Figure 1.21.: Transients of Au(111) in 0.05 M sulphuric acid 1 mM copper sulphate at different surface defects for the deposition (B,left) and dissolution (B',right) of the second stage of the Cu-UPD with the potential steps (E vs SCE) indicated in the figures. The surfaces have different step densities expressed through the surface orientation or have been modified by oxidation-reduction cycles (ORC). Reprinted from reference 54, Copyright 1995, with permission from Elsevier.

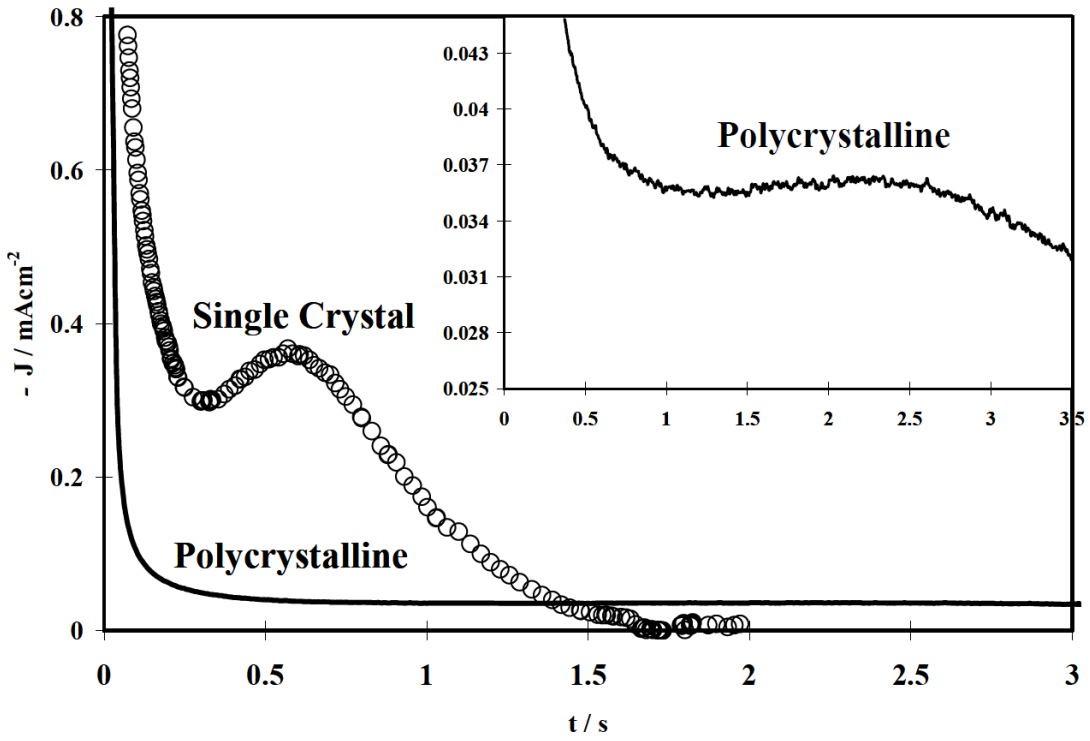

Figure 1.22.: Transients of the whole Cu-UPD process on Au(111) and polycrystalline gold in 0.1 M sulphuric acid 10 mM copper sulphate. Potential step:-50 mV_{SSE} to -445 mV_{SSE}. Republished with permission of Electrochemical Society, from reference 55; permission conveyed through Copyright Clearance Center, Inc..

In Fig. 1.20, the deposition and dissolution of the first and second stage of the Cu-UPD are investigated separately, showing the distinctive shape of each stage. The current peak for B,B' and A' is an indication of a nucleation and growth process.[53] The implications for the kinetics has been discussed previously. Fig. 1.21 shows the dependence of the form of the transients for the second Cu-UPD stage on the amount of surface defects. It has been shown that the surface defects have a strong effect on the shape of the transient, and especially on the nucleation and growth process.[53,54] For an Au(111) single crystal, the whole Cu-UPD process still shows a current peak as seen in Fig. 1.22. Similar to the studies done by Hoelzle et al.,[53,54] the work of Garfias-Garcia et al.[55] shows that the current peak is greatly reduced on polycrystalline gold.

1.4.3. Au(111) in perchloric acid

Perchlorate is one of the most weakly adsorbing anions on Au(111).[37,64–67] While it is often considered non-specifically adsorbing or inert,[20,32,36] other studies show it to actually be weakly specifically adsorbing.[37,68–70] Evidence of the specific adsorption was found using ECQM and SEIRAS, while no evidence was found in STM.[37,68] However, there is no evidence of an ordered perchlorate structure in the double-layer region and mobile anions cannot be seen with STM, which could explain the lack of evidence using that method.[37] Other studies have found evidence that the supposed evidence of specific adsorption of perchlorate may be due to the specific adsorption of trace chloride.[71] Thus, the debate on the specific adsorption of perchlorate is not fully settled.
Nevertheless, due to its much weaker adsorption compared to sulphate, perchlorate influences the electrochemical processes less than sulphate.[67] This makes it useful for comparison with sulphate to see the influence of the adsorbed anions on the processes. However the inherent trace amounts of chloride contained within perchlorate as well as the possible decomposition into chloride can make it somewhat problematic to work with, leading to fewer studies. Although to my knowledge no systematic study of the effect of the temperature in the double-layer region has been published, Hamelin et al.[69] showed that the CVs of perchloric acid are dependent on the temperature. Also, higher temperatures showed no increase in surface defects after oxidation due to the increased effect of electrochemical annealing, while the slower electrochemical annealing at low temperatures leads to an increase of the surface defects which is visible in cyclic voltammetry.[72] Electrochemical annealing refers to the surface quality being restored after the introduction of defects due to specifically adsorbing anions enhancing the mobility of the gold surface atoms.[21,72] The effect of the annealing increases with the strength of the gold-anion interaction.[21] Furthermore, higher temperatures lead to a higher onset potential of the hydrogen evolution reaction (HER).[72]
Fig. 1.23 is an example CV from the literature for illustration. In the CV, there should be one anodic and one cathodic peak for a well-ordered Au(111) surface, though higher surface defects lead to a low potential shoulder and less intensity in the peaks (see Fig. 1.23).[72] These peaks should be due to perchlorate adsorption/desorption coupled with the surface reconstruction lifting/formation.[67,68,72]

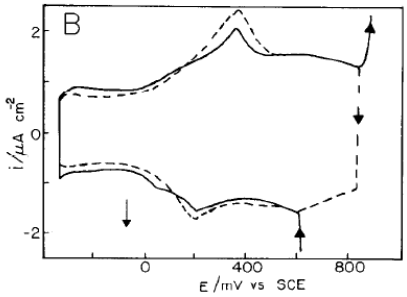

Figure 1.23.: CVs in the double-layer region on Au(111) at 5 mV/s in 0.1 M perchloric acid at 1°C. Solid line after 6 cycles at 50 mV/s between -0.3 V_{SCE} and 1.4 V_{SCE}, the surface has an increased defect density due to going into the oxidation region. Dashed line after 6 cycles at 50 mV/s between -0.3 V_{SCE} and 0.8 V_{SCE}. Reprinted from reference 72, Copyright 1991, with permission from Elsevier.

Below 10 V/s, the peaks are asymmetric due to the coupling with the surface reconstruction and the peak position is also dependent on the scan rate.[65,67,72] The adsorption/desorption process itself is rather fast, with a standard heterogeneous rate constant $k_s^\circ = 23 \pm 11 \cdot 10^3 s^{-1}$, with a slow surface reconstruction and reconstruction lifting leading to the kinetic limitation.[65,67] For 0.1 M perchloric acid and 10 mV/s, the anodic peak would be at 445 $mV_{Ag/AgCl}$ while the cathodic peak would be at 325 $mV_{Ag/AgCl}$.[67] The reconstruction lifting peak is less intense and shifted positive compared to sulphuric acid due to the weaker adsorbability of perchlorate.[28] Since the reconstruction lifting is due to the adsorbed anions, more weakly adsorbing anions lead to a a larger potential range where the reconstruction is stable. Due to the rather large size of the adsorbed hydrated perchlorate, the perchlorate coverage is rather low.[67] The saturation coverage was found to be close to 0.25 using ECQM[37] or around 0.15 by integrating the CVs[68] or from SEIRAS.[67]

1.4.4. Cu-UPD on Au(111) in perchloric acid

Few publications about the Cu-UPD on Au(111) in perchloric acid are available, with all experiments done at room temperature. The discussion of whether perchlorate is weakly specifically adsorbing or not also applies to the Cu-UPD in perchloric acid, where the discussion similarly is not settled completely. Fur-

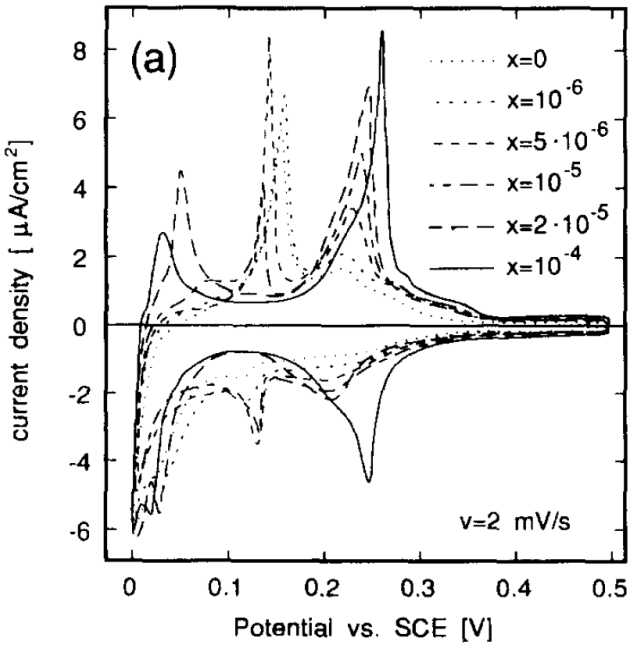

Figure 1.24.: CVs of the Cu-UPD on Au(111) in 0.1 M perchloric acid 10 mM copper perchlorate with x M hydrochloric acid added and a scan rate of 2 mV/s. Reprinted from reference 74, Copyright 1995, with permission from Elsevier.

thermore, chloride has a strong affinity to copper,[46] as well as being strongly specifically adsorbing, which means traces of chloride have a strong influence on the Cu-UPD on Au(111) in perchloric acid.[73,74] Traces of chloride found even in the purest commercially available perchloric acid, while copper also catalyses the reduction of perchlorate to chloride, though the decomposition still has a time scale of weeks.[74] However, this means that there will always be traces of chloride in the electrolyte while investigating the Cu-UPD in perchloric acid, which has to be taken into account in the interpretation of any results.

Both Krznaric et al.[73] and Hotlos et al.[74] have investigated the effect of chloride on the Cu-UPD in perchloric acid on Au(111) and both found a strong influence of even traces of chloride on the system. This is seen in Fig. 1.24, as the peaks change with the chloride concentration and the CV for 10^{-4} M chloride is the same as for pure hydrochloric acid.[74] Hotlos et al.[74] found two structures at different potential ranges using STM which also showed a dependence on the chloride concentration. One was a commensurate quasi-hexagonal (2×2) superstructure

with a likely copper coverage of 0.75 ML, which was found at lower potentials and lower chloride concentrations.[74] The other was a "(5×5)" incommensurate hexagonal layer with a copper coverage of 0.64 ML, stable at higher potentials than the (2×2) structure at low chloride concentrations or over the full range at higher chloride concentrations.[74]
For both structures, a dependence on chloride was found which indicated that both adlayers incorporated copper and chloride, but especially the "(5×5)" structure.[74] A possible disordered, metastable adlayer was additionally found in the potential range of the "(5×5)" structure at very low chloride concentrations.[74] However, the STM measurements by Hotlos et al.[74] were done without the exclusion of oxygen, which could affect the found structure.
Hotlos et al.[74] also observed a growth of small irregular protrusions at potentials below 0.1 V_{SCE} in all chloride-containing electrolytes, which disappear if the potential is raised above that value. They indicated surface alloying of gold and copper as a possible source, though no further investigation into the phenomenon or its origin was presented.[74]
Zei et al.[75] used ex-situ LEED, reflection high-energy electron diffraction (RHEED) and Auger electron spectroscopy (AES) to investigate the structures of the Cu-UPD on Au(111) in perchloric acid. However, it has to be remembered that due to the loss of the environment, the structures found in ex-situ methods can be rearranged and thus different from the in-situ structure. A (2.2×2.2) incommensurate superstructure was found at lower emersion potential, while a commensurate $(\sqrt{3} \times 2)$ structure was found at higher emersion potentials, though the later is debatable, since it was also found without copper, but not in a reproducible fashion.[75] The (2.2×2.2) structure likely correspond to the (2×2) structure found by Hotlos et al.[74] There are several considerations: for one, due to the distortion of the STM images used by Hotlos et al.,[74] it is possible the slight diversion might not have been found. On the other hand, if the surface alloys as indicated as a possibility by Hotlos et al.,[74] the surface alloy could change the lattice constant, with a wrongly assumed lattice constant changing the structures seen via LEED and RHEED. As such, while there is a difference between the structures, they could be consistent within the constraint of the measurement methods and assumption. Of course, as said previously, ex-situ structures are less reliable due to the change in the environment possibly influencing the structure.

The $(\sqrt{3} \times 2)$ structure could be an ordered structure at low chloride concentrations in the potential range above the (2×2) structure, comparable to the "(5×5)" structure at higher chloride concentrations. However, due to the ex-situ nature of the method as well it being found sometimes even without copper, the disordered adlayer found by Hotlos et al.[74] at low chloride concentrations seems more reliable.

For the composition of the adlayer Zei et al.[75] found peaks due to copper, chlorine and oxygen using AES. They attributed this to a coadsorption of copper and perchlorate.[75] However, from the work of Hubbard et al.,[76] both chloride and perchlorate show the same chlorine peak, only differing in whether or not an oxygen peak is present. It is known that perchlorate solutions always contain chloride, which is more strongly adsorbing than perchlorate. As such, while the work of Zei et al.[75] does show coadsorption between copper and at least one anion, summarily attributing the coadsorption to perchlorate might be incorrect. Considering the strong influence of chloride on the Cu-UPD in perchloric acid shown by Krznaric et al.[73] and Hotlos et al.,[74] it is likely that there is at least partly chloride coadsorption. However, the oxygen in the AES found by Zei et al.[75] would support the assertion of Krznaric et al.[73] that the adlayers consist of copper, chloride and perchlorate.

For the CV, Hotlos et al.[74] attributed the peaks around 0.24 V_{SCE} (see Fig. 1.24)to the formation/dissolution of the "(5×5)" structure and the peaks around 0.14 V_{SCE} to the transition to and from the (2×2) structure, with the other peaks being due to increased chloride. Krznaric et al.[73] found a difference in the potential dependence of the anodic peaks around 0.24 V_{SCE}, which indicated that there are two different peaks in that potential range depending on the chloride concentration and which were due to two different structures. They agreed with the assignment of the "(5×5)" structure to the peak at chloride concentrations above 7 µM chloride, but postulated another unspecified structure for the lower chloride concentrations.[73] Additionally, they found that at the same chloride concentration, the anodic peak seen around 50 mV_{SCE} in Fig. 1.24 appears while the peak found at 0.14 V_{SCE} disappears.[73] Therefore, there seem to be four different anodic peaks in perchloric acid, two of which appear at low chloride concentrations and two at high chloride concentrations. While Hotlos et al.[74] found the "(5×5)" structure at lower chloride concentrations in the STM measurements, the potential

in the STM is modified by the tip, which especially influences species with low concentration. The tip-induced effects could lead to a higher local concentration of chloride, which would make the effective chloride concentration in the measurements unknown. Thus, while the STM measurement found the "(5×5)" structure at low total chloride concentrations, the relevant local concentration might have been higher and thus falsified the chloride concentrations at which the structure appears. Additionally, as previously mentioned, they did find a disordered adlayer in the "(5×5)" range, which could be the structure for the peaks around 0.24 V_{SCE} at the low chloride concentrations.
However, the experiments of Hotlos et al.[74] have been done in 0.1 M perchloric acid with pH 1, while Krznaric et al.[73] worked in electrolyte with 2 mM perchloric acid (pH 2.7) and 10 mM perchloric acid (pH 2), with sodium perchlorate at different concentrations as a supporting electrolyte. While the effect of the pH on the Cu-UPD in perchloric acid has to our best knowledge not been investigated, and thus there is no way to establish the influence of the pH, the difference in the electrolytes has to be considered. For the influence of the perchlorate concentration or the ionic strength, some measurements had been done by Krznaric et al.,[73] with the increase of the concentration of sodium perchlorate shifting chloride concentration at which the appearing anodic peaks change towards a higher chloride concentration. Therefore, the perchlorate seems to stabilize the structures found at low chloride concentrations and it was postulated by Krznaric et al.[73] that these adlayer structures are composed of copper, chloride and perchlorate.
While the CV also contains the cathodic copper deposition peaks, they tend to be rather broad due to the strong kinetic hindrance of the Cu-UPD in perchloric acid.[73,74] Due to the strong influence of the chloride concentration on the CVs and structures, Hotlos et al.[74] claimed that the rate-determining step for the Cu-UPD is the slow diffusion of chloride to the interface, which would be responsible for the kinetic hindrance. They also postulate an island-growth mechanism for the different adlayer structures from the in-situ STM.[74]
Uchida et al.[37] also investigated the Cu-UPD in perchloric acid on Au(111) with ECQM, however the published CV (Fig. 1.25) shows strong signs of a heightened chloride concentration. It has been previously shown that chloride has a strong influence on the Cu-UPD in perchloric acid, and thus its effects have to be considered, especially with a heightened chloride concentration. However, any

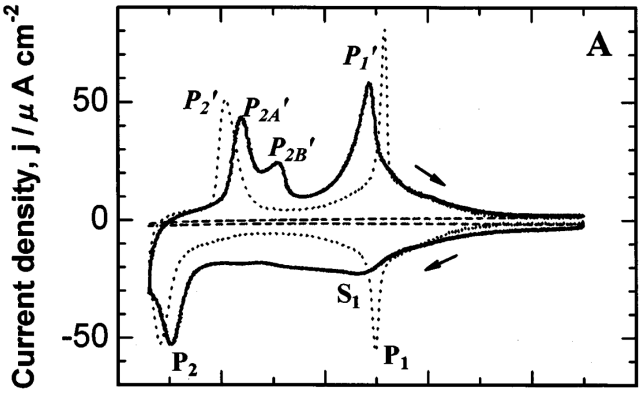

Figure 1.25.: CVs on Au(111) in 0.1 M perchloric acid (dashed line), 0.1 M perchloric acid 5 mM copper perchlorate (solid line) and 0.05 M sulphuric acid 5 mM copper sulphate (dotted line) with a scan rate of 10 mV/s. Reprinted from reference 37, Copyright 1998, with permission from Elsevier.

contribution of chloride was neglected in the analysis of Uchida et al.,[37] and thus the results were deemed to not be reliable. Manne et al.[77] also investigated using AFM, though they show the structure left by the dissolution of the bulk copper, not the UPD. Furthermore, the choice of potential step by Manne et al.[77] is questionable, as the potential is stepped positive enough that the honeycomb phase in sulphate is presented as the full monolayer in that electrolyte. Thus, the work of Manne et al.[77] was also disregarded.

2. Methodology

Fig. 2.1 shows the setup used for the experiments. An Isotemp 5150 R28 (Fisher Scientific) with distilled water as the heat transfer fluid and a temperature precision of ±5°C was used as the thermostat. It has a reservoir of 8 l, where the fluid is brought to the specified temperature. Using tubing to connect the cell and the thermostat, the fluid is circulated. A special cell was used with the thermostat which had a mantle with inlets to allow for circulation of a heat transfer fluid and heat transfer to the enclosed electrolyte. Given enough time, the electrolyte in the cell can be assumed to be at the temperature set for the heat transfer fluid, though there is no way to measure the temperature at the electrode surface. A time of at least 15 minutes after the heat transfer fluid reached the specified temperature was used for the equilibration time in the experiments.
The hanging meniscus configuration was used for contacting the working electrode with the electrolyte. A rod-shaped crystal holder was used to hold the working electrode to increase stability. The working electrode was an Au(111) single crystal (Mateck, misscut<0.05°, diameter 10 mm) was used as the working electrode with

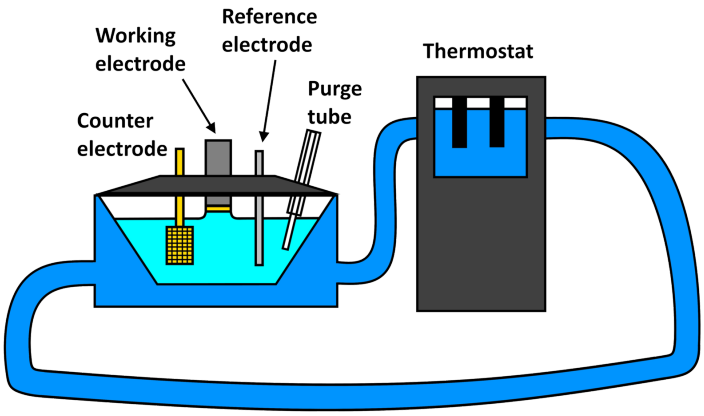

Figure 2.1.: Schematical representation of the experimental setup

a gold mesh counter electrode and an Ag/AgCl 3.4 M KCl reference electrode. Since chloride is a very strongly specifically adsorbing anion, even trace levels of chloride have a strong effect on the electrochemistry of Au(111) in an electrolyte with any weaker adsorbing anion. Both perchlorate and sulphate have weaker specific adsorption than chloride. Thus, to eliminate chloride contamination from the reference electrode, it was kept in a bridge tube filled with the copper-free electrolyte used in the main experiment. The single crystal was flame-annealed in a butane flame for at least 5 minutes and cooled in normal atmosphere for the surface preparation. The procedure was done two times to ensure a consistent surface before the crystal was transferred into the cell. The electrolyte was purged with nitrogen (BOC) prior to the experiment and kept under a nitrogen atmosphere during the experiment to eliminate dissolved oxygen. For the perchloric acid experiments, the influence of oxygen was found to be stronger than in sulphuric acid. When purging the electrolyte and filling the cell with a nitrogen atmosphere, the CV still showed oxygen. To further eliminate oxygen, a glove bag was used. For that, the single crystal was transferred into the cell, but not brought into contact with the electrolyte, and the setup prepared before the bag was closed. The glove bag was then filled with nitrogen and the electrolyte purged for at least an hour in the nitrogen atmosphere before the start of the experiments. The working electrode was put into contact with the electrolyte at the open circuit potential (OCP). An Ivium Compactstat.e was used to conduct the experiments. For the metal deposition, the single crystal was cycled in metal-free electrolyte after the experiments to remove any leftover deposited metal from the surface.
As the temperature influences the potential of the reference electrode, a temperature correction had to be applied to the potential. The used correction is

$$E = E_e - (0.73 \cdot (T - 25)) \tag{2.1}$$

with E_e being the experimentally applied potential, T the temperature in °C and all potentials in mV.[78]
Analytical grade perchloric acid (70%, Aldrich, 99.999% trace metal basis), copper(II) perchlorate hexahydrate (Aldrich, 98%), sulphuric acid (95-98%, Aldrich, 99.999% trace metal basis), copper(II) sulphate pentahydrate (Aldrich, 99.999% trace metal basis) and milli-Q water were used to prepare the electrolytes. The

prepared solutions were 0.1 M perchloric and sulphuric acid as well as 0.05 M copper sulphate or copper perchlorate in 0.1 M sulphuric or perchloric acid. For the Cu-UPD experiments, 50 ml of the base electrolyte and 1 ml of the copper solution were pipetted in the cell as electrolyte. Before use, the cells as well as any equipment in contact with the electrolyte were acid cleaned in a 1:1 mixture of concentrated sulphuric and nitric acid and then rinsed and boiled in milli-Q water to remove contaminations.

2.1. Au(111) in sulphuric acid

For the measurements in 0.1 M sulphuric acid, CVs of an Au(111) single crystal surface at temperatures of 10°C, 20°C, 30°C, 40°C and 50°C were recorded at scan rates of 50 mV/s,20 mV/s, 10 mV/s and 5 mV/s. The single crystal surface was freshly prepared for each temperature. A set of measurement consisted of CVs in the range of -0.2 V to 0.9 V (uncorrected), with the potential being held for 90 s at -0.1 V (uncorrected) before each CV. The starting potential was the lower potential limit. The crystal was contacted at OCP. The scan rates were in order 10 mV/s, 50 mV/s, 20 mV/s, 10 mV/s and 5 mV/s. The first 10 mV/s measurement changed the surface from the thermal reconstruction to the potential-induced reconstruction and was cycled until the change with cycling was negligible, reaching an equilibrium surface state. It was also used to compare against the second 10 mV/s measurement to check if the surface was changing with prolonged cycling. The other measurements had three cycles each.
A longer holding time would increase the quality of the single crystal surface. However, since the used electrolyte is water-based, elevated temperatures gave a noticeable increase in electrolyte evaporation. Thus, the associated drop in electrolyte levels could lead to a smaller meniscus or even to the loss of the meniscus during the measurement. Additionally, small bubbles were also formed in the electrolyte at high temperatures, and the likelihood of any bubbles influencing the meniscus increased with the measurement time. As such, an increased equilibration time was not used in these measurements since the necessary time increase would have been impractical, as the holding time was constant for all temperatures to ensure they are comparable. The current density at 50°C had

to be scaled by a factor of 0.4 for the temperature comparison as all CVs at that temperature have an increased current at all potentials compared to other temperatures. Due to experimental difficulties, the measurements for 50°C could not be repeated. Generally, for potentials below 0.3 V, the current response at all temperatures was nearly identical, except for 50°C, which indicates it is unlikely to be a temperature effect. It is more likely that the contact area of the single crystal with the electrolyte was larger than for the other temperatures, as the current density is dependent on that contact area. It is assumed that the contact area is the surface of the single crystal, although surface defects introduce an unknown roughness factor. The single crystal surface showed no change when compared under the same conditions, so the roughness factor should stay constant. This means that all presented measurements are internally consistent, eliminating this factor from the reasons of the increased current response. Therefore, the increased contact area should likely come from a broader meniscus. That introduces a chance that the sides of the single crystal had been wetted, which would introduce an additional polycrystalline area that would influence the measurement.
After the measurements, the potential was corrected for the temperature dependence of the reference electrode using Eq. 2.1.

2.2. Cu-UPD on Au(111) in sulphuric acid

In 0.1 M sulphuric acid 1 mM copper sulphate, the CVs of Au(111) were recorded at 10°C, 20°C, 25°C, 30°C, 35°C, 40°C, 45°C, 50°C and 55°C for scan rates of 50 mV/s, 20 mV/s, 10 mV/s and 5 mV/s in that order. The potential range for the CVs was 0 V to 0.5 V (uncorrected) for 10°C and 20°C, with the lower potential limit increasing to 0.01 V (uncorrected) for 25°C, 0.02 V (uncorrected) for 30°C, 0.03 V (uncorrected) for 35°C and 40°C and 0.04 V (uncorrected) for 45°C, 50°C and 55°C. This was due to an earlier onset of the bulk deposition necessitating the limitation of the lower potential limit. The crystal was contacted at OCP. Each measurement consisted of three cycles. The crystal was freshly prepared for each temperature.
For the chronoamperometric transients, the crystal was contacted at OCP and a CV with 3 cycles at 5 mV/s in the potential range for that temperature taken

before and after measuring the transients. The starting potential for the transients was 0.5 V (uncorrected). After each lower potential, the reverse potential jump was executed. The end potential for each transient is indicated in the data. Again, the single crystal was prepared for each temperature, with the investigated temperatures being 10°C, 20°C, 30°C, 40°C and 50°C. The transients for the different peaks in the CV were investigated at 20°C, with the CVs taken before and after measuring the transients. The potential sequence was 0.5 V, 0.11 V, 0.07 V, 0.5 V, 0.11 V, 0.035 V, 0.075 V, 0.1 V, 0.075 V, 0.13 V, 0.075 V, 0.2 V, 0.25 V, 0.075 V, 0.2 V, 0.3 V (all uncorrected), with 40 s at each potential. The potential step back to 0.5 V (uncorrected) for the cathodic and 0.075 V (uncorrected) for the anodic transients was to ensure comparable starting surfaces for the transients of each peak.
The correction for the temperature dependence of the reference electrode potential (Eq. 2.1) was applied after the measurements, and not considered for the choice of the starting and end potentials of the chronoamperometric transients. Thus, these transients were not taken for the same starting and end potential for each temperature.

2.3. Au(111) in perchloric acid

The measurements in 0.1 M perchloric acid were done similarly to Ch. 2.1 at 10°C, 20°C, 30°C, 40°C and 50°C with scan rates of 50 mV/s,20 mV/s, 10 mV/s and 5 mV/s each. The single crystal surface was freshly prepared for each temperature and the glove bag purged and filled each time to eliminate oxygen as described previously. Each measurement set consisted of CVs in the range of -0.3 V to 0.75 V (uncorrected). The crystal was contacted at OCP and the starting potential was the lower limit. The scan rate order was the same as for 0.1 M sulphuric acid due to the same reasons, with the same amount of cycles. The measured potential was afterwards corrected for the temperature dependence of the reference electrode using Eq. 2.1.

2.4. Cu-UPD on Au(111) in perchloric acid

The measurements of the CVs in 0.1 M perchloric acid 1 mM copper perchlorate were done similarly to the cyclic voltammetry without copper, from 0.7 V(uncorrected) to the lower potential limit, which varied with the temperature. The CV was started at 0.7 V(uncorrected), to investigate the deposition. The lower limit was -0.1 V(uncorrected) at 10°C, and 0 V for the other temperatures. The electrolyte was freshly mixed from two stock solutions for each day of experiment, with 50 ml of 0.1 M perchloric acid and 1 ml of 0.1 M perchloric acid 0.05 M copper perchlorate. Although the decomposition of perchlorate to chlorate, even with the catalysation from the copper, takes several weeks for a noticeable increase of the chloride concentration,[74] this would help reduce a possibly increased chloride concentration of the electrolyte due to the copper solution.
The chronoamperometry for that electrolyte encompassed two experiments: the stepwise investigation of the deposition kinetics and coverage as well as the investigation of the surface change in the deposition range. For the former, the starting potential was 0.6 V, and it was stepped to the end potential for at least 1 minute, before being stepped back to the starting potential for the next transient. The end potential was in the range of 0 V-0.3 V in 50 mV steps. This was done for each temperature. For the later, the change in the transients for the jump 180 mV→600 mV with t=60 s were investigated for 10°C and 50°C by first holding the potential at 180 mV before the jump to obtain a baseline and then holding at potentials lower than 180 mV for either 60 s or 120 s, before holding at 180 mV for 60 s and then measuring the transient.
The potentials were corrected for the temperature dependence of the reference electrode (Eq. 2.1). For the chronoamperometry, this correction was considered while choosing the starting and end potentials, so that the same potentials were used for all temperatures.

3. Au(111) in 0.1 M sulphuric acid

Since the temperature may well affect processes on the single crystal electrode besides the metal deposition, it was considered necessary to first establish the effect of the temperature in metal-free electrolyte.

3.1. Experimental results

For the investigation in the temperature dependence, CVs have been recorded at different scan rates and different temperatures (see Ch. 2.1). Due to the scan rate incorporating a time component, the different scan rates can influence the shape of the CV depending on the speed of the processes in that potential range. Thus, the combination of the scan rate dependence and temperature dependence can be used to gain additional information on the processes. As the temperature dependence and scan rate dependence can influence each other, the analysis of the results will incorporate both dependences.
Fig. 3.1 shows CVs of the Au(111) single crystal in sulphuric acid with the peaks labelled for ease of referencing. SAD1 to SAD3 and SDD1 as well as SDD2 are each overlapping peaks which sometimes express as shoulders depending on the maximum current density relative to each other, which heightens the error in estimating the peak position.
Fig. 3.2 shows the CVs at different scan rates for each temperature, with the current density j multiplied by the ratio of 50 mV/s to the used scan rate. This scaling was done to make the peaks at lower scan rate more visible due to the different maximum current densities at different scan rates. The measured current density comes from the faradaic current induced by electrochemical processes and a double-layer charging current.[5] The double-layer charging current is proportional to the scan rate, while the faradaic current increases with increased scan rate due to induced concentration gradients.[5] The scaling in Fig. 3.2 does not accurately

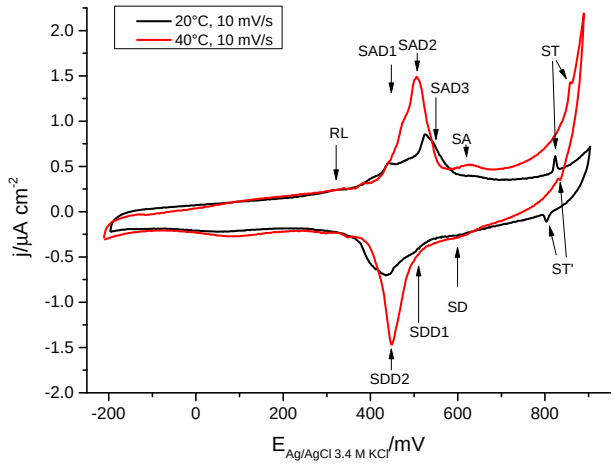

Figure 3.1.: CVs of the Au(111) single crystal in 0.1 M sulphuric acid at 20°C and 40°C for 10 mV/s with labelling for peaks

portray the relative peak heights, but allows for easier comparison of the peak forms and positions.

The same CVs are shown in Fig. 3.3 at different temperatures for each scan rate for easier visualization of the temperature dependence. The current density at 50°C has been scaled as it is uniformly higher than at the other temperatures. As the current density is dependent on the surface area of the crystal in contact with the electrolyte, the higher current density might be due to an increased area compared to the CVs of the other temperatures. Further discussion of both the reason for this as well as possible consequences will be in the later section for the discussion of the results. Fig. 3.4 and 3.5 as well as 3.6 and 3.7 show the peak positions of the different peaks depending on the scan rate and temperature, respectively.

SAD1 (Fig. 3.4a and 3.6a) shows a very slight increase in the peak potential with increasing scan rate, except for 30°C. It also shows a generally increasing trend with increasing temperature, though there is some scattering. Since SAD1 is mostly expressed as a shoulder, except at 50°C (Fig. 3.2e), this does affect the accuracy of the determination of the peak position. For 30°C (Fig. 3.2c), the shoulder is very faint, which is likely the reason for the exception in the scan rate dependence. For the temperature dependence, the scattering along the general

trend could also be due to the inaccuracy from the overlap. Also, due to the increase in potential with the scan rate being only around 5 mV, it is uncertain whether the effect is due to an actual scan rate dependence or due to better peak separation at lower scan rates. Furthermore, at 5 mV/s (Fig. 3.3d) SAD1 is seen only weakly expressed below 40°C, where it shows as a slightly stronger shoulder, while it is a distinguishable peak at 50°C. At higher scan rates, SAD1 is slightly weaker expressed and less distinguishable.

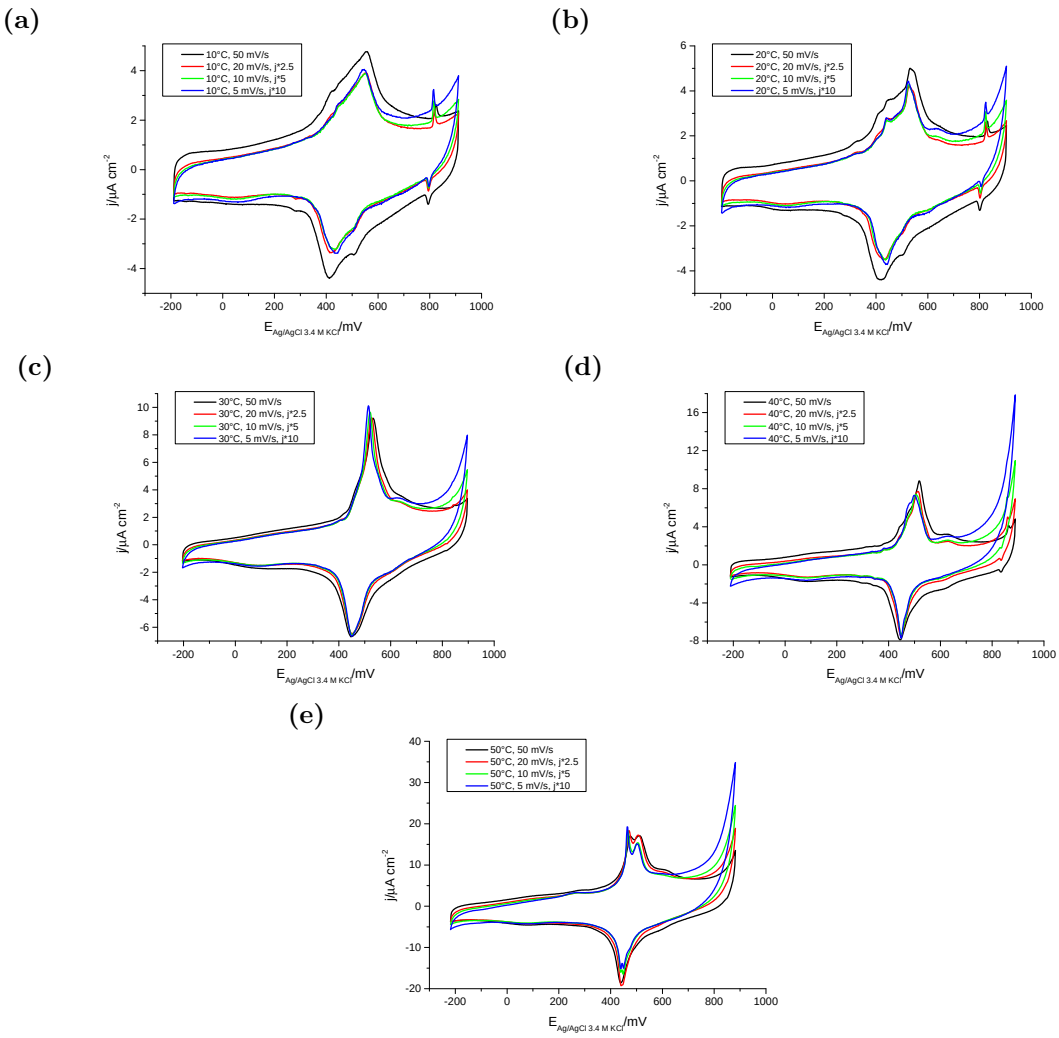

Figure 3.2.: CVs of Au(111) in 0.1 M sulphuric acid at scan rates of 50 mV/s, 20 mV/s, 10 mV/s and 5 mV/s for (a) 10°C, (b) 20°C, (c) 30°C, (d) 40°C and (e) 50°C. The CVs for 20 mV/s, 10 mV/s and 5 mV/s have the current density j scaled for convenience by a factor of 2.5, 5 and 10, respectively.

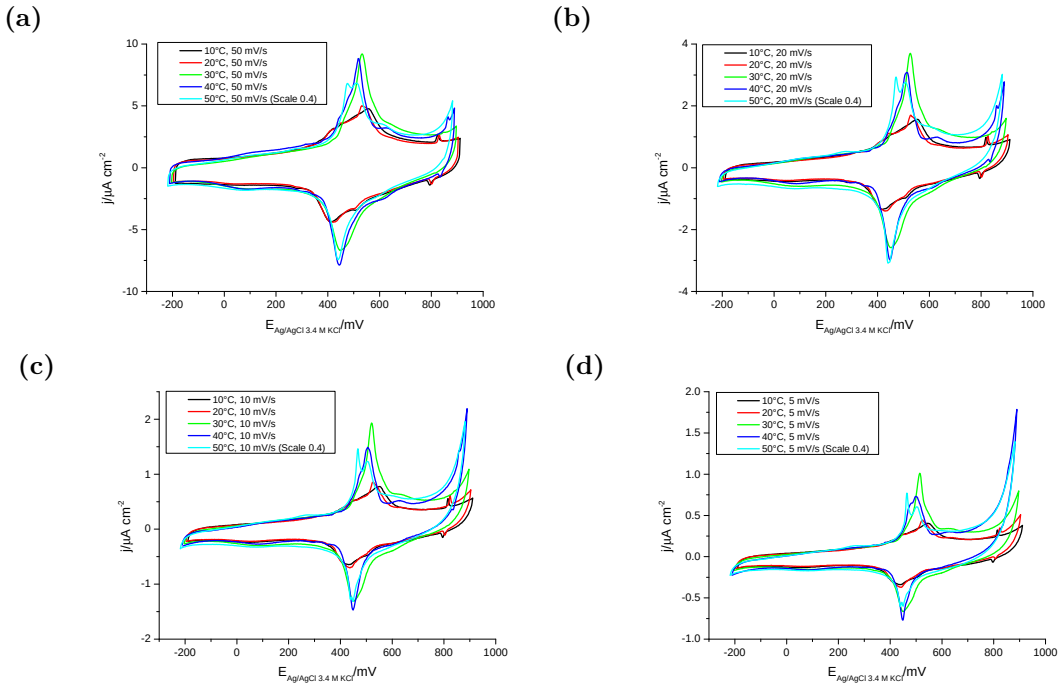

Figure 3.3.: CVs of Au(111) in 0.1 M sulphuric acid at 10°C, 20°C, 30°C, 40°C and 50°C for (a) 50 mV/s, (b) 20 mV/s, (c) 10 mV/s and (d) 5 mV/s. The current density of the 50°C CVs are scaled by a factor of 0.4 for easier comparison.

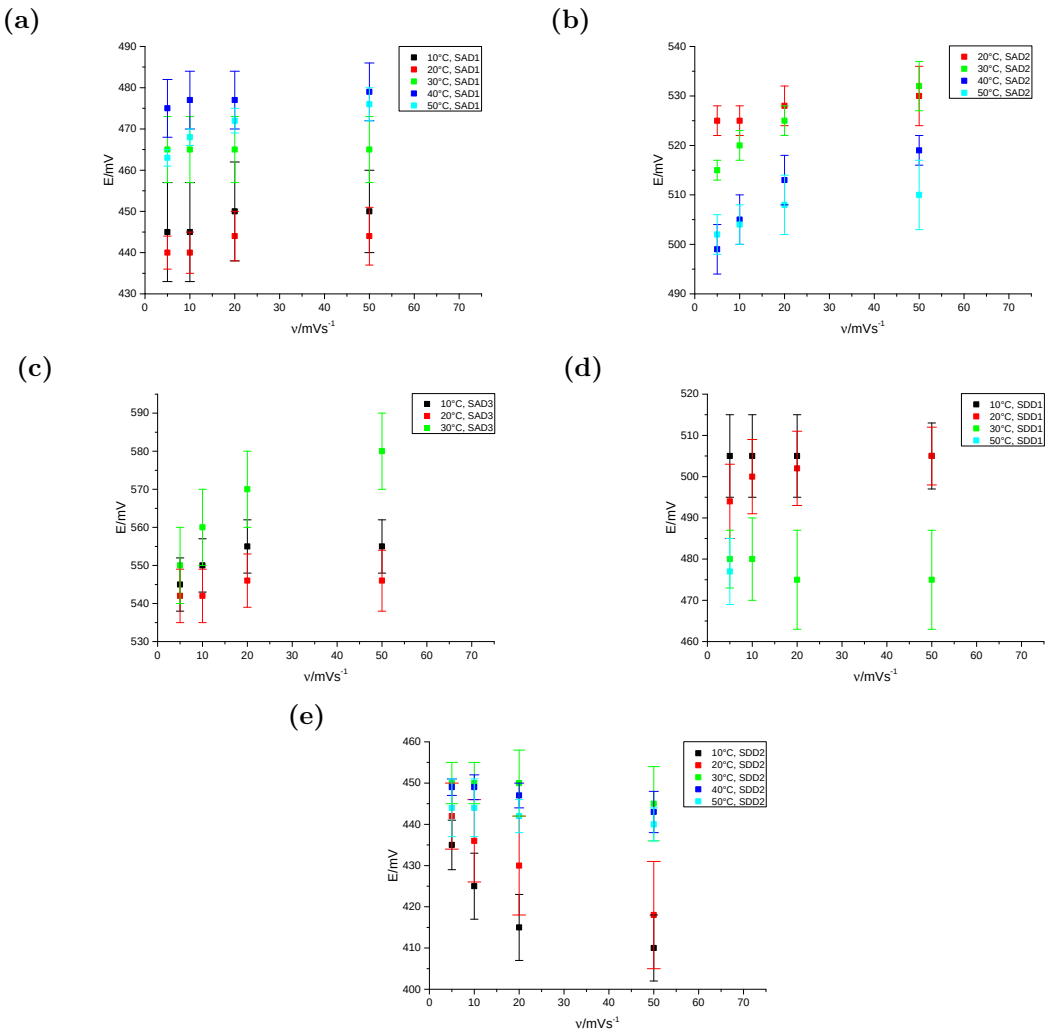

Figure 3.4.: Change of the peak positions with the scan rate ν at different temperatures for (a) SAD1, (b) SAD2, (c) SAD3, (d) SDD1 and (e) SDD2.

All in all, while SAD1 shows little change in the peak potential with the scan rate, it is slightly weaker with increasing scan rate. With increasing temperature, the peak potential also increases, while the peak is also more strongly expressed at high temperatures.

SAD2 (Fig. 3.4b and 3.6b) shows an increasing potential with the scan rate, with the peak not apparent at 10°C and only slight changes with the scan rate at 20°C. The peak potential decreases with increasing temperature. Also, the peak height increases with the temperature up to 30°C, at which point the trend changes to decreasing.

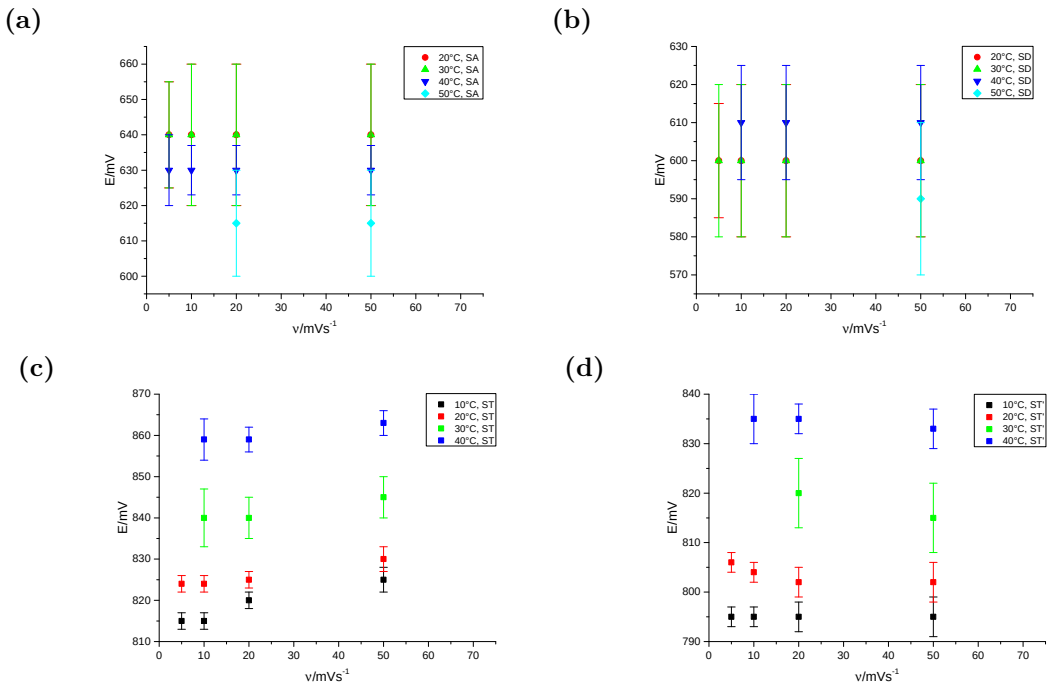

Figure 3.5.: Change of the peak positions with the scan rate ν at different temperatures for (a) SA, (b) SD, (c) ST and (d) ST'.

SAD3 (Fig. 3.4c and 3.6c) is only visible at low temperatures, as the main peak at 10°C and then as a shoulder for 20°C and 30°C. It has an increasing peak potential with increasing scan rate, with the amount of change varying for each temperature. However, due to being a faint shoulder with strong overlap at 20°C and 30°C, the peak potentials for these temperatures might have been affected by the overlap. Due to these factors as well as only having three temperature, the trend for the temperatures is hard to determine.

SDD1 is a weak shoulder at all temperatures, though it is slightly stronger expressed at low scan rates. Most temperatures do not show much change in the peak potential with the scan rate, which coupled with the overlap makes it likely that there is no or only a very weak scan rate dependence (Fig. 3.4d). It does show a decreasing peak potential with increasing temperature (Fig. 3.6d) .

SDD2 (Fig. 3.4e and 3.6e) shows a strongly decreasing peak potential with increasing scan rates under 30°C, with only a slight decrease afterwards. At the same time, there is a strong increase in the peak height from 20°C to 30°C, as well as the peak being sharper at temperatures above 20°C (Fig. 3.3).

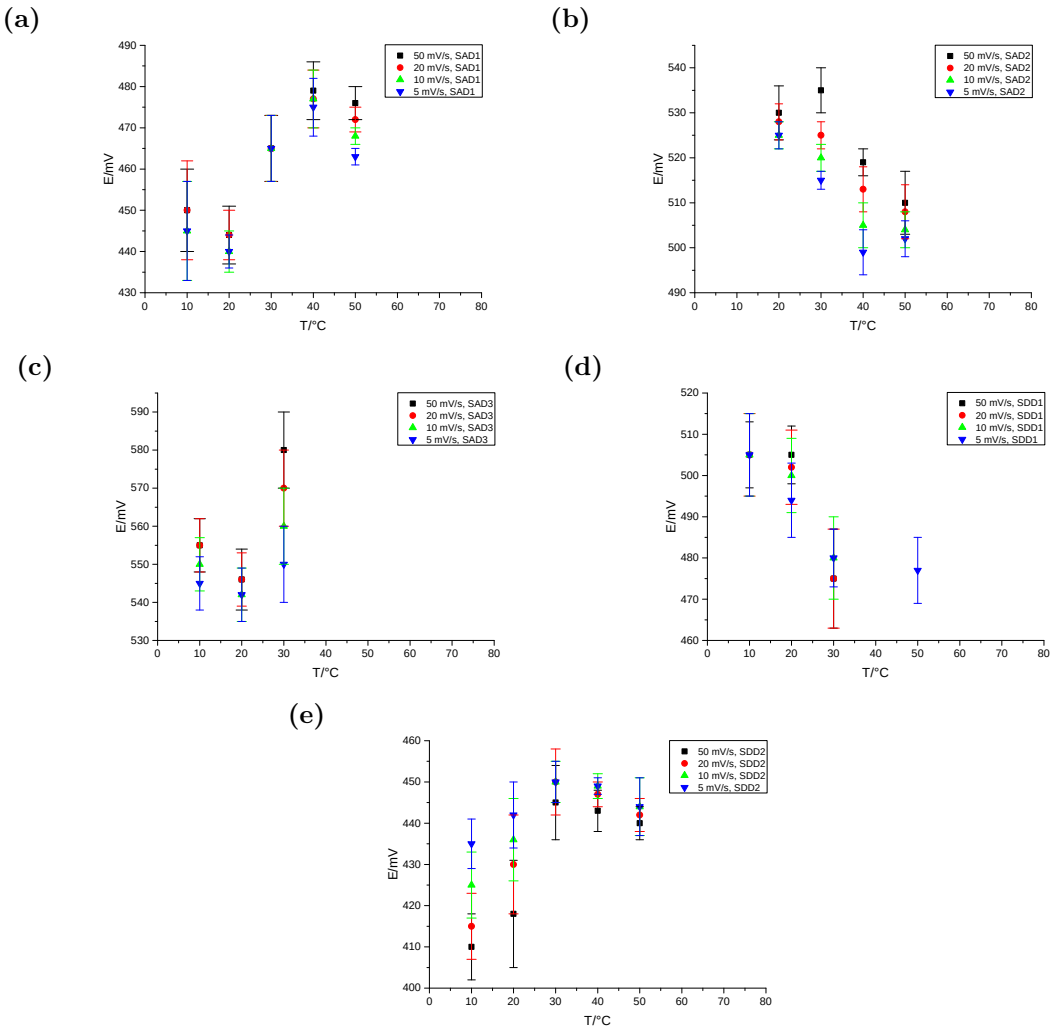

Figure 3.6.: Change of the peak positions with the temperature at different scan rates for (a) SAD1, (b) SAD2, (c) SAD3, (d) SDD1 and (e) SDD2.

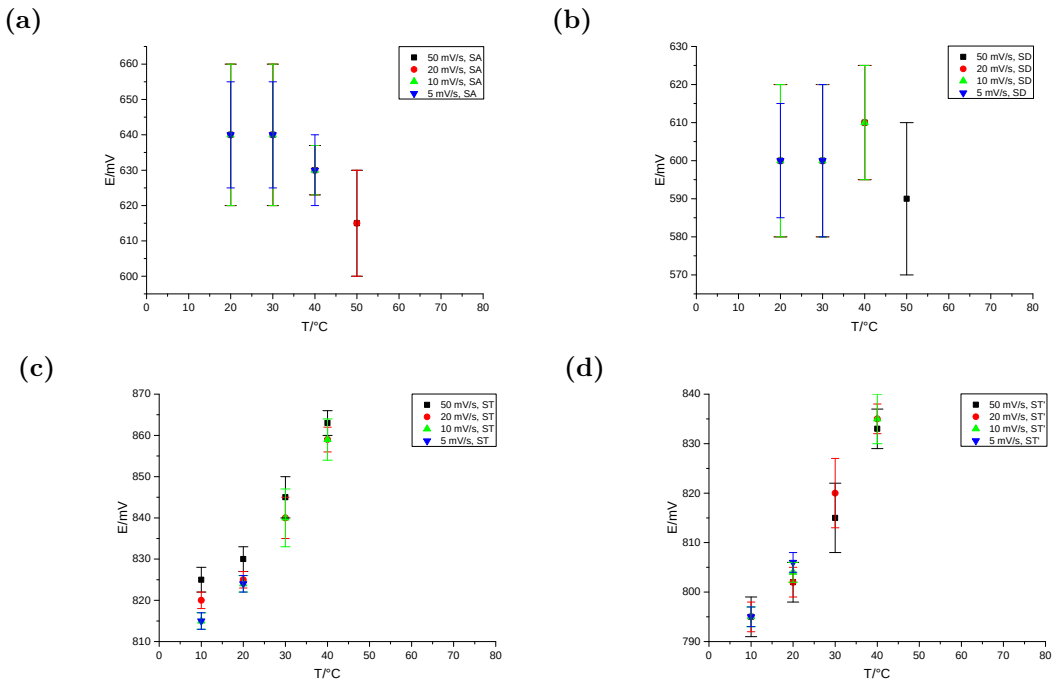

Figure 3.7.: Change of the peak positions with the temperature at different scan rates for (a) SA, (b) SD, (c) ST and (d) ST'.

For the temperature dependence of SDD2, there is a strong increase of the peak potential with the temperature up to 30°C, while the trend changes to a slight decrease at the other temperatures. However, the change is comparatively low, around 5 mV between 30°C and 50°C. Also, for 5 mV/s and 10 mV/s at 50°C (Fig. 3.2e), SDD2 is split into two peaks with a very small peak separation. Furthermore, at 10°C and 20°C, there might be a slight shoulder at lower potentials. Possibly, there are two peaks with very strong overlap which cannot be visually separated in most of the CVs.

The peak potential of SA (Fig. 3.5a and 3.7a) shows no change with the scan rate, while there is a decrease with increasing temperatures above 30°C. It is a weakly expressed, broad peak (Fig. 3.2 and 3.3), which is not visible at some temperatures and scan rates. For SD (Fig. 3.5b and 3.7b), the peak potential does not change with the scan rate but does fluctuate with the temperature. However, like SA, it is a weakly expressed broad peak, and furthermore this part of the CV has a convex shape at higher temperatures, where the peak potential changes. It is possible that the overlap between the broad peak and the convex baseline of

the CV influenced the peak position.
ST and ST' are a small, sharp pair of peaks (see Fig. 3.1). ST (Fig. 3.5c and 3.7c) shows a slight increase of the peak potential with increasing scan rate, mostly at 10°C, and a strong increase with increasing temperature. ST' (Fig. 3.5d and 3.7d) shows little change with increasing scan rate, though some temperatures show a decreasing peak potential, while the temperature dependence is the same as for ST. For 30°C and above, ST and ST' are not visible at the lower scan rates, while they are not visible at all for 50°C (Fig. 3.3). Those higher temperatures also have a strong rising current at the upper potential limit for the positive going part of the CV, while the negative going part due to this has a strong falling current in that area. As ST and ST' should be in or near that area, due to their low height it is possible that they were masked by this current change.

3.2. Discussion

As Au(111) in sulphuric acid is a well-studied system, existing literature can be used to interpret the CVs.

3.2.1. Reconstruction lifting

A sharp peak for the lifting of the gold surface reconstruction would be expected from the literature, though the potential would depend on the type of reconstruction.[29,33] The thermal reconstruction from the flame-annealing would be expected at 380 mV, while the potential-induced reconstruction would be shifted negatively to around 320 mV.[29,33] As the potential-induced reconstruction is less well-ordered than the thermal reconstruction, this results in the reconstruction lifting peak being smaller and shifted towards more negative potentials.[29,33] Since in this work the single crystal was contacted with the electrolyte at the OCP, it would also show the potential-induced reconstruction.
The very small peak at 325 mV in Fig. 3.1 designated RL has been shown to become more pronounced if the potential was held around -100 mV for 10 minutes instead of the 90 s used in the data shown in this chapter. As the surface reconstruction is a slow process, the measurement time in the potential region of the reconstruction can be too low for the reconstruction to fully form. Therefore,

holding in the potential range of the reconstruction increases the time available for the reconstruction to proceed and thus increases the reconstructed surface area. An increase in the peak with increasing holding time thus points towards it being due to the reconstruction lifting, as the charge of the reconstruction lifting depends on the reconstructed surface area. However, experimental considerations made longer holding in the reconstruction potential range impractical. Considering this peak is at the expected potential as well as showing the expected behaviour, it is very likely to be the reconstruction lifting peak.
As the charge of RL is very low in the CVs, not much of the surface of the crystal was reconstructed during the CVs. Considering the literature, more reconstruction would have been expected. However, as RL increased with increased holding time, it seems that the reconstruction process was only slower than expected. The reconstruction lifting peak has also been found to be affected by surface defects.[29,33] An increased surface defect density leads to RL being smaller and at more negative potential, as mentioned previously.[29,33] Thus, the low charge of RL might be due to a higher than expected surface defect density. An increase in surface defects would also explain the slower reconstruction, as surface defects can inhibit the reconstruction. This is due to the reconstruction being formed to relieve surface stress, which is also relieved around surface defects, and thus the driving force of the reconstruction is reduced.[22–24,26,27]

3.2.2. ST/ST'

The current spike ST represents the transition of the unordered adsorbed sulphate to the ordered $(\sqrt{3} \times \sqrt{7})$ sulphate adlayer, while ST' is the reverse transition from the ordered to the disordered adlayer, both of which are characteristic to the Au(111) surface.[29,33] Like the reconstruction lifting, ST/ST' have been found to be affected by surface defects.[29,33] An increased step density has been shown to lead to a decrease in the charge density as well as a slight decrease in the peak potential of ST and ST'.[29] The small size of ST/ST' could thus be another indicator of a higher surface defect density.
According to Dretschkow et al.,[29] and as explained in Sec. 1.4.1, the ordering is a nucleation and 2D surface diffusion-controlled growth process on terraces, which has a fast adsorption of a small amount of sulphate prior to it. As previously

mentioned, the decrease of the peak potential of an anodic peak with decreasing scan rate is due to the process being slow compared to the scan rate. ST shows this mentioned scan rate dependence, which is also more pronounced at 10°C (see Fig. 3.2 and Fig. 3.5c). Since the process is surface diffusion-controlled, meaning the limiting factor is the speed of the surface diffusion, this scan rate dependence should be due to diffusion limitation at higher scan rates. The more pronounced scan rate dependence at 10°C is also expected, as decreasing the temperature also decreases the kinetic energy of the anions in the system. With a decrease in the kinetic energy of the anions, the mobility of the anions also decreases. Therefore, the surface diffusion would be slower, thus increasing the effect of the scan rate.However, there is a limit to this diffusion limitation, as once the speed of the diffusion is high enough, a further increase of the mobility will not affect the scan rate dependence.

Due to this diffusion-control, one would expect a decreasing potential with increasing temperature, yet the actual temperature dependence is the opposite. If this is compared to the reverse process ST', there is nearly no scan rate dependence, with only 20°C showing a very slight increasing peak potential with decreasing scan rate (see Fig. 3.2 and Fig. 3.5d). Considering the shape in the baseline current density at that temperature depending on the scan rate, and the fact that that there is not much of a scan rate dependence at the other temperatures, it might also be an overlap effect. If it is an actual effect of the scan rate, it does fit with the trend for cathodic peaks with diffusion limitation, though it would be unclear why the other temperatures aren't affected. However, a clear temperature dependence of ST' is shown, which matches the one shown by ST(see Fig. 3.3, Fig. 3.7c and Fig. 3.7d).

This means that with increasing temperature, the potential range of stability of the ordered sulphate structure shifts towards higher potentials. Dretschkow et al.[29] had found a decreasing peak potential for the sulphate order↔disorder transition spikes with increasing surface defect density, while also finding an increase in the rate of nucleation. However, this decreasing peak potential was also connected to a strongly decreasing charge density of the process due to the decrease of the size of the ordered domains with increasing surface defect density.[29] Considering the connection between electrochemical annealing, the temperature and the surface defect density, it could be possible that a lower surface defect density at higher

temperatures would lead to the potential shift, but that is likely not the case. While the trend would fit a decreasing surface defect density, ST and ST' do not show an increasing charge density with increasing temperature. However, it is still possible that the potential shift is due to a decreasing rate of nucleation with increasing temperature, but further experiments, for example chronoamperometric measurements, would be needed to verify this.
More likely this is due to the potential range of stability of the ordered structure. An inhibition of the formation of the ordered phase due to the decreasing degree of order with increasing temperature had already been reported by Jerkiewicz et al. [13] for Pt(111) in sulphuric acid. With increasing temperature, the kinetic energy and thus the mobility of the adsorbed sulphate increases. An increase in the mobility of the adsorbed sulphate would make a mobile adlayer energetically favourable. The formation of an ordered adlayer involves the immobilization of the adspecies, which would require more energy for more mobile adspecies. Thus, an increase in the mobility of the adspecies increases the activation barrier for the formation of the ordered adlayer. The formation of the ordered $(\sqrt{3} \times \sqrt{7})$ sulphate adlayer is due to the more positive charge at the electrode surface with increasing potential. As the positive charge is attractive for the anions, the ordered adlayer is formed so the surface coverage of sulphate can be increased. If the activation barrier for the ordered adlayer formation is increased, then a more positive surface charge would be required and thus a higher potential. Therefore, the increase in the peak potential of ST/ST' with increasing temperature is likely due to the increased stability of the mobile sulphate adlayer with increased temperature.

3.2.3. SA,SAD1 to SAD3

Unordered adsorption/desorption of sulphate on the Au(111) crystal would be expected as a set of broad peaks with no hysteresis between 0.2-0.7 V according to the literature. [29,32,33,36,39] SA is a broad peak in the expected potential range and thus should be due to the unordered sulphate adsorption (see Fig. 3.1). However, the peaks SAD1 to SAD3 are also in the range expected for the unordered sulphate adsorption and could also be related to it. Due to the possible increased surface defect density, there is the possibility that SAD1 to SAD3 are adsorption on different type of surface defects, while SA represents the adsorption on the

terraces. However, the available information on the exact surface state of the single crystal as well as of the effects of all types of defects on the shape of the CV is insufficient to be certain that this is the case.
SAD1 to SAD3 show changes with the temperatures and scan rate (see Fig. 3.2, Fig. 3.3, Fig. 3.4 and Fig. 3.6). While a systematic trend might be possible, the sensitivity of cyclic voltammetry to the quality of the surface structure as well as the number of defects make it hard to establish. As the crystal surface was freshly prepared for each temperature, small differences in the surface structure are possible. The overlap of the peaks would also obscure trends.
Furthermore, it is possible that the crystal surface and thus also the number and type of defects changed with temperature due to electrochemical annealing. Hamelin et al.[72] found for perchloric acid that the electrochemical annealing is faster at elevated temperatures, where certain types of defects then do not have the stability to affect the measurement. The specific type of defects were said to be monoatomic pits and terrace edges.[72] As electrochemical annealing also takes place in sulphuric acid, it is possible that the same temperature dependence for electrochemical annealing is also applicable for sulphuric acid.
For the 50°C CVs, further considerations have to be made. It was mentioned earlier that these CVs show an overall increased current density compared to other temperatures. While the maximum current density of the peaks does vary, the base current density, especially in the potential range under 300 mV. is very similar for all other temperatures. As explained before, the current density depends on the surface area of the single crystal electrode in contact with the electrolyte through the formed meniscus. This is assumed to be the surface area of the single crystal. Even if the area covered by the meniscus might be different, as long as the meniscus for each measurement covers approximately the same area, the results are comparable. Moreover, if the CVs show an increase of the current density for all potentials compared to other temperatures, the most likely explanation is that the area covered by the meniscus is larger. Then, the assumed surface area is too low, and the scale would be different.
However, if there is a much larger than usual area covered by the meniscus, then the most likely reason for this is that the sides of the single crystal are whetted. Since the sides of the crystal are not cut for a specific face, this would mean an area of polycrystalline gold has been included in the measurement, which in turn

means the surface used for 50°C is different than for the other temperatures.
An interesting change with the temperature for SAD1 to SAD3 is that above 20°C, the combined charge density for SAD1 to SAD3 seems to be higher than for the lower temperatures. As the charge density for the adsorption process should be proportional to the anion coverage, this would mean that if the assumption about SAD1 to SAD3 being sulphate adsorption is correct then more sulphate is adsorbed at elevated temperatures. However, the sulphate coverage at 30°C is likely not higher than the maximum sulphate coverage of the disordered sulphate layer in the literature. Due to the unknown baseline of the CV, calculating the sulphate coverage from the CV would not be reliable and thus the coverage was not extracted from the CVs. If SAD1 to SAD3 are adsorption of sulphate at defects, then the lower sulphate coverage at lower temperatures might be due to the surface state.

3.2.4. SD,SDD1 and SDD2

Peak SD (see Fig. 3.1) should be due to desorption of the unordered sulphate. It shows a similar form as well as similar scan rate dependence as SA, while being a cathodic peak shifted around 40 mV towards lower potential than SA (see Fig. 3.2, Fig. 3.5a and Fig. 3.5b). Therefore, it should be the reverse process to peak SA. Additionally, SDD1 and SDD2 (see Fig. 3.1) should be the reverse processes to SAD1 to SAD3, and thus due to unordered sulphate desorption. Considering that SDD1 and SDD2 are likely connected to SAD1 to SAD3, it is quite interesting that the shape of those desorption peaks at higher temperatures is slightly different from the adsorption peaks. This could indicate a difference in the adsorption and desorption processes, or perhaps the distribution of the location of the adsorbed sulphate changed after the disordering of the ordered sulphate layer. It would make sense for the majority of the adsorbed sulphate to be on the terraces after the order-disorder transition, as that is where the ordered adlayer structure is formed.
SDD2 has an increasing peak potential with decreasing scan rate, though the effect a lot weaker above 20°C (see Fig. 3.4e). It also has a general increase of the peak potential with increasing temperature (see Fig. 3.6e), though the higher temperature actually show a slight decrease in peak potential instead. This

would match with a kinetic limitation for a cathodic peak, with the temperature increasing the rate of the process, and thus leading to a less pronounced scan rate dependence at higher temperatures. SDD2 does sharpen with increasing temperature, which would further indicate that the speed of the process increases with increasing temperature. SDD1 on the other hand does not have a scan rate dependence but has the opposite temperature dependence of SDD2 (see Fig. 3.4d and Fig. 3.6d), with a decreasing peak potential with increasing temperature. This temperature dependence would indicate that the potential range of stability for the unordered sulphate adlayer increases with increasing temperature, although SDD2 should also be affected by it in that case. As the temperature dependence as well as the scan rate dependence for SDD2 (see Fig. 3.6e and Fig. 3.4e) changes around 30°C, it could be that it is both affected by a kinetic limitation as well as the changing range of stability. In this case, it is likely that the kinetic limitation dominates the temperature dependence at the lower temperatures for SDD2.

3.3. Summary

CVs of Au(111) in 0.1 M sulphuric acid at different scan rates and temperatures have been measured. The reconstruction and reconstruction lifting of the Au(111) surface could not be observed as the time scale for the measurements was insufficient due to an additional kinetic hindrance of the reconstruction on the single crystal.

An influence of the temperature could be observed. The potential range of stability of the ordered sulphate adlayer shifted to higher potentials with increasing temperature. This is likely due to the increased mobility of the adsorbed sulphate at higher temperatures. The increased mobility of the sulphate would make the mobile phase energetically more favourable, while the ordered phase would be less favourable. As such, the phase transition between the ordered and the mobile phase is shifted to higher potentials.

SA, SAD1 to SAD3 as well as SD, SDD1 and SDD3 are assumed to be connected to the unordered adsorption and desorption of sulphate, respectively. SAD1 to SAD3 as well as SDD1 and SDD2 show a difference in the total charge above 20°C compared to at or below 20°C. However, there is not enough information available to assign more specific processes to the peaks and thus confidently interpret the

temperature dependence.
All in all, the temperature appears to have an effect on the stability of the phases of the sulphate adlayer. It is also possible that a change in the surface state due to faster electrochemical annealing at higher temperatures is responsible for some of the temperature effects.

4. Copper underpotential deposition on Au(111) in 0.1 M sulphuric acid

The UPD of copper on Au(111) was investigated in regards of the temperature dependence through cyclic voltammetry and chronoamperometry to determine the kinetics as well as the copper coverage at different potentials.

4.1. Experimental results

As two different techniques were used to gather data, this section will be split into two, one dealing with the cyclic voltammetry and one dealing with the chronoamperometry, with the overall results being discussed later. The measurement conditions and protocols can be found in Ch. 2.2. For convenience, the peaks in the CV are labelled for easier reference in Fig. 4.1.

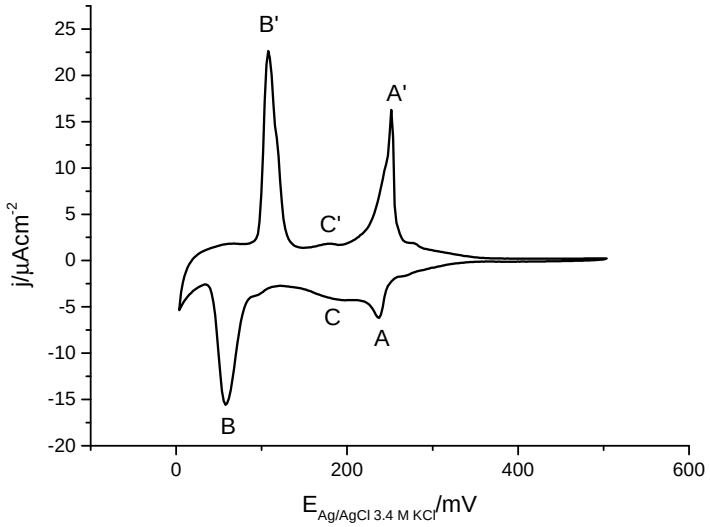

Figure 4.1.: CV of the Au(111) single crystal in 0.1 M sulphuric acid 1 mM copper sulphate at 20°C for 5 mV/s with labelling for the peaks.

4.1.1. Cyclic voltammetry

CVs at the different temperatures and different scan rates were taken to investigate the system. As stated in earlier chapters, both the scan rate and the temperature can influence the shape of the CV, and the two dependences as well as their dependence on each other can give more information than looking at only one dependence. The CVs were taken at 5°C intervals above 20°C to better establish the trend at higher temperatures. Fig. 4.2 and 4.3 show the CVs depending on the scan rate and the temperature, respectively. As before, the CVs are from the same dataset but presented differently to show the different dependences. For the scan rate, the current density was scaled for easier comparison, as already explained in Ch. 3. The peak position of peak A, A', B, B' and C' are shown against the scan rate and the temperature in Fig. 4.4 and 4.5, respectively. For peak C, the peak position couldn't be estimated accurately due to the broadness of the peak.

(a)

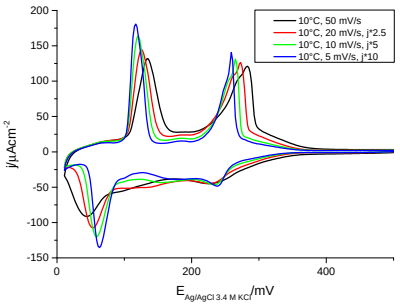
10°C, 50 mV/s
10°C, 20 mV/s, j*2.5
10°C, 10 mV/s, j*5
10°C, 5 mV/s, j*10
j/µAcm-2
E Ag/AgCl 3.4 M KCl/mV

(b)

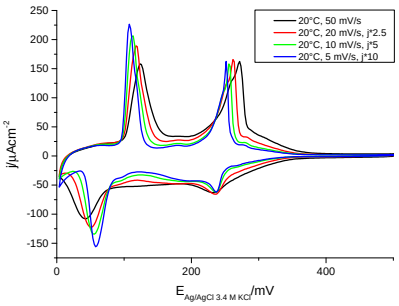
20°C, 50 mV/s
20°C, 20 mV/s, j*2.5
20°C, 10 mV/s, j*5
20°C, 5 mV/s, j*10
j/µAcm-2
E Ag/AgCl 3.4 M KCl/mV

(c)

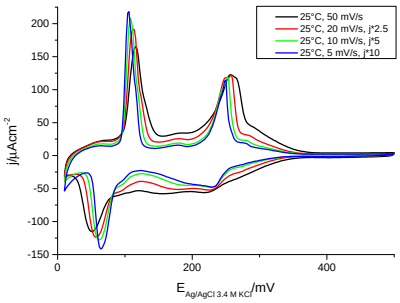
25°C, 50 mV/s
25°C, 20 mV/s, j*2.5
25°C, 10 mV/s, j*5
25°C, 5 mV/s, j*10
j/µAcm-2
E Ag/AgCl 3.4 M KCl/mV

(d)

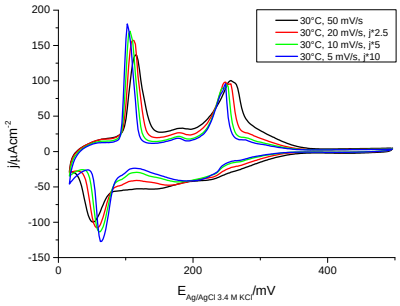
30°C, 50 mV/s
30°C, 20 mV/s, j*2.5
30°C, 10 mV/s, j*5
30°C, 5 mV/s, j*10
j/µAcm-2
E Ag/AgCl 3.4 M KCl/mV

(e)

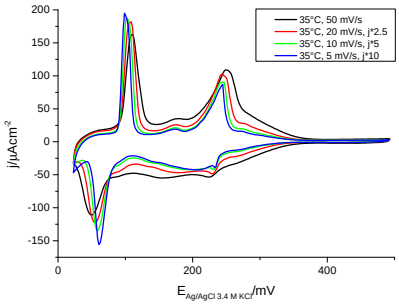
35°C, 50 mV/s
35°C, 20 mV/s, j*2.5
35°C, 10 mV/s, j*5
35°C, 5 mV/s, j*10
j/µAcm-2
E Ag/AgCl 3.4 M KCl/mV

(f)

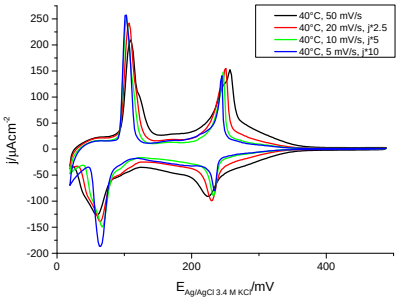
40°C, 50 mV/s
40°C, 20 mV/s, j*2.5
40°C, 10 mV/s, j*5
40°C, 5 mV/s, j*10
j/µAcm-2
E Ag/AgCl 3.4 M KCl/mV

(g)

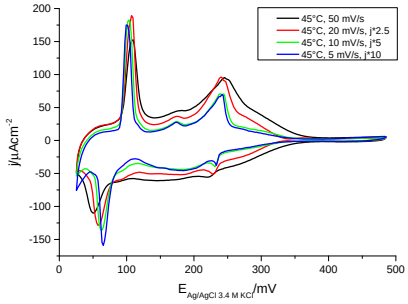
45°C, 50 mV/s
45°C, 20 mV/s, j*2.5
45°C, 10 mV/s, j*5
45°C, 5 mV/s, j*10
j/µAcm-2
E Ag/AgCl 3.4 M KCl/mV

(h)

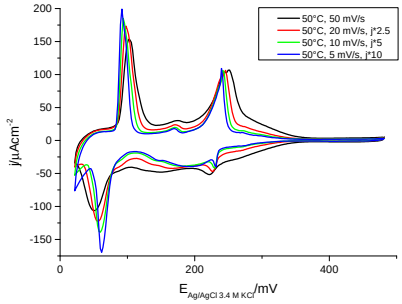
50°C, 50 mV/s
50°C, 20 mV/s, j*2.5
50°C, 10 mV/s, j*5
50°C, 5 mV/s, j*10
j/µAcm-2
E Ag/AgCl 3.4 M KCl/mV

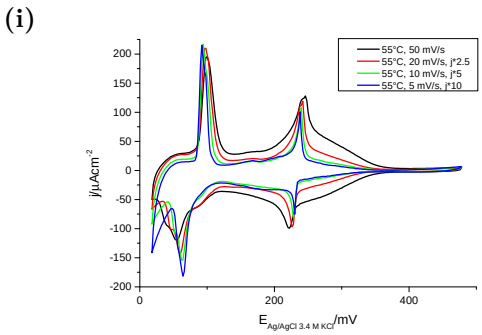

Figure 4.2.: CVs of Au(111) in 0.1 M sulphuric acid 1 mM copper sulphate at scan rates of 50 mV/s, 20 mV/s, 10 mV/s and 5 mV/s for (a) 10°C, (b) 20°C, (c) 25°C, (d) 30°C, (e) 35°C, (f) 40°C, (g) 45°C, (h) 50°C and (i) 55°C. The CVs for 20 mV/s, 10 mV/s and 5 mV/s have the current density j scaled for convenience by a factor of 2.5, 5 and 10, respectively.

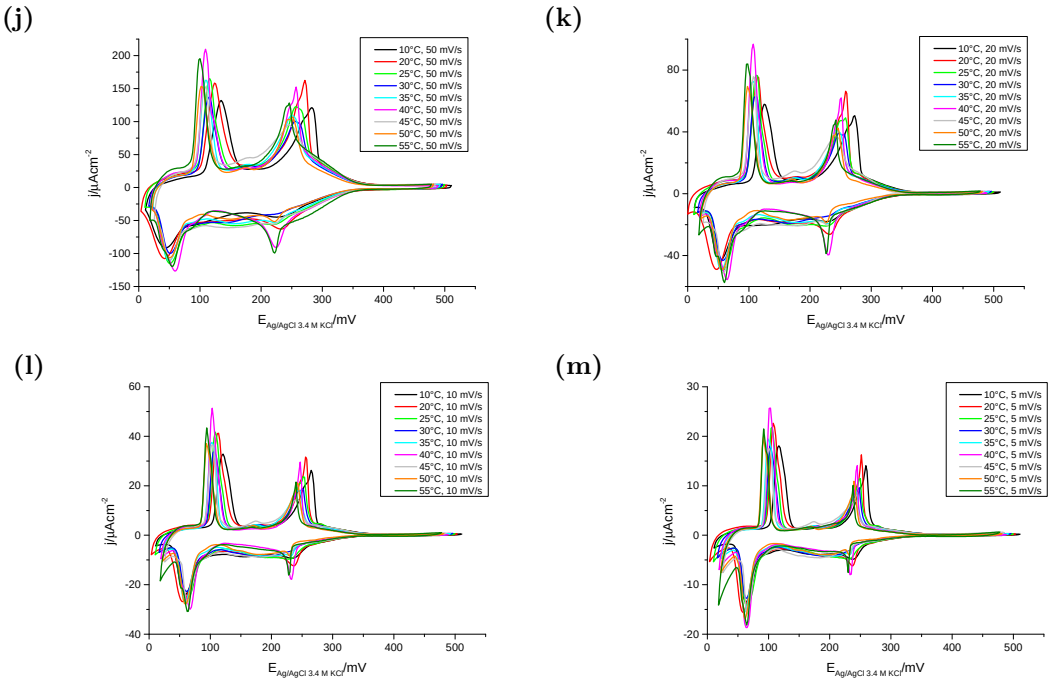

Figure 4.3.: CVs of Au(111) in 0.1 M sulphuric acid 1 mM copper sulphate at 10°C, 20°C, 25°C, 30°C, 35°C, 40°C, 45°C, 50°C and 55°C for (j) 50 mV/s, (k) 20 mV/s, (l) 10 mV/s and (m) 5 mV/s.

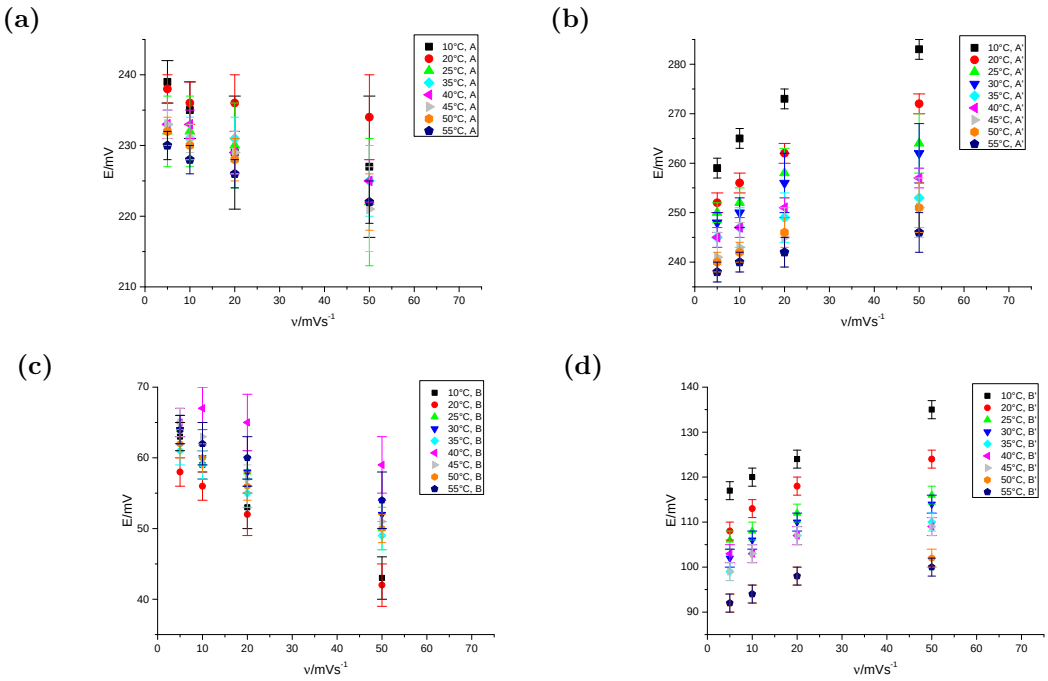

Figure 4.4.: Change of the peak positions with the scan rate ν at different temperatures for (a) A, (b) A', (c) B and (d) B'.

The shape of the CVs shows a strong dependence on the scan rate, as can be seen in Fig. 4.2. In general, the peaks sharpen with decreasing scan rate, with the effect being more pronounced at lower temperatures. Also, the anodic peak shift towards lower potential with decreasing scan rate while the cathodic peaks shift towards higher potentials (see Fig. 4.4 and 4.5).

For peak A (see Fig. 4.4a and 4.5a), the peak potential shows an increase with decreasing scan rate as well as a decrease with increasing temperature. From Fig. 4.2, it can also be seen that the peak becomes more prominent with decreasing scan rate, especially at low temperatures. It has also been said that the peaks sharpen with decreasing scan rate, but the effect is especially strong for peak A. For 10°C, it is very broad at higher scan rates. It is nearly absent at all scan rates for 25°C and 30°C and is only strongly expressed at 40°C and 55°C. It is of note that at the temperatures where A is strongly expressed, peak C is nearly absent. In Fig. 4.3, the peak is broader at low temperatures, but as said before the intensity of the peak seems to be linked to peak C.

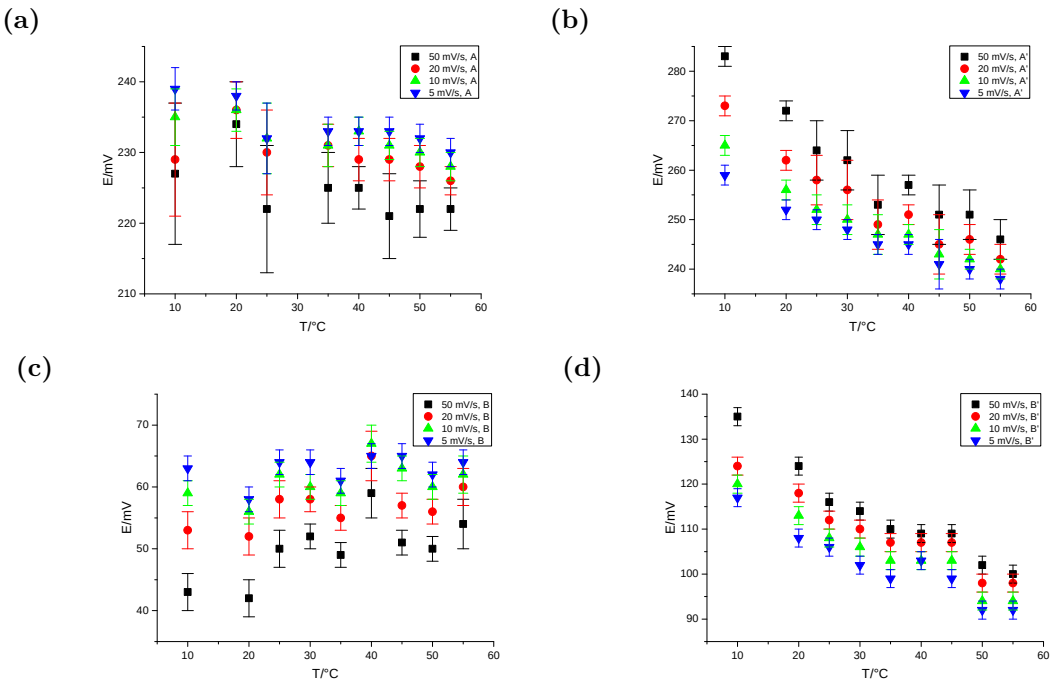

Figure 4.5.: Change of the peak positions with the temperatures at different scan rates for (a) A, (b) A', (c) B and (d) B'.

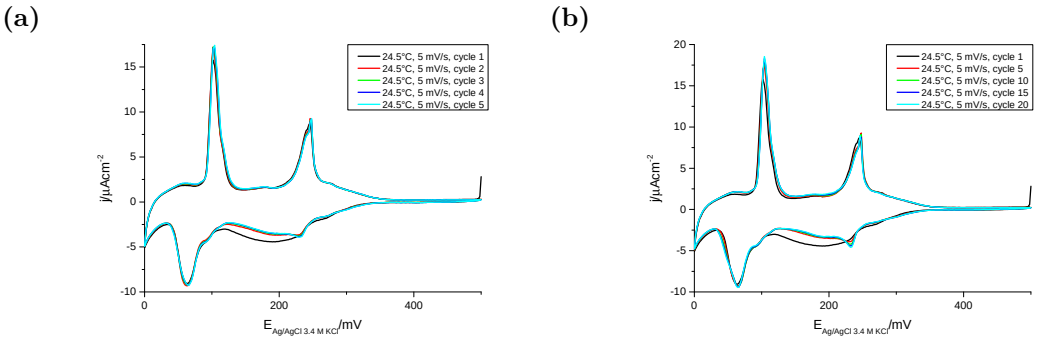

Figure 4.6.: Change with cycling for the CV of Au(111) in 0.1 M sulphuric acid 1 mM copper sulphate at room temperature (24.5°C) for (a) the first five cycles and (b) every five cycles.

Because of this, the change of the CV with cycling was investigated, as the repeated cycling tends to influence the surface of the crystal. Fig. 4.6 shows the change with cycling at room temperature over 20 cycles at 5 mV/s. While there is little change in the other peaks, there is a change in peak A and C. For the first cycle, peak A cannot be seen, and peak C is much stronger compared to

subsequent cycles. For the following cycles, there is a slight decrease of peak C with increasing number of cycles while peak A increases with the same. As there is no other change, the decrease of peak C seems to be linked to the increase of peak A.
As for peak C, while it is different at different temperatures for one scan rate, it does not show a discernible trend with the temperature (see Fig. 4.3). However, it does show changes with the scan rate, especially at low temperatures. For 10°C, it seems to show a strong shift towards higher potential with decreasing scan rate, while the same is true for the higher temperatures, though the change is not quite as strong. Fig. 4.2e and 4.2h also make it appear as if there might be two overlapping broad peaks involved. There is also a higher potential shoulder of peak B, though this seems to simply overlap with peak C at low temperatures or high scan rates.
Peak B (see Fig. 4.4c and 4.5c) appears at an increasing potential with decreasing scan rate as well as no change with the temperature at low scan rates. At 50 mV/s and 20 mV/s, the peak potential above 20°C is higher than at 20°C and 10°C. Since the strength of the scan rate dependence decreases with increasing temperature, the scan rate dependence is influenced by the temperature and vice versa. Also, the peak sharpening with decreasing scan rate is stronger at lower temperatures, with higher temperatures showing less of a difference (see Fig. 4.2). At 5 mV/s, the peak does not sharpen with increasing temperature, but it does at 50 mV/s (see Fig. 4.3m and 4.3j), also showing that the sharpening of the peaks depends on both temperature and scan rate. Furthermore, in Fig. 4.2f and 4.2i, peak B has a lower potential shoulder, though in both it is less apparent at 5 mV/s. Interestingly, for both temperatures there seems to be a relative increase of peak C at 5 mV/s.
Peak A' has a decreasing peak potential with decreasing scan rate and increasing temperature (see Fig. 4.4b and 4.5b) as well as the peak becoming sharper with decreasing scan rate (Fig. 4.2). The scan rate dependence is also dependent on the temperature, with the effect of the scan rate stronger at lower temperatures. Also, there are actually two peaks in A' which strongly overlap, which usually manifests as a lower potential shoulder, though at some higher scan rates the two peaks aren't visibly separated at all (f.e. Fig. 4.2e, at 50 mV/s).
For peak B' (see Fig. 4.4d and 4.5d), the temperature dependence and scan rate

dependence mirrors the one for peak A', though there is barely any influence of the temperature on the scan rate dependence. The peak sometimes has a higher potential shoulder, which seems to be connected to the lower potential shoulder of peak B.
Peak C' is a rather broad peaks that has a tendency to be sharper at higher temperatures as well as lower scan rates (see Fig. 4.2). There is a slight trend of decreasing peak potential with decreasing scan rate as well as increasing temperature.

4.1.2. Chronoamperometry

To investigate the kinetics of the Cu-UPD, two types of transients were measured. For the first, the potential was stepped from a value before peak A, B, A' and B', respectively, to the potential of the peak or a potential after the peak at 20°C. This was to isolate the kinetics of each peak similar to the experiment done by Hoelzle et al.[53,54] This is shown in Fig. 4.7, with peak A, B and A' only showing a falling current density over time, while peak B' shows a current peak for the transient from 79 mV to 134 mV.
The second type of transient had one starting potential, with several end potentials chosen at certain intervals for several temperatures each. The potential was returned to the starting potential after each transient. The temperature range was from 10°C to 50°C in 10°C intervals. As the effect of the temperature on the reference electrode had been overlooked at the time of the measurement, the exact measured potentials shift slightly with the temperature. The correction for the temperature dependence of the reference electrode has been shown in Ch. 2. These transients sorted by temperature are shown in Fig. 4.8. They all show only a falling current density with increasing time.

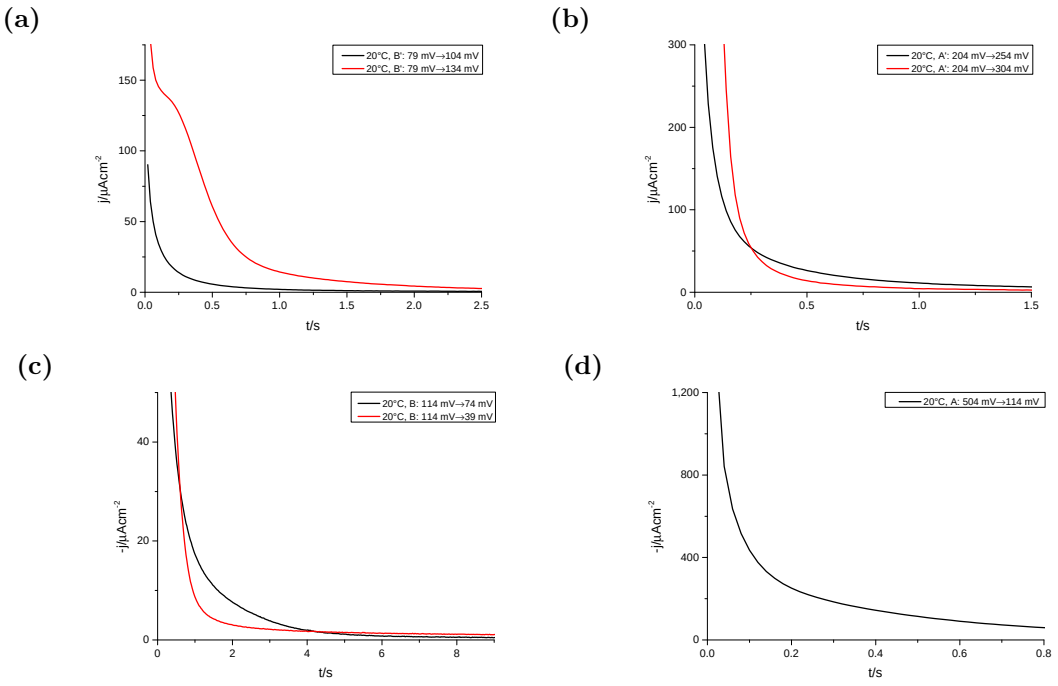

Figure 4.7.: Transients of Au(111) in 0.1 M sulphuric acid 1 mM copper sulphate at 20°C for (a) B', (b) A', (c) B and (d) A.

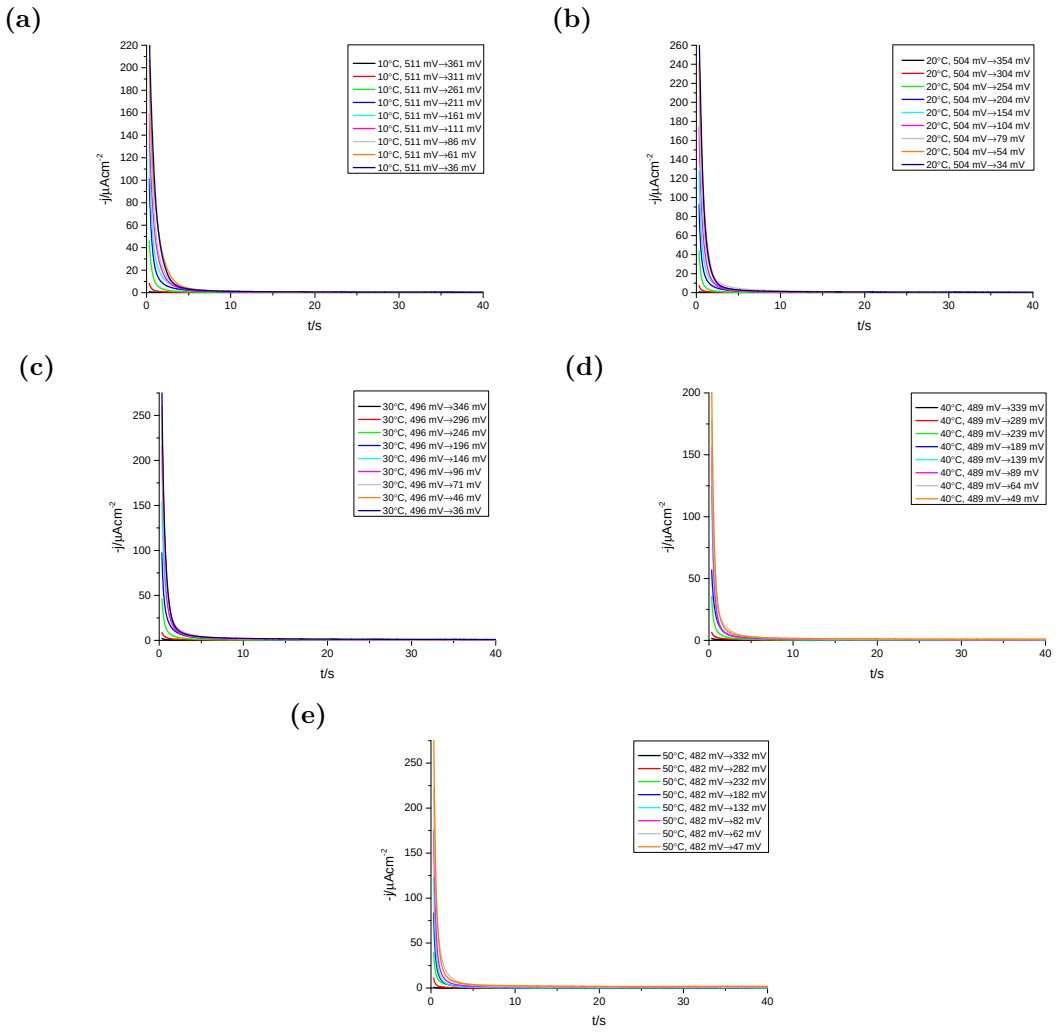

Figure 4.8.: Transients for Au(111) in 0.1 M sulphuric acid 1 mM copper sulphate with fixed starting potential at (a) 10°C, (b) 20°C, (c) 30°C, (d) 40°C and (e) 50°C.

4.2. Analysis & discussion

4.2.1. Cyclic voltammetry

A/A' & C

The CVs in this work show the known features which are supported by the literature.[18,37,40,52–54,56] In the CV (see Fig. 4.1), Peak A/A' are the formation/dissolution of the $(\sqrt{3} \times \sqrt{3})$R30° structure of coadsorbed copper and sulphate, with the higher potential shoulders the random coadsorption of copper and sulphate in a mobile adlayer.[17,18,40,43,47,49,51,56] The coadsorption of copper and sulphate is known to enhance the adsorption, as the coverages of each species on its own would be much lower in that potential range.[18,37]
Legault et al.[59] found that the formation of the ordered structure is a first-order phase transition, while Vasiljevic et al.[47] and Xia et. al[79] found a nucleation and growth process for the formation of the honeycomb copper layer using STM. Xia et al.[79] postulated a two-dimensional instantaneous nucleation and growth process for the formation of the honeycomb structure, however a two-dimensional nucleation and growth process would lead to a current peak in the chronoamperometric transients. While Hoelzle et al.[53] did not specify the kinetics for peak A in their investigation of the kinetics of the different stages using chronoamperometry, the transients did not show the current peak inherent in a two-dimensional nucleation and growth process. Furthermore, the transient for peak A presented in this work (Fig. 4.7d) also does not show the current peak, which means the two-dimensional nucleation and growth should not be the dominant process for this structural transition. However, for peak A', the transition to the disordered mobile adlayer, Hoelzle et al.[53] showed that a two-dimensional instantaneous nucleation and growth process contributes to the process.
The appearance of peak C is connected to peak A, as seen in Fig. 4.6, with peak C decreasing when peak A increases. As only peak C is visible in the first cycle after the lifting of the thermal reconstruction and it decreases with cycling while peak A increases, peak C is likely to be connected to surface defects. The lifting of the thermal reconstruction leads to the formation of gold islands of monoatomic height, with the amount of defects lowered with cycling due to electrochemical annealing. This would indicate that while both peak C and peak A are due to the

coadsorption of copper and sulphate, peak C is the process at or around surface defects, while peak A takes place on the ordered Au(111) surface. The discrepancy in the peak size of peak A and A', which should have a similar charge density due to peak A' representing the reverse process, also indicates that peak A is only one part of the process. Xia et al.[79] found no influence of the surface defects, especially the monoatomic islands, on the formation of the ordered honeycomb structure in their STM measurements, although they indicated that the coverage of the islands might not be complete. However, they neglected to show the associated CVs, and their postulated nucleation and growth mechanism for the honeycomb phase is contrary to the evidence in the chronoamperometry, as discussed earlier. Furthermore, while the work of Hoelzle et al.[54] does not show indications of peak C, which could be due to it being from a different type of defect than the investigated steps, they did show an influence of the step density on the shape of peak A, which would also indicate an effect of surface defects on the formation of the honeycomb phase.

This overlap of peak A and C is important when looking at the scan rate dependence of peak A, which is an increasing peak potential with decreasing scan rate (Fig. 4.4a). Meanwhile, Hoelzle et al.[53] found little change of the peak potential for peak A with the scan rate at room temperature in their investigation. As peak A is the first-order phase transition to the honeycomb phase, it is expected to be fast and not be governed by diffusion effects. Therefore, no significant scan rate dependence would be expected. While this seems contrary to the findings of this work, it is not if other factors are considered. Peak C shows a shift towards higher potentials with decreasing scan rate, the same as peak A. Considering the strong overlap of peak C and peak A, the scan rate dependence of peak A is very likely due to peak C, with peak A not depending significantly on the scan rate.

With increasing temperature, the peak potential for peak A decreases slightly (Fig. 4.5a). This again implies the dependence of peak A on temperature and scan rate is not due to diffusion, as the opposite trend would have been expected. As had been said previously for the scan rate dependence, diffusion-control is not expected for the process behind peak A, and this supports that assumption. While the observed sharpening of peak A in the CV would indicate the process becoming faster with increasing temperature, the peak shift is not due to the earlier onset of a faster process. However, the temperature dependence can be explained by the

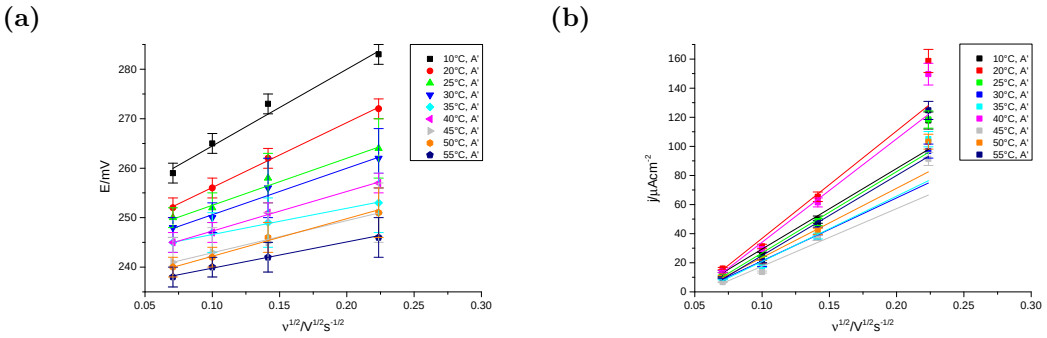

Figure 4.9.: Change of (a) the peak potential and (b) the peak current density with $\nu^{\frac{1}{2}}$ at different temperatures for peak A'.

increase of kinetic energy and thus the mobility of the adspecies. It is important to remember that peak A is the transition of the unordered mobile copper and sulphate adlayer to the ordered $(\sqrt{3}\times\sqrt{3})$R30° structure. Thus, an increase in the kinetic energy of the adspecies and therefore their mobility can increase the potential range of stability of the unordered phase. As the transition to the ordered phase requires the ordered state to be energetically advantageous to the unordered state, an increase in the mobility of the adspecies would increase the energy needed for the ordered state to be advantageous and thus could be said to lead to a higher activation barrier for the transition. A lower potential also decreases the surface charge, with a lower surface charge being more attractive for the adsorption of copper, which is a cation. Thus, with decreasing potential the single crystal becomes more attractive towards the copper cations, until the formation of the ordered adlayer and thus further copper deposition is more advantageous. The charge of the single crystal also depends on the pzc, which is dependent on the system. There is, to our best knowledge, no information on the influence of the temperature on the pzc. If the pzc shifts with the temperature, a similar shift of peak A would be expected due to the dependence of the $(\sqrt{3}\times\sqrt{3})$R30° adlayer formation on the surface charge of the crystal outlined before. While this is an alternative explanation, there is not enough evidence to support or reject it.

Table 4.1.: χ^2_{red} for the linear fits of the peak potential and peak current density for peak A' shown in Fig. 4.9.

	10°C	20°C	25°C	30°C	35°C	40°C	45°C	50°C	55°C
E_P	0.713	0.048	0.068	0.055	0.006	0.034	0.005	0.036	0.016
j_P	10.62	14.58	13.06	17.15	23.99	12.75	35.41	13.82	21.70

The order-disorder transition of the $(\sqrt{3} \times \sqrt{3})$R30° structure to a mobile adlayer of coadsorbed sulphate and copper, which is seen in the CV as peak A', is, according to Hoelzle et al.[53] a two-dimensional instantaneous nucleation process coupled with a desorption process. For the limit of $\nu \to 0$, Bosco et al.[80] found a dependence of the peak potential as well as the peak current density on $\nu^{\frac{1}{2}}$ for instantaneous nucleation. As such, at low scan rates and for instantaneous nucleation, the peak potential and the peak current density plotted over $\nu^{\frac{1}{2}}$ should show a linear trend. Fig. 4.9 shows this plot as well as the accompanying linear fits, while Tab. 4.1 shows the χ^2_{red} as an indication of the goodness-of-fit. While the linear fit for the peak potential has a χ^2_{red} below one, which would indicate a good agreement with the assumption of linearity as well as likely overestimation of the error, the peak current density does not agree quite as well. From Fig. 4.9b it can be seen that the values for 50 mV/s strongly deviate from the expected trend. The χ^2_{red} values (Tab. 4.1) also are generally over 10. While a value this large would indicate the wrong choice of model, there are also other factors to be considered in this case. For one, if there are other errors that have not been considered, this would impact the χ^2_{red}. The error for the current density was estimated as 5% of the value to account for the accuracy of the determination of the peak potential. However, the CVs (Fig. 4.2) show at the very least a shoulder for peak A' at all scan rates and temperatures, which means there is an overlap with another peak. While the impact of this on the peak potential is not too strong and easily accounted for in the error, the same cannot be said for the peak current density. A strong overlap with a peak of similar broadness, as is the case, strongly impacts the peak current density. This is not easily estimated as an error, as the contribution of the overlapping peak to the peak current density of peak A' is unknown. As such, the real value of the peak current density is unknown. Furthermore, the overlapping peak is likely connected to peak C, which would mean two different processes taking place. While this would complicate the

analysis for both peak potential and the peak current density, if the assumptions of the overlapping peak being connected to peak C as well as the assumptions about peak C are correct, the process would not be in competition with the process for peak A', as they would be at different surface sites. The reason the overlap is not seen as strongly in the peak potential is likely that the influence of the overlap on the peak potential is much smaller than on the peak current density, and that it could be sufficiently accounted for in the error. As such, the scan rate dependence of peak A' shows indications of an instantaneous nucleation and growth process in accordance to the findings of Hoelzle et al.[53] However, due to a strong overlap, further data would be required to ascertain this.

The temperature dependence of peak A' (Fig. 4.5b) shows a decreasing peak potential with increasing temperature. Generally, for an anodic peak, lower peak potentials can point towards an increasing speed of the process if it was kinetically limited. Both the decreasing scan rate dependence as well as the sharpening of the peak with increasing temperature would point towards a faster process at higher temperatures. On the other hand, peak A had the same temperature dependence, if not as strongly expressed, as peak A', so the same reason for the temperature dependence should be considered. For peak A, it was seen as likely that the increasing mobility of the adspecies with increasing temperature extended the range of stability of the unordered mobile adlayer, with the onset of the ordered honeycomb structure shifted towards lower potentials as a result. While the work of Hoelzle et al.[53] showed that the processes for the disorder-order transition (peak A) and the order-disorder transition (peak A') have different kinetics, with a two-dimensional instantaneous nucleation and growth for peak A' but no strong evidence of the same for peak A, this should not impact consideration of phase stability. Thus, it is expected that the considerations for the stability of the unordered mobile adlayer for peak A also apply to peak A'. However, the temperature dependence does not necessarily only have one component. Comparing the temperature dependence for peak A and A' shows the trend to be much stronger for peak A'. As such the hysteresis between the peaks lessens with increasing temperature. The effect of changing kinetics on the anodic and cathodic peaks has opposite trends due to the direction of the potential scan. As said earlier, an increase in the speed of the process would induce a shift towards lower potentials for anodic peaks, while it would shift towards higher potentials for

cathodic peaks. Furthermore, the sharpening of peak A and A' in the CVs with increasing temperature also points towards a faster process. As such, it is likely that for both peak A and A' the increasing temperature leads to both a faster process as well as an increase in the stability range of the unordered adlayer. Since the potential shift with an increasing speed of the process is opposite for peak A and A', peak A' shows a much stronger temperature dependence than peak A, since for peak A, the influence of the change in kinetics and of the stability have opposite effects.

For the Cu-UPD on Pt(111) in sulphuric acid, Jerkiewicz et al.[13] also found sharper peaks at higher temperatures, which was attributed to synergetic effects of the coadsorbed species. As the degree of order decreases with increasing temperature, they had expected less ordering at high temperatures, which would have lead to broader peaks in the CV.[13] However, the expected increased disorder can be seen on Au(111) in this work for peak A and A', since the potential at which the order↔disorder transition occurs changes with the temperature as explained previously. Therefore, the effect of the changed degree of order seems to be in the relative stability of the ordered and disordered phase. Furthermore, the results indicate that the phase transition on Au(111) is faster at higher temperatures, likely due to the increased mobility of the adspecies.

B/B'

Peak B and B' are the transition of the $(\sqrt{3} \times \sqrt{3})$R30° structure to and from the Cu-(1x1) layer, respectively.[17,18,37,40,43,47,56] The hysteresis between the peaks is explained by Uchida et al.[37] to be due to the copper-sulphate interaction, with the removal of the sulphate requiring a large overpotential due to the strong coadsorption. According to Hoelzle et al.,[53] it is an indication of the two-dimensional phase transition, with the chronoamperometric transients showing a two-dimensional instantaneous nucleation and growth behaviour. Peak B shows peak splitting at 40°C and 55°C (see Fig. 4.2f and 4.2i), though for both it does not show for 5 mV/s, only showing at the higher scan rates. This peak splitting is attributed to the surface quality by Hoelzle et al.,[53,54] with the lower potential shoulder being due to nucleation on Au(111) terraces, with the higher potential peak being attributed to nucleation on defects. Considering it is only seen at these two temperatures, and not a systematic change with increasing temperature, it is

likely because of slightly differing conditions for these measurements instead of a temperature effect. Interestingly, Peak C is strongly reduced compared to other measurements at the same scan rate at these two temperatures, which would point towards a difference in the surface for these two temperatures. When investigating the peak splitting of peak B, Hoelzle et al.[54] found that when the potential was held slightly before the maximum of peak B, the lower potential peak was reduced with increased holding time. Both surface defects and the domain boundaries of the honeycomb phase can be used as nucleation sites for the Cu-(1x1) layer,[47,54] with the domain boundaries serving as nucleation sites on Au(111) terraces.
As the nucleation on defects occurs at higher potentials, it seems to be energetically preferred. Likely, the disappearance of the lower potential shoulder with increasing surface defect density is due to the increasing availability of the surface defects providing sufficient nucleation sites. This would also explain the reduction of the lower-potential peak with increased holding time Hoelzle et al.[54] found, as the nucleation on the domain boundaries is only relevant if the phase transition is not complete. This would explain why the shoulder in Fig. 4.2f and 4.2i is reduced with decreasing scan rate. The scan rate represents the time domain in cyclic voltammetry, with a higher scan rate resulting in less time at a potential. Thus, at high scan rates, the transition to the Cu-(1x1) layer on defects was not complete before the potential for the nucleation on the domain boundaries was reached, so both processes took place. At lower scan rates, more time was available for the nucleation on defects, so that likely at 5 mV/s the transition to the Cu-(1x1) was complete before nucleation on the domain boundaries could begin. As an increase in surface defects means an increase in nucleation sites and thus a faster process, it is likely that the other temperatures had a higher surface defect density and thus had a sufficiently fast nucleation on defects so no nucleation on domain boundaries was observed even at higher scan rates. This also correlates well with the lower intensity of peak C at the two temperatures showing the nucleation on domain boundaries.

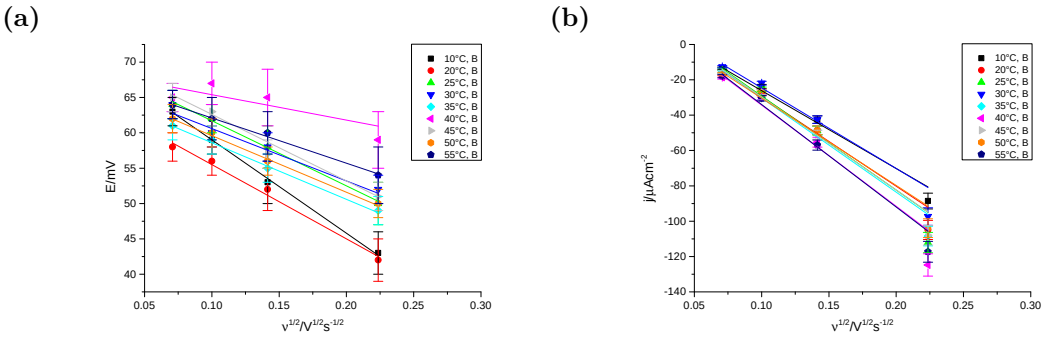

Figure 4.10.: Change of (a) the peak position and (b) the peak current density with $\nu^{\frac{1}{2}}$ at different temperatures for peak B.

Table 4.2.: χ^2_{red} for the linear fits of the peak potential and peak current density for peak B shown in Fig. 4.10.

	10°C	20°C	25°C	30°C	35°C	40°C	45°C	50°C	55°C
E_P	0.023	0.127	0.036	0.215	0.034	0.504	0.315	0.034	0.017
j_P	3.72	5.93	9.32	10.49	4.06	10.26	6.48	5.70	5.26

The scan rate dependence for peak B is shown in Fig. 4.10 with the assumption of a linear dependence on the peak potential and the peak current density on $\nu^{\frac{1}{2}}$. As explained previously, this linear dependence for low scan rates is a sign of instantaneous nucleation.[80] Fig. 4.10a shows a good agreement of the peak potential with this dependence, which is also seen in the values for χ^2_{red} in Tab. 4.2. The values below one for χ^2_{red} indicate that the model is appropriate but the error variance is larger than necessary for the values of the fit to fall within. For the peak current density, Fig. 4.10b shows 50 mV/s to be an outlier. The values for χ^2_{red} in Tab. 4.2 are above one, which has been previously stated to be due to a wrong assumption of the model or an underestimation of the error variance. For peak B, the CVs show some overlap with peak C at high scan rates (Fig. 4.2). This is similar to what was seen for peak A'. As explained there, this would have a strong impact on the peak current density that is not easily estimated with the error. There is also the peak splitting at 40° C and 55°C which would have similar effects on the peak current density, and also depends on the scan rate. This is furthermore a sign of two different processes taking place, which would influence the scan rate dependence. Furthermore, the assumption made for the determination of the

baseline is important. While measuring in copper free electrolyte could be seen as the way to determine the baseline, it is impractical as the double-layer charging current depends on the meniscus, which, while similar, cannot be guaranteed to be identical in different measurements. Additionally, the properties of the electrochemical interface depend on the composition of the system. As copper is an electrochemically active species, it could change the properties of the interface beyond the Cu-UPD taking place, which would invalidate the use of copper-free electrolyte as a baseline. Instead, the current density at 420 mV was taken as the baseline. While this is in the range of sulphate adsorption, the relative current density for it is low compared to the Cu-UPD. Lower potentials risked including the start of the random copper and sulphate coadsorption, while higher potentials could include a slight raising or falling trend due to oxygen. Of course, taking this value assumes that without the deposition process the CV would show no change in the current density. So a neglected error due to the choice of baseline is possible. Furthermore, peak B is near the lower potential limit, which shows a falling current density likely from the start of the bulk deposition, although a slight influence of oxygen cannot be ruled out. This falling current density could also influence the peak current density and thus introduce an error that had not been accounted for.

While the agreement of the scan rate dependence of peak B with the model of linear dependence on $\nu^{\frac{1}{2}}$ is not good for the peak current density, peak B still seems to show reasonable indications of instantaneous nucleation considering the likely influences on the peak current density that the error did not account for.

Peak B does not show a temperature dependence of the peak position (see Fig. 4.5c), which means the formation of the full copper monolayer is not affected by the temperature. The UPD takes place at higher potentials than the bulk deposition due to the strength of the copper-gold interaction exceeding that of the copper-copper interaction, making the deposition of the first monolayer energetically favourable compared to the bulk deposition. For the Cu-UPD in sulphuric acid, the strong interaction between copper and sulphate also results in the codeposition during the first stage of the Cu-UPD process at higher potentials than the copper monolayer formation. Furthermore, according to Uchida et al.,[37] the strong potential shift between peak B and B' is due to the need to overcome the copper-sulphate interactions. Thus, besides the kinetics of the process, the

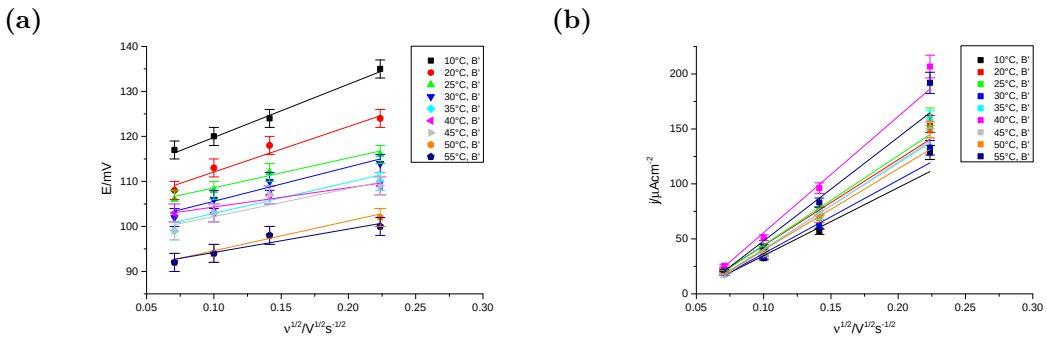

Figure 4.11.: Change of (a) the peak position and (b) the peak current density with $\nu^{\frac{1}{2}}$ at different temperatures for peak B'.

strength of the copper-gold and copper-sulphate interactions relative to each other would govern the onset of the formation of the Cu-(1x1) phase and thus the peak potential. There is no significant difference in the temperature dependence at different scan rates. As such, there should be no influence of the kinetics on the temperature trend at one scan rate. Therefore, the temperature dependence of the peak potential is governed by the previously mentioned copper-gold and copper-sulphate interactions. Considering the temperature range is over 45°C, the change in energy due to the temperature would not be expected to be relevant compared to the strength of these interactions. As such, it is reasonable that there is no temperature dependence of the peak potential of peak B.

Since peak B' is the transition of the Cu-(1x1) layer to the $(\sqrt{3}\times\sqrt{3})$R30° structure, there are some connections between the processes for peak B and B'. For peak B', the appearance of the higher-potential shoulder is due to the lower-potential shoulder of peak B, which has also been shown by Hoelzle et al.[54] While the relevant sites for the two processes for peak B' are not specified, the connection between the peak splitting for peak B and B' shown by Hoelzle et al.[54] makes it likely that it is similarly related to the surface structure. Like for peak B, the shoulder only appears if the first process is sufficiently slow compared to the scan rate so that the transition is not complete before reaching the potential for the second process.

Table 4.3.: χ^2_{red} for the linear fits of the peak potential and peak current density for peak B' shown in Fig. 4.11.

	10°C	20°C	25°C	30°C	35°C	40°C	45°C	50°C	55°C
E_P	0.146	0.650	0.170	0.559	0.770	0.331	1.016	0.170	0.449
j_P	6.26	3.71	3.86	4.51	6.97	4.00	3.61	5.80	7.62

Similar to peak B, peak B' shows indications of instantaneous nucleation in the scan rate dependence (see Fig. 4.11 and Tab. 4.3). Like peak B, the peak potential shows a good agreement with the linear dependence on $\nu^{\frac{1}{2}}$, while the peak current density shows worse agreement, especially at 50 mV/s. However, the values for χ^2_{red} are generally better for the peak current density of peak B' than for peak B. The same basic considerations made for peak B also apply here, with the baseline possibly adding an unaccounted for error. Also, possible competing processes, which the peak-splitting indicated as a possibility, would also influence the scan rate dependence. Therefore, the scan rate dependence of peak B' shows indications of an instantaneous nucleation process.
Peak B' also has a temperature dependence, unlike peak B, indicating a difference in the two processes. As said previously, the hysteresis between peak B and B' is due to sulphate strongly coadsorbing with copper and needing a large overpotential for removal,[37] while for peak B', copper has to be replaced with sulphate. The copper-sulphate interactions not needing to be overcome in peak B' could be the reason for the different dependence. The temperature dependence of peak B' also shows a slight dependence on the scan rate, which would indicate that the speed of the process increases with the temperature. This could be due to an influence of diffusion or surface diffusion on the process. An increase in the speed of a kinetically limited process would lead to a lower peak potential with increasing speed.

4.2.2. Chronoamperometry

To access the kinetics of the Cu-UPD, the transients were fitted. For the fit, it was assumed that each process could be described by the Avrami equation (Eq. 1.3), and that the whole transient was a superposition of several processes. The used

form of the equation, which has been covered in more depth in Sec. 1.1.2, was

$$j_i(t) = q_i \cdot m_i \cdot k_i \cdot t^{(m_i-1)} \cdot e^{(-k_i \cdot t^{m_i})}$$

with the current density j, the charge density q, the rate constant k and m representing the type of process.[12] m=1 represents either a surface diffusion-controlled two-dimensional instantaneous nucleation and growth process or a one-dimensional instantaneous nucleation and growth process,[11] m=2 is instantaneous nucleation and growth and m=3 is progressive nucleation and growth.[5,12]

Transients for peak A, A', B and B'

The transients for each peak (Fig. 4.7) were measured similarly to the ones measured by Hoelzle et al.[53] (Fig. 1.20). The form of the transients for peak A, B and B' differs from the transients of Hoelzle et al.[53] insofar as the current peaks seem to be reduced. Only the transient for peak B' shows a current peak, though compared to the work of Hoelzle et al.,[53] the current peak is less prominent. The sulphuric acid concentration in this work was 0.1 M, while the work of Hoelzle et al.[53,54] uses 0.05 M. While Shi et al.[41] found that the copper deposition is slow in electrolytes with low sulphate concentration, they worked with comparatively low sulphate concentration compared to the ones used in this work and by Hoelzle et al.[53] As there are, to our best knowledge, no systematic studies on the influence of the sulphate concentration on the kinetics of the Cu-UPD, it is not certain whether the change in kinetics was due to the sulphate concentration or other factors.
Also, for peak B and B', a study from Hoelzle et al.[54] showed a decrease in the current peak with increasing step density or after introducing defects by oxidation, which means surface defects could also be an influence. However, the current peak visible for the transient of peak B' supports the instantaneous nucleation found from the scan rate dependence of peak B' in the CV.
For the transient of peak A', analysis of the peak potential found indications of a possible instantaneous nucleation, but this could not be seen in the peak current density, likely due to a strong overlap with another peak. The transient also does not show the current peak that would be characteristic for the expected two-dimensional instantaneous nucleation and growth process found

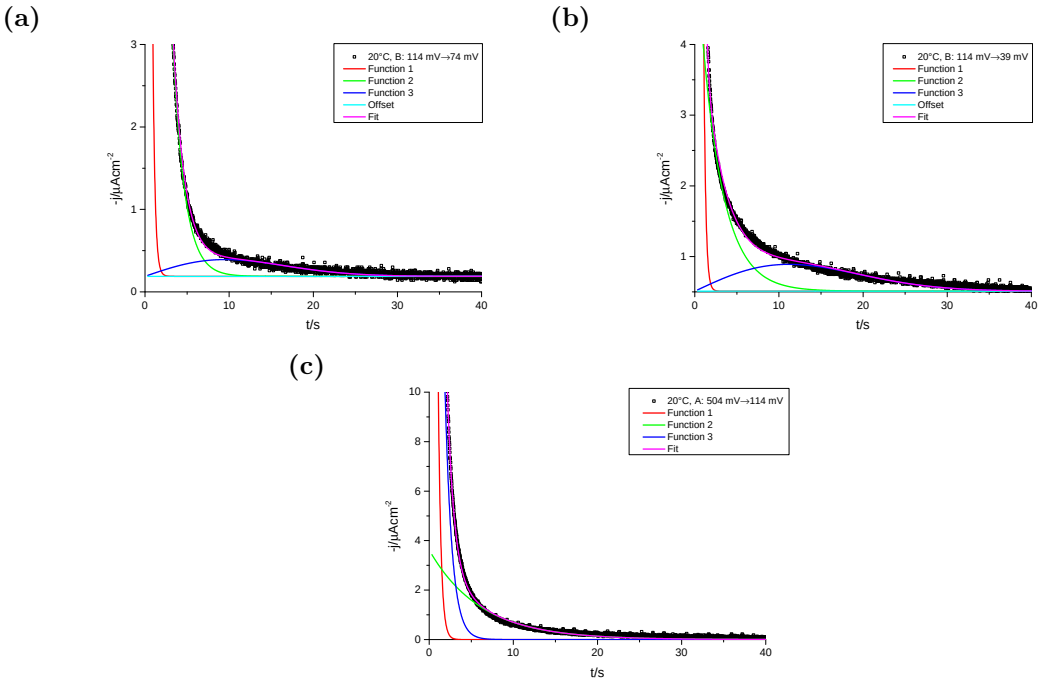

Figure 4.12.: Fits for the transients of Au(111) in 0.1 M sulphuric acid 1 mM copper sulphate at 20°C for (a),(b) B and (c) A.

by Hoelzle et al.[53] It might be possible that the current peak is masked by the process from the overlapping peak, but there is no strong evidence of the two-dimensional instantaneous nucleation and growth. So while it is possible that the two-dimensional instantaneous nucleation and growth plays a role in the order-disorder transition of the $(\sqrt{3}\times\sqrt{3})$R30° structure to the mobile adlayer, the evidence in this work points towards it not being the main process in our experiments.

Hoelzle et al.[53] found in their investigation of the Cu-UPD on Au(111) in sulphuric acid that the transients for peak B, B' and A' could be described as a combination of an adsorption/desorption process and an instantaneous nucleation. In the Avrami equation detailed in Sec. 1.1.2, this could be modelled with a m=1 and m=2 process, respectively. This was used as approach for fitting the transient for peak B in Fig. 4.7, while the transient for peak A was assumed to be a superposition of exponential decays. The resulting fits can be seen in Fig. 4.12, while the corresponding fit parameters are in Tab. 4.4. The transients can be fitted with the above assumption, though the contribution of the instantaneous

Table 4.4.: Parameters for the fits of the transients of Au(111) in 0.1 M sulphuric acid 1 mM copper sulphate shown in Fig. 4.12.

	114 mV→39 mV	114 mV→74 mV		504 mV→114 mV
$q_1/\mu Ccm^{-2}$	-79.12±0.01	-27.45±0.03	$q_1/\mu Ccm^{-2}$	-91.5±0.4
k_1/s^{-1}	4.274±0.002	3.852±0.007	k_1/s^{-1}	3.068±0.007
m_1	1	1	m_1	1
$q_2/\mu Ccm^{-2}$	-13.21±0.08	-42.57±0.03	$q_2/\mu Ccm^{-2}$	-22.06±0.09
k_2/s^{-1}	0.39±0.004	0.7176±0.0008	k_2/s^{-1}	0.164±0.001
m_2	1	1	m_2	1
$q_3/\mu Ccm^{-2}$	-7±0.3	-3.2±0.08	$q_3/\mu Ccm^{-2}$	-80.6±0.4
k_3/s^{-2}	0.004±0.0002	0.0055±0.0001	k_3/s^{-1}	1.204±0.005
m_3	2	2	m_3	1

nucleation and growth process to the transients of peak B is rather small and not readily apparent from the form of the transient. Hoelzle et al.[53] found a decrease of the nucleation and growth process with increasing surface defect density, which could be one explanation. As mentioned previously, the different concentrations of sulphate might also play a role. Also, a second adsorption process has been used for the transients of peak B compared to the work of Hoelzle et al.[53] As there are differences between the CVs in this work and the ones from Hoelzle et al.,[53] it seems plausible that there are differences in the transients. The additional process might be either the small higher potential shoulder of peak B or possibly a slight contribution from peak C. It should also be noted that although the parameters for the transients for both A and B are labelled the same, the functions for A and for B do not necessarily represent the same processes.

The transient for peak A should include the processes for peak A and peak C, as the potential step for this transient covers the potential range in which these peaks can be seen in the CV. These processes are likely to be function 1 and function 3 seen in Tab. 4.4 and Fig. 4.12c, respectively, since they should be the main contributions to the process. Considering that in the CV, peak C is much broader than peak A, this likely means it also is a slower process, which also fits with its strong shift with the scan rate. Thus, the process for peak C should have a lower rate constant than the one for peak A.

For the transients for peak B (see Tab. 4.4 and Fig. 4.12), function 3 represents the two-dimensional instantaneous nucleation and growth process on terraces. In the work of Hoelzle et al.,[53] the adsorption process on defects was fast, thus

function 1 could be the adsorption on defects due to its large contribution as well as high rate constant. As mentioned earlier, the shoulder of peak B or a partial influence from peak C may be explanations for function 2. While the interpretation of m=1 as an adsorption process is possible, the interpretation of the Avrami equation would be either a surface diffusion-controlled instantaneous two-dimensional nucleation and growth or an one-dimensional instantaneous nucleation and growth process. Considering the low contribution of function 3 as well as the indication of instantaneous nucleation and growth from the scan rate dependence of peak B, these two interpretations seem more likely compared to an adsorption. Since one-dimensional growth would usually be expected from step edges or similar defects, which are not as likely to be the cause in this work, surface diffusion-controlled instantaneous two-dimensional nucleation and growth would be the more appropriate interpretation of the two.

The overall charge density of the different processes is around 0.3 $mCcm^{-2}$, which is below the charge density for a full monolayer of copper, which is 0.44 $mCcm^{-2}$.[17] However, this has not been corrected for the coadsorption of copper and sulphate. With the assumption of 0.22 ML of copper masked by sulphate adsorption,[57] the value would be around 0.38 $mCcm^{-2}$. As the transients for peak B did not go to zero at long times, as also found by Hoelzle et al.,[53] it is possible that the offset used to correct this might have falsified some of the charge. Schultze et al.[81] proposed a side reaction of $Cu^{2+} + e^- \rightleftharpoons Cu^+$ with a charge around 0.01 $mCcm^{-2}$ for the second Cu-UPD stage, which was the side process assumed by Hoelzle et al.[53] as the reason for the offset of the transient. It is important to note that the assumed main reaction in this case is $Cu^{2+}_{sol} + 2e^- \rightleftharpoons Cu^0_{ad}$, which makes the reduction to Cu^+ the side reaction. There is another proposed reaction scheme with the following two steps: $Cu^{2+}_{sol} + e^- \rightleftharpoons Cu^+_{ad}$ and $Cu^+_{ad} + e^- \rightleftharpoons Cu^0_{ad}$, although Shi et al.[40] found evidence to the contrary, as the amount of charge per adsorbed copper atom did not vary significantly between the two Cu-UPD stages. Due to this, it is assumed in this work that the charge transfer does not happen in two steps with an Cu(I) intermediate. The charge from the side reaction is however not enough to explain the difference between the known charge for one monolayer and the overall charge density from the transients for each peak. It is also known that the deposition processes for the system are slower than the dissolution processes,[40,57] with Shi et al.[40] finding that several minutes are needed for equilibration at

the negative potential step. While the low sulphate concentration in the work of Shi et al.[18,40,41] would further slow the copper deposition,[41] the hysteresis as well as lower peak current densities for the negative peaks in the CV[57] also show this at higher sulphate concentrations. Because of this, it is also possible that due to the long equilibration time, the measurement time for the transients in this work was not sufficient to establish equilibrium for the transients of peak B and the full process wasn't measured. Furthermore, Shi et al.[18,40] found in their calculation of the surface concentration of copper that the number of electrons exchanged per copper atom varied between 1.6 and 1.8. The charge density for a full monolayer, 0.44 $mCcm^{-2}$, is calculated assuming a transfer of 2 electrons. Using the values of Shi et al.[18,40] would give 10-20% lower charge density, which would be consistent with the charge density in this work.

Temperature-dependent transients

The fits described above can be used as a starting point for fitting the transients at different temperatures. While a nucleation and growth process should have been used at the lower potentials, due to the transients including all processes and thus having a superposition of several functions as well as the contribution of the nucleation and growth process being rather small, it was not represented in the temperature-dependent transient fits. From the known information about the Cu-UPD process as well as the CVs, the process can be divided into three potential regions which should have different kinetics. The first region of 350 mV to 250 mV has the unordered copper and sulphate codeposition, the second region of 250 mV to approximately 100 mV has the $(\sqrt{3} \times \sqrt{3})$R30° structure and the third region below 100 mV is the formation of the Cu-(1x1) monolayer. The processes in the transients should depend on the potential region. Although the fit parameters in Tab. 4.4 can be used as an approximation, the transients in Fig. 4.12a and 4.12b have a different starting surface, which would change the kinetics even if only the processes for peak B take place in the third region when starting from the clean gold surface.
Fig. 4.13 and 4.14 show the parameters for the fits of the temperature dependent transients against the potential for each function at the different temperatures. All processes have m=1. The charge density q had been converted to the coverage θ assuming an electron transfer of two electrons per deposited copper atom using

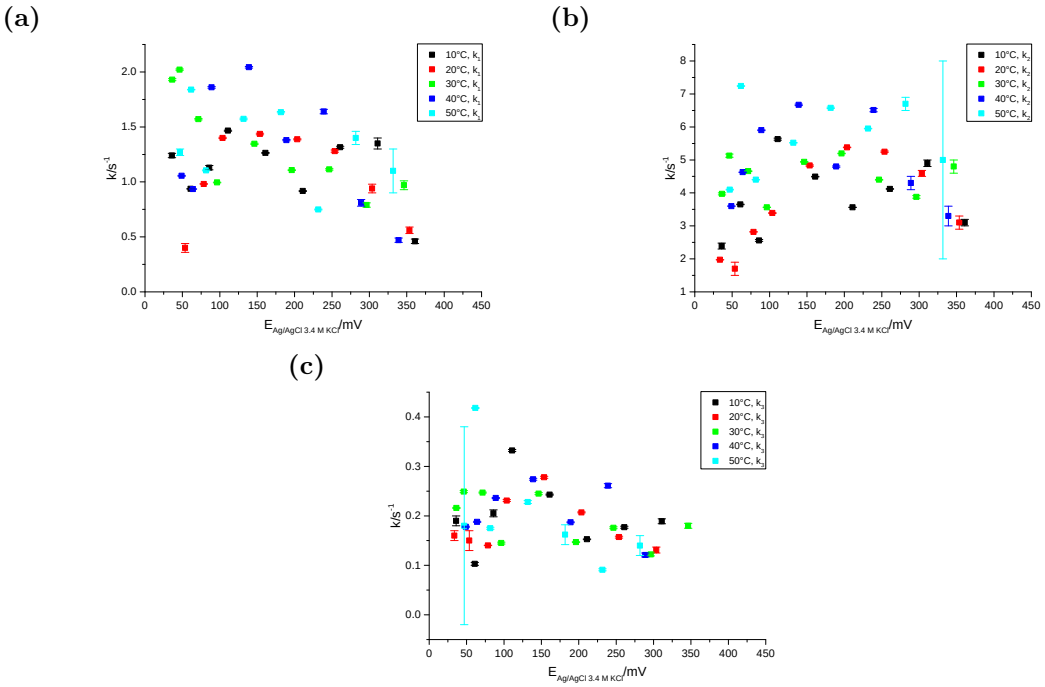

Figure 4.13.: Plot of the rate constants (a) k_1, (b) k_2 and (c) k_3 over the potential for the fit the temperature dependent transients of the Cu-UPD on Au(111) in 0.1 M sulphuric acid.

$\theta_i = \frac{q_i}{-2e \cdot n_A}$, with e being the elementary charge and $n_A = 1.39 \cdot 10^{15} cm^{-2}$ [40] being the number of gold atoms on an ideal Au(111)-(1x1) surface. Due to the coadsorption of copper and sulphate, the shown calculated coverages in Fig. 4.14d are 0.22 ML [57] lower than their actual value. This brings the total coverage at the full monolayer to around 0.9 ML, which is lower than the 1 ML that should exist. However it is consistent with the summed up charge for the transients in Fig. 4.12, which is about 86% of the expected value. Similar to the previously discussed fits, an offset was used to account for the side reaction, although its charge should not account for 0.1 ML. Also, there were slight differences between the output of the fitted model and the actual transient, as the model did not describe the transient perfectly. This might also contribute to the lower coverage obtained. Moreover, for the calculation of the coverage, a full charge transfer with two electrons flowing to the interface per copper atom was assumed. As said before, Shi et al. [18,40] found that instead of 2, the number of electrons exchanged per copper atom varied between 1.6 and 1.8. If the coverage of this value is compared to the one assuming

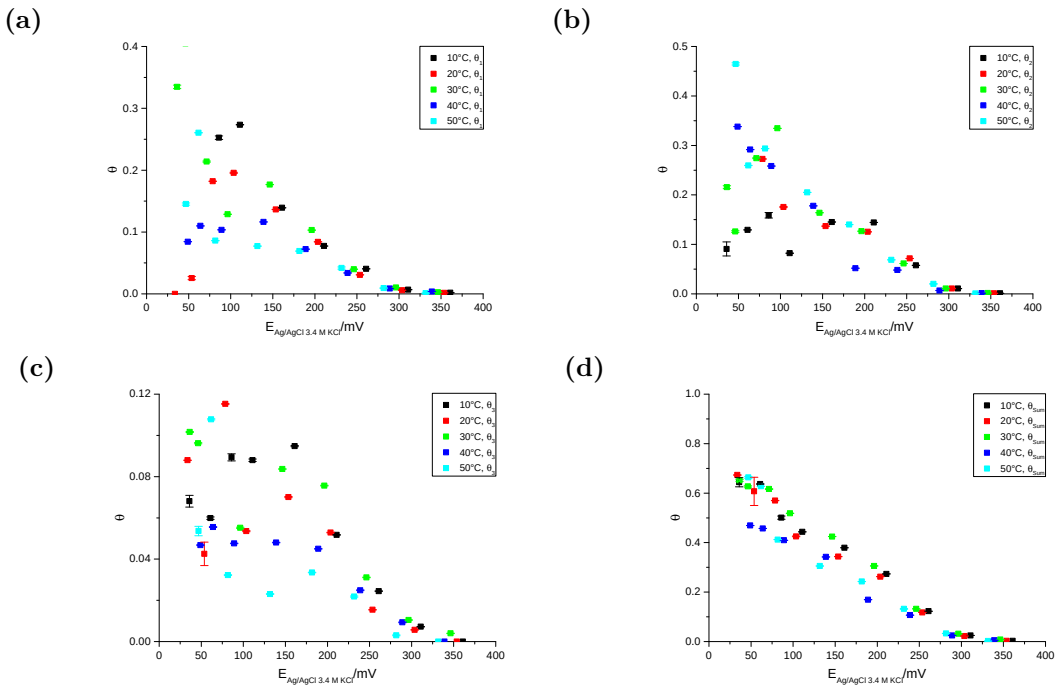

Figure 4.14.: Plot of the coverages of (a) function 1, (b) function 2, (c) function 3 and (d) the overall coverage over the potential for the fit of the temperature dependent transients of the Cu-UPD on Au(111) in 0.1 M sulphuric acid. The coverages were not corrected for sulphate coadsorption.

a transfer of 2 electrons, it would be 10-20% higher, which would account for the discrepancy. Since the coverage correction has to be applied in region three to obtain coverages consistent with the total charge for the processes in peak A and B, and the potential was in this case stepped directly from the clean Au(111) surface to the region for Cu-(1x1) formation, the coadsorption seems to affect the charge in this region, too. As Frittmann et al.[57] found that the Faradaic charge in that region is equal to the obtained coverage, this would imply that even in region three a process with coadsorption happens when stepping from the clean Au(111) surface.

Fig. 4.14d also shows a decreased coverage for 40°C at low potentials, which is not observed for any other temperature. As the coverage is consistently lower for 40°C compared to other temperatures, it is likely connected to the actual measured transients. A possible reason would be a smaller meniscus during that measurement compared to the other measurement sets. As the deposition is only on the single crystal surface covered by the meniscus, a smaller meniscus means

the assumed surface area used to calculate the charge density was too large, which leads to an artificially decreased charge density, which in turn would lead to an artificially lowered coverage. Otherwise, the total coverage doesn't change with the temperature, which would be expected.
The dependence of the coverage on the potential shows approximately the form found in the literature (see Fig. 1.14 and 4.14d). The steps seen in the potential dependence of the coverage are not as strongly expressed, though this is likely due to the difference in the approach. Frittmann et al.[57] and Shi et al.[40] show similarly clear steps in the coverage with the potential as Hoelzle et al.[53] does, but all use data from positive potential steps and thus from the dissolution of the phase rather than the deposition, which was used in this work. It is known that the deposition processes for the system are slower than the dissolution processes,[40,57] with Shi et al.[40] finding that several minutes are needed for equilibration at the negative potential step. While the low sulphate concentration in the work of Shi et al.[18,40,41] would further slow the copper deposition,[41] the hysteresis as well as lower peak current densities for the negative peaks in the CV[57] also show this at higher sulphate concentrations. Thus, it is not surprising that for the slower process, less clear steps are revealed. Furthermore, correlations between the CV and the coverage-potential curve can be drawn. Due to peak C, the CVs in this work have a continuation of deposition between peak A and B, in the same area where the coverage step is less strongly expressed than in the previously mentioned literature. If there is a potential range of continuous deposition after peak A in the CV, the coverage change in that area would also be expected to be more gradual.
Both the coverage and the rate constants of each function don't show a clear consistent trend with the temperature as well as no consistent difference in each region. Considering the clear trends in the cyclic voltammetry, especially the sharpening of peak A, there should be a temperature trend. While it is possible that the temperature has no effects on the kinetics of the Cu-UPD, there are other indicators to consider. Due to the different processes in the three regions, there should also be a difference in the processes or at least a change in the number of processes. It has been said previously that the model for the transients of peak B in Fig. 4.12 imply at least one m=2 process in the third region. While it could be argued that the process could change from a nucleation and growth

process due to the different starting surface when starting from the bare Au(111) surface, Garfias-Garcia et al.[55] also found a current peak when investigated the monolayer formation from bare Au(111). The current peaks in the transients are signs of a nucleation and growth process. While the transients found in this work do differ from the ones published by other people, there was some indication of a nucleation and growth process found even without the current peak. Thus, it is not unreasonable to assume that the model should include this contribution. There was also a strong correlation between parameters, which increased the difficulty of obtaining a reasonable fit. While the fits presented in this work are the attempt that has been consistently able to fit the transient, and attempts had been made to include nucleation and growth processes, the behaviour of the transients is rather complex and there are several indications that the used model doesn't reflect the processes in the transients.
Furthermore, the model used for the chronoamperometric transients is a simple nucleation model. It is well-known that the coadsorption of copper and sulphate strongly influences the Cu-UPD in sulphuric acid. However, the Avrami equation does not account for the coadsorption, which could be part of why the used model represent the processes in the transients.
Regardless of the applicability of the fitting model, the total coverage at each temperature still contains valid information. For the overall coverage, there is a slight shift of the θ-E curve towards lower potential with increasing temperature (see Fig. 4.14d). While the neglect of the temperature dependence of the reference electrode during measurement means the coverage values for each temperature are at slightly different potentials, the coverages above 70 mV have a trend of either decreasing with increasing temperature for similar potentials or at the least stay approximately constant. If there was no change with the temperature, they would be expected to show an increase with increasing temperature, as higher temperatures are shifted towards lower potentials by the reference electrode temperature dependence. Instead, the θ-E curves imply that with increasing temperature, the start of the first Cu-UPD stage shifts towards lower potentials, which is also consistent with the trend of peak A in the CV. Similarly, it is unlikely to be a temperature dependence of the kinetics, as generally an increase in temperature would be expected to increase the speed of a process, which would lead to a positive potential shift instead. Rather, it is a shift in the onset potential

of the formation of the ordered honeycomb phase with increasing temperature. As discussed for peak A in the CV, the mobile adlayer is most likely stable over a higher potential range at increased temperatures due to an increase in the mobility of the adspecies.

4.3. Summary

The Cu-UPD on Au(111) in sulphuric acid was investigated using cyclic voltammetry and chronoamperometry.
A temperature dependence of the $(\sqrt{3} \times \sqrt{3})$R30° structure was found in the CVs as well as the coverage obtained from the chronoamperometry. The potential range of stability of the ordered structure shifts to lower potentials with increasing temperature due to the increasing mobility of the adspecies. The higher mobility leads to the mobile adlayer being energetically favourable compared to the ordered structure. Furthermore, the phase transition becomes faster with increasing temperature, which is also likely to be due to the increased mobility of the adspecies. The formation of the full copper monolayer does not show a temperature dependence, with no change of the peak position in peak B as well as the potential of the second step in the θ-E curves. However, the transition of the copper monolayer to the $(\sqrt{3} \times \sqrt{3})$R30° structure is affected by the temperature. The transition becomes faster with increasing temperature, possibly due to the increased mobility of the ions.
All in all, the Cu-UPD on Au(111) in sulphuric acid shows a dependence on the temperature mainly due to the increased mobility of the adspecies with increasing temperature.

5. Au(111) in 0.1 M perchloric acid

It is known that sulphate specifically adsorbs on Au(111) and also has a strong influence on the UPD process when copper is added. Perchlorate has a more strongly bound hydration shell and is thus also less strongly adsorbing than sulphate.[19] It can be considered to have a weaker influence on the UPD than sulphate on Au(111), and is thus good as contrast when investigating whether the effects are due to the nature of the anion. For the investigation of the temperature effect on the Cu-UPD in perchloric acid it had been necessary to first systematically establish the effects on the electrochemistry without copper. While some studies have been done on that previously, it was thought prudent to perform a study under the same conditions as the Cu-UPD for better compatibility.

5.1. Experimental results

For the investigation of Au(111) in perchloric acid, CVs at different scan rates and temperatures (see Ch. 2.3) have been taken to show the scan rate as well as temperature dependence. Since the scan rate and the temperature both can affect the CV, both dependences as well as their dependence on each other have to be considered. Fig. 5.1 shows CVs of Au(111) in 0.1 M perchloric acid at 20°C and 40°C with the peaks labelled for convenience. PA2 expresses as shoulder of peak PA1, which heightens the error on the estimation of the peak potential because of the overlap. Peak B also shows some overlap with PA2, leading to the same problem. For peak D/D', the peak position cannot be estimated with sufficient accuracy due to the broadness of the peak. Peaks PD1, PD2 and PD3 may also be affected by overlap with each other.
Fig. 5.2 and 5.3 show the same CVs in 0.1 M perchloric acid depending on the scan rate and temperature, respectively. For the scan rate dependence, the current density j was scaled for easier comparison as already explained in Ch. 3.

(a)

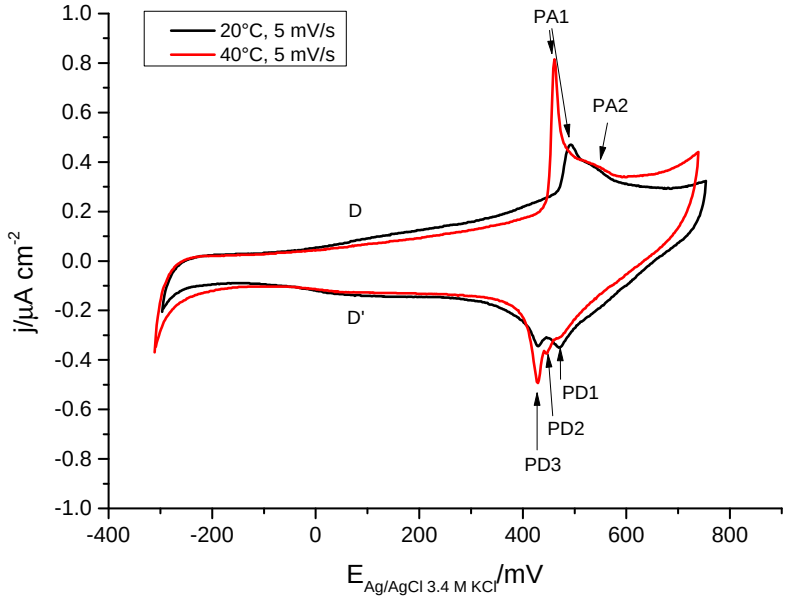

(b)

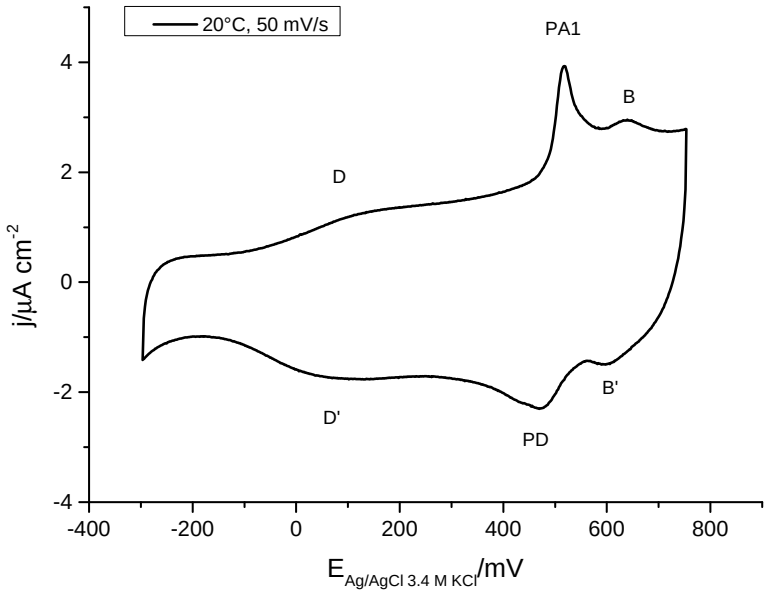

Figure 5.1.: CVs with labelled peaks for (a) 5 mV/s at 20°C and 40°C and (b) 50 mV/s at 20°C

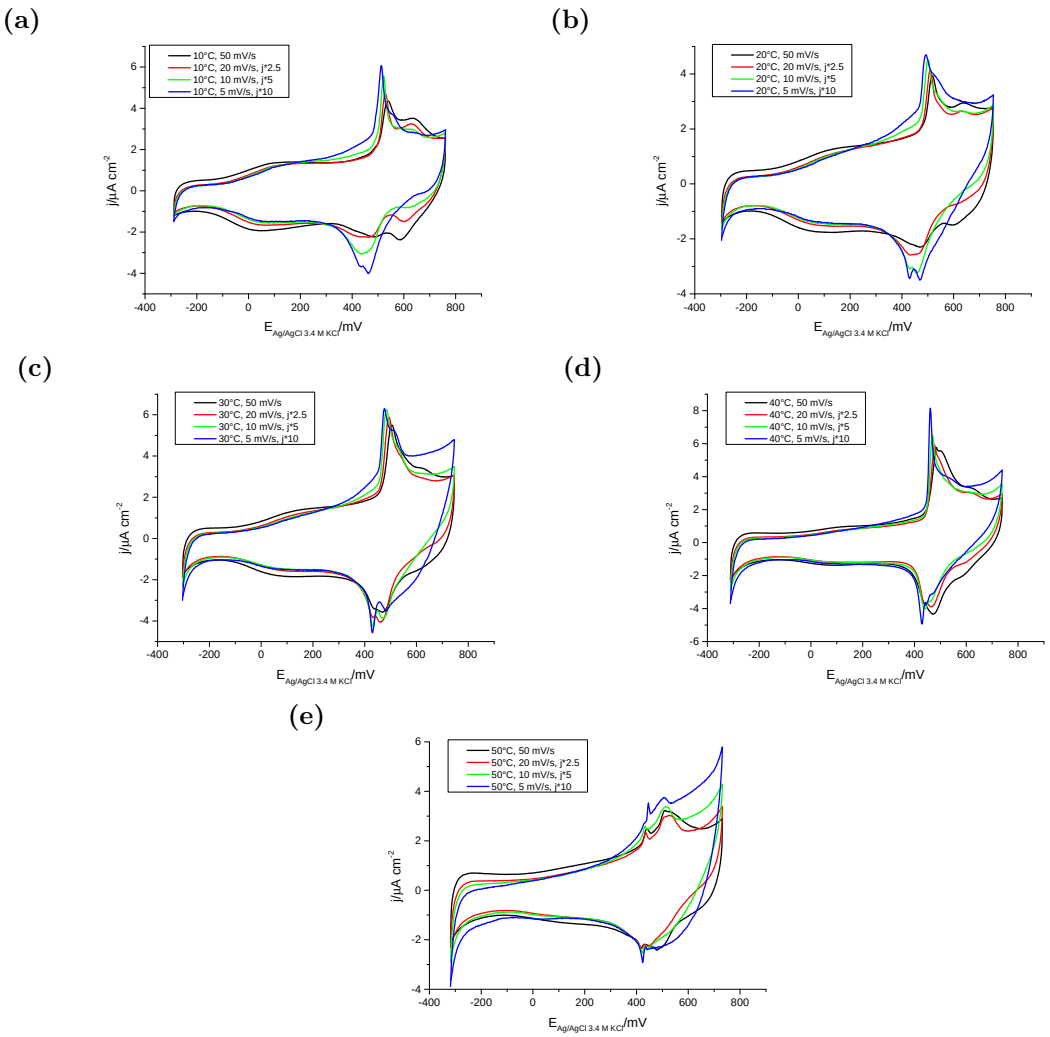

Figure 5.2.: CVs of Au(111) in 0.1 M perchloric acid at scan rates of 50 mV/s, 20 mV/s, 10 mV/s and 5 mV/s for (a) 10°C, (b) 20°C, (c) 30°C, (d) 40°C and (e) 50°C. For the lower scan rates, the current density j has been scaled.

Meanwhile, Fig. 5.4 and 5.5 show the approximate potential of the peak maxima depending on the scan rate and temperature respectively. For the temperature dependence, there is a decrease in the potential window with increasing temperature.

Peak PA1 shows decreasing peak potential with increasing temperature as well as with decreasing scan rate (see Fig. 5.5a and 5.4a). However, the scan rate dependence shows no change with the temperature, except for 50°C, where the trend differs from the one seen at the other temperatures. 50°C also shows a

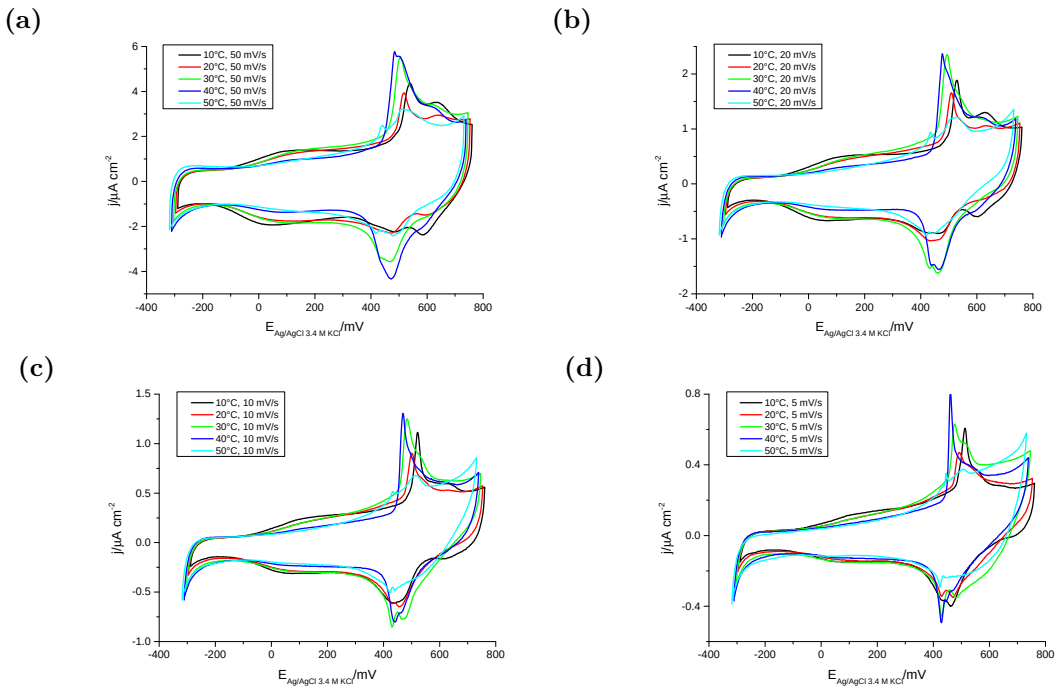

Figure 5.3.: CVs of Au(111) in 0.1 M perchloric acid at 10°C, 20°C, 30°C, 40°C and 50°C for (a) 50 mV/s, (b) 20 mV/s, (c) 10 mV/s and (d) 5 mV/s.

marked decrease in the peak current density of peak PA1 compared to the other temperatures (see Fig. 5.3d).

Peak PA2 expresses as a higher-potential shoulder of peak PA1, which impacts the determination of the peak position, as mentioned previously. A strong overlap can also mask the peak, especially at high scan rates, thus at some scan rates and temperatures the peak position for peak PA2 could not be determined. It also shows decreasing peak potential with increasing temperature and decreasing scan rate like peak PA1 (see Fig. 5.5b and 5.4b). The temperature and scan rate dependences do not show a dependence on each other.

Peak PD1 (see Fig. 5.5c and 5.4c) does not show a clear temperature or scan rate dependence. The peak current density of PD1 also seems to decrease with decreasing scan rate, especially at high temperatures (see Fig. 5.2).

Peak PD3 (Fig. 5.5d and 5.4d) does not show a clear temperature dependence. There is little change with the scan rate except for 10°C and 40°C. Furthermore, PD3 seems to grow with decreasing scan rate, especially at higher temperatures (see Fig. 5.2). The peak current density for PD3 is higher at 30°C and 40°C

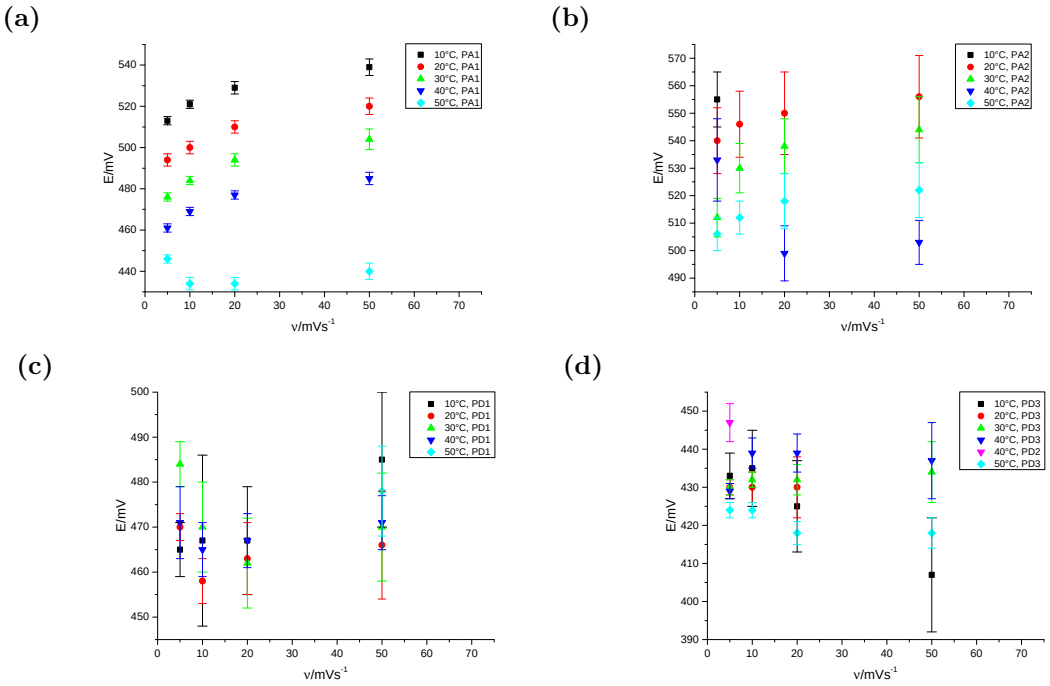

Figure 5.4.: Change of the peak positions with scan rate ν at different temperatures for (a) PA1, (b) PA2, (c) PD1 and (d) PD3 (PD2 included for 40°C).

compared to the lower temperatures. It does decrease at 50°C compared to the other temperatures, but is still higher at that temperature compared to the surrounding peaks (see Fig. 5.3d).

Generally, Fig. 5.2 and 5.3 show strong overlap and broad peaks for PD1 to PD3 at high scan rates and low temperatures, with the overlap decreasing as well as the peaks becoming sharper with decreasing scan rate as well as increasing temperature.

Peak B and B' appear at high scan rates and low temperatures and show a decrease in the peak current density with decreasing scan rate as well as increasing temperature. The peak position does not appear to show a strong dependence on the scan rate or the temperature, though the peak position could not be determined accurately enough to determine if there is a less strong dependence.

The peak current density of peak D and D' decreases with increasing temperature (see Fig.5.3). At high scan rates, strong changes in the peak current density happen at 20°C and at 40°C, while at lower scan rates the change is mostly at 40°C. At high temperatures D and D' vanish. Furthermore, at low scan rates the

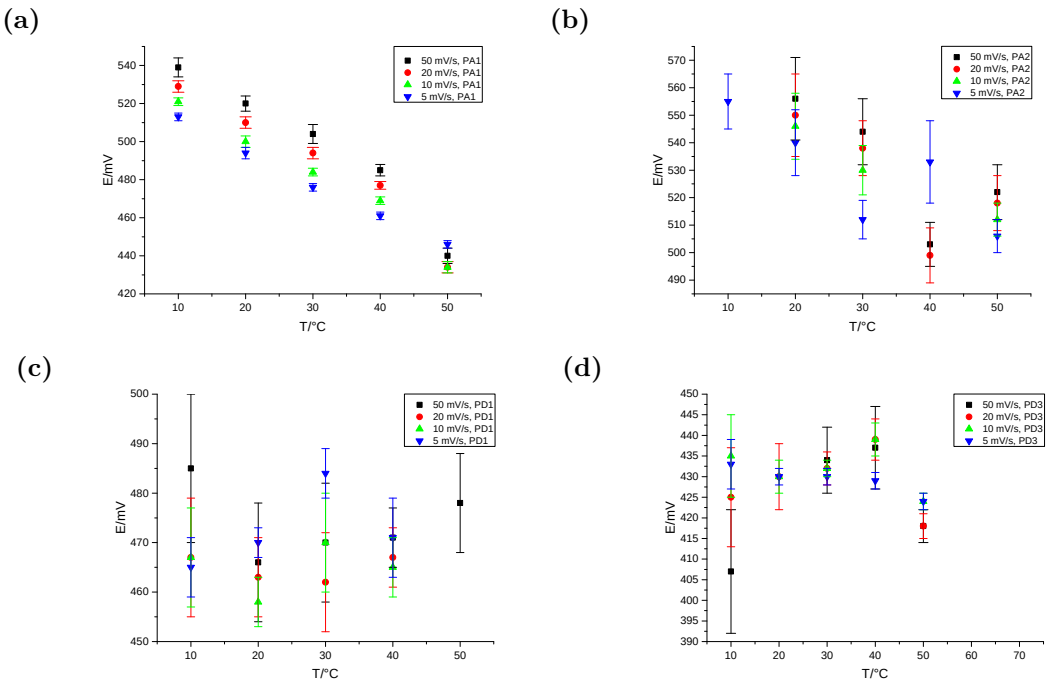

Figure 5.5.: Change of the peak positions with the temperature at different scan rates for (a) PA1, (b) PA2, (c) PD1 and (d) PD3

change in the peak current density with the temperature is less strong than at high scan rates, implying a scan rate dependence that cannot be determined from Fig. 5.2 due to the scaling possibly influencing the relative peak heights.

5.2. Discussion

The decrease of the potential window with increasing temperature is likely due to the HER starting at higher potentials with increasing temperature as well as a possible earlier onset of the oxidation with increasing temperature. The onset potential of the HER increasing at higher temperatures has also been shown by Hamelin et al.[72] for Au(111) in perchloric acid and was thus to be expected.

5.2.1. PA1,PA2 and PD1 to PD3

Peak PA1 and PA2 as well as PD1 to PD3 are likely connected to the adsorption/desorption of the anion, which could be either chloride or perchlorate or both.

The potential range matches the one in the literature for the perchlorate adsorption/desorption coupled with the surface reconstruction lifting/formation.[65,67,72] However, the set of peaks found in the literature is broader, as well as being composed of one anodic and one cathodic peak.[65,67,72] Furthermore, they show a strong hysteresis due to the coupling with the surface reconstruction.[65,67] Zhumaev et al.[65] showed that the hysteresis of the peaks disappears if the surface reconstruction is decoupled from the adsorption/desorption process. This was achieved by Zhumaev et al.[65] by using a high scan rate, which meant the measuring time was too fast for the formation of the reconstruction.
In Ch. 3 it was already shown that the surface reconstruction on the single crystal seemed to be at the very least inhibited. Thus, the low hysteresis of PA1 and PA2 and PD1 to PD3 might indicate that the adsorption/desorption process was decoupled from the reconstruction due to the inhibition of the reconstruction. While Zhumaev et al.[65] only saw a broad peak for the decoupled adsorption/desorption, this could be due to the very high scan rate of 10 V/s masking details of the peaks. As such, it is assumed that PA1 and PA2 are due to anion adsorption, while PD1 to PD3 represent the anion desorption.

PA1

PA1 has a decrease of the peak potential with both increasing temperature as well as decreasing scan rate, except for no significant trend with the scan rate at 50°C. There is also a strong decrease in the charge density compared to the other temperatures at 50°C. Assuming the peak is the adsorption of perchlorate, the complete process consists of diffusion to the surface, partial stripping of the hydration shell and adsorption on the surface. As the coverage of perchlorate is rather low and the electrolyte is 0.1 M perchlorate, any diffusion limitation seems unlikely. Furthermore, the work of Zhumaev et al.[65] suggests no diffusion or charge-transport limitation of the adsorption/desorption of perchlorate. If it is due to the adsorption of trace chloride, the process would most likely be diffusion limited due to the low chloride concentration.
Besides 50°C, the form of the scan rate dependence is the same at all temperatures, which further indicates that it is unlikely to be diffusion limited. If it were diffusion limited, the speed of the diffusion would increase with the temperature, thus at elevated temperature the diffusion limitation would be at higher scan rates

compared to lower temperatures. As such, it is more likely to be the adsorption of perchlorate as it shows no diffusion limitation.
The adsorption of perchlorate on the surface itself is also unlikely to be the cause, leaving the partial stripping of the hydration shell. Perchlorate has a strongly bound hydration shell which is the reason for it being only weakly adsorbing. The most likely explanation would be that the increase in kinetic energy due to the increase in temperature weakens the bonds to the hydration shell, as it would increase the movement of the water molecules in the hydration shell. Donets et al.[82] found for chloride and bromide that the increased thermal motion with increased temperature distorts the net of hydrogen bonds and weakens the structure of the solvation shell, even increasing the number of water molecules in the hydration shell. While these results were not for perchlorate, it is assumed that increasing temperature would have similar effects. A more weakly bound solvation shell would allow for the removal of the water molecules from the hydration shell at lower potentials without influencing the speed of the removal. At 50°C, there is a change in the process, as it shows no scan rate dependence as well as having a strongly decreased charge density. While not enough information is available to reliably ascertain the nature of the change, the decreased charge density indicates a lower coverage of perchlorate, while the change in scan rate dependency indicates a change in the kinetics of the process compared to lower temperatures.

PA2

Due to overlap, PA2 cannot be seen at higher scan rates at 10°C, and the position cannot be estimated at 10 mV/s at 40°C. The general trend is a decreasing peak potential with increasing temperature as well as decreasing scan rate. Furthermore, the dependence on the scan rate at different temperatures stays very similar. However, 40°C does not follow the trends concerning scan rate and temperature. It had been noted that at 40°C and 10 mV/s there could possibly be two shoulders. Furthermore, if one assumed this was true, then 50 mV/s and 20 mV/s mainly expressed the lower potential shoulder while 5 mV/s showed the higher potential shoulder, explaining the rather strong potential shift at 5 mV/s. Also, at 50°C 50 mV/s and 20 mV/s, the CVs the peak assigned PA2 could be the overlap of two peaks.
If there are actually two peaks and the distinction at 40°C is clearer, that would

account for the deviation at 40°C, as the peak potential of the separate peaks would be different from the one gotten from overlap. The trends excluding 40°C are very similar to PA1, except without the strong change at 50°C. As said previously, it is in the right potential range for perchlorate adsorption, but there is not enough evidence to be able to confidently assign the peak to a process. However, it is unlikely to be due to trace chloride adsorption since the scan rate dependence does not show a systematic change with the temperature. This would indicate that there is no diffusion limitation, which would be expected for the adsorption of an anion only present in trace amounts.
If PA2 is due to perchlorate adsorption, the considerations made for PA1 should also apply to it, except the change at 50°C. Furthermore, due to the strong overlap between PA1 and PA2, the scan rate and temperature dependence of PA2 may also be affected by the overlap with PA1, which would also explain the similarities. Last but not least, considering that any evidence of PA2 being two overlapping peaks is only visible at or above 40°C, it is possible that this is due to the change in the surface defects due to better electrochemical annealing at those temperatures.

PD1 to PD3

For peak PD1 to PD3, the strong overlap at high scan rates tends to mask the individual peaks, which makes the peak potential less reliable at high scan rates due to the higher error. As previously said, they are likely to be the desorption processes for the adsorption connected to PA1 and PA2. PD1 and PD3 also show a strongly decreased peak current density at 50°C, mirroring PA1 and PA2, which would be expected if they are the desorption processes. PD1 does not show a systematic change with the scan rate or temperature, however the peak current density decreases with decreasing scan rate, especially at high temperatures. This is the opposite of PD3, which shows an increasing current density with decreasing scan rates, also especially at high temperatures. Since both of the peaks are likely to be connected to the same type of process, this might be due to a change in the contribution of each process.
PD3 also does not show a systematic change with the temperature or scan rate. At 10°C, there is an increasing peak potential with decreasing scan rate, but due to the broadness of the peak and the high overlap this might be falsified by the aforementioned factors. 40°C shows a strong change in the peak potential at

5 mV/s compared to higher scan rates, which might be due to PD2, which appears at 5 mV/s at 40°C and has the same displacement towards higher potentials as PD3 has towards lower potentials at this scan rate compared to the higher ones. This might indicate a peak splitting that is only visible at that scan rate.
The lack of a change in the peak potential with the scan rate or temperature for PD1 to PD3 contrasts with the dependences of PA1 and PA2. Since the adsorption peaks do have a peak potential dependent on the scan rate and temperature, the kinetics of adsorption and desorption are different. However, the lack of dependence is not surprising if one looks at the reverse of the previously assumed steps for the process of the adsorption peak, namely desorption of perchlorate, re-establishment of the full hydration shell and diffusion away from the surface. The diffusion would not affect the kinetics of the desorption. The desorption of perchlorate is likely to be fast as well, due to perchlorate being a rather weak adsorbate. For the adsorption, the likely reason for the temperature and scan rate dependence is the stripping of the hydration shell being slow. However, due to perchlorate having a strongly bound hydration shell and water being the solvent, the re-establishment of the hydration shell should also be a fast process. Thus, no part of the whole process should limit the reaction, leading to no temperature or scan rate dependence, contrary to the adsorption, where the partial stripping of the hydration shell likely limits the process.

5.2.2. B/B'

Peak B and B' are linked, as the later only appears together with the former, thus showing B' to be due to the reverse process of peak B. Due to the rather broad peak and the shape of the CV being convex in that part of the CV, B' is sometimes not visible while B can still be seen. No clear trend of the peak potential with the temperature or scan rate can be established for either peak, though the peaks disappear with decreasing scan rate and increasing temperature. There is not enough information to be able to ascertain the process connected to the peaks.

5.2.3. D/D'

Peak D and D' are due to surface defects according to Hamelin et al.,[72] more specifically they found these peaks after oxidation. Therefore, Hamelin et al.[72] postulated that they were due to monoatomic pits and terrace edges. Furthermore, Hamelin et al.[72] found that they vanished at 41°C, which was attributed to faster electrochemical annealing at higher temperatures.
Electrochemical annealing, which happens in the double-layer region, can remove these surface defects.[72] The stability of those surface defects during cycling depends on the kinetics of the electrochemical annealing.[72] At low temperatures, the electrochemical annealing is slow and thus does not remove the defects on a time scale that would not affect the measurement.[72] At higher temperatures, the reaction becomes faster and thus at 40°C and above the defects are not stable enough to affect the measurement.[72]
Similarly, Fig. 5.2 and 5.3 show that peak D/D' decrease at 20°C and vanish at 40°C, though the change is less at lower scan rates. This is in accordance with the findings of Hamelin et al.[72] The appearance of D and D' thus depends on how long the surface defects are stable compared to the measuring time of the CV. At low temperatures, they are stable for longer times, while the faster annealing at high temperatures decreases the time the defects are stable for. For the appearance of the peaks in the CV, the other factor would be the time scale of the measurements. High scan rates mean a short measuring time, while low scan rates increase the measuring time. Thus, for the peaks to appear in the CV, the stability time of the defects cannot be small compared to the measuring time. As such, the found decrease of peak D and D' with increasing temperature as well as peak D and D' being stronger expressed at higher scan rates is to be expected. Similar to the results of Hamelin et al.,[72] the electrochemical annealing at 40°C and above is too fast for the defects to appear in the measurement. Otherwise, the peak current density depend on the ratio of the measurement time to the time it takes to anneal the defects. Thus, at high scan rates peak D/D' is more strongly expressed as the measurement time is shorter than at lower scan rates, where more time is available during the measurement for the surface defects to be annealed.
Moreover, as the temperature dependence shows thresholds rather than a steady

decrease, it is likely that the faster electrochemical annealing with increasing temperature is due to overcoming activation energy barriers. If the effect was due to an increased kinetic energy and thus higher mobility leading to faster surface diffusion, there would be a slight change with each increase in temperature, as each increase in temperature would be an increase in the speed of the surface diffusion. Thresholds point towards discrete barriers that would need to be overcome.

5.3. Summary

CVs of Au(111) in perchloric acid at different scan rates and temperatures were measured to investigate the temperature dependence of the system. Indications of faster electrochemical annealing with increasing temperature in accordance with the results of Hamelin et al.[72] were found. Similar to the results in sulphuric acid in Ch. 3, the surface reconstruction of the Au(111) crystal was not observed. The adsorbed anion is likely to be perchlorate as the anodic peaks, which represent the anion adsorption, do not show indications of a diffusion limitation. As chloride, which would be the other possible anion, is at the most present at a trace concentration, the adsorption of chloride would be diffusion limited. Therefore, since no diffusion limitation was observed, the adsorbed anion is unlikely to be chloride.

While the anodic peaks show a dependence on both the temperature and the scan rate, the cathodic peaks show a dependence on neither. As the cathodic peaks represent the perchlorate desorption, the temperature dependence seems to be due to one of the steps inherent in the adsorption of perchlorate. Since perchlorate has a strongly bound solvation shell, the temperature dependence is likely due to the increasing temperature decreasing the energy necessary to partially strip the solvation shell of the perchlorate.

All in all, there is an influence of the temperature and the scan rate on CVs of Au(111) in 0.1 M perchloric acid. The main effects seem to be due to electrochemical annealing and the partial stripping of the hydration shell requiring less additional energy with increasing temperature.

6. Copper underpotential deposition on Au(111) in 0.1 M perchloric acid

The temperature dependence of the Cu-UPD on Au(111) in perchloric acid was investigated using cyclic voltammetry as well as chronoamperometry to determine the copper coverage as well as the kinetics of the process. Furthermore, the possibility of surface alloying was investigated using chronoamperometry.

6.1. Experimental results

Due to the use of two different electrochemical techniques, the section is split into parts pertaining to the results from each technique. The analysis and discussion of the results is left for the next section. The used measurement conditions and protocols can be found in Ch. 2.4. The peaks of the CV are labelled in Fig. 6.1 for convenience.

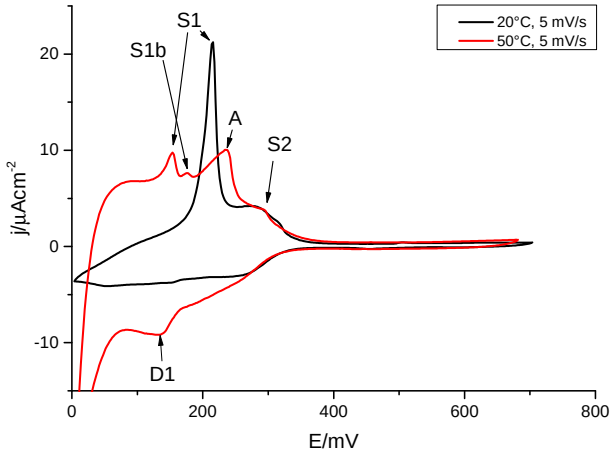

Figure 6.1.: CV of the Au(111) single crystal in 0.1 M perchloric acid 1 mM copper perchlorate at 20°C and 50°C for 5 mV/s with labelling for the peaks.

6.1.1. Cyclic voltammetry

For the investigation of the system, CVs at different temperatures and different scan rates were taken. Both the scan rate and the temperature can, as stated before, influence the CV, and thus investigating both dependences provides more information as well as precluding erroneous conclusions due to neglecting one influence. The CVs are presented to show the scan rate dependence in Fig. 6.2 and the temperature dependence in Fig. 6.3. Again, the current density for the scan rate dependence was scaled to allow for easier comparison, as explained in Ch. 3. The peak potential for the anodic peaks was plotted against the scan rate in Fig. 6.4 and against the temperature in Fig. 6.5. Due to the kinetic hindrance, the cathodic peaks for the copper deposition are very broad and thus the peak potential could not be established with sufficient accuracy to be of use.
Generally, the peak separation of the anodic peaks increases with decreasing scan rate, with a strong overlap at high scan rates which can preclude the identification of separate peaks. Furthermore, at low scan rates there is a falling current at the lower potential limit, which increases with increasing temperature. Thus, at higher temperatures it can also be seen at higher scan rates compared to lower temperatures.

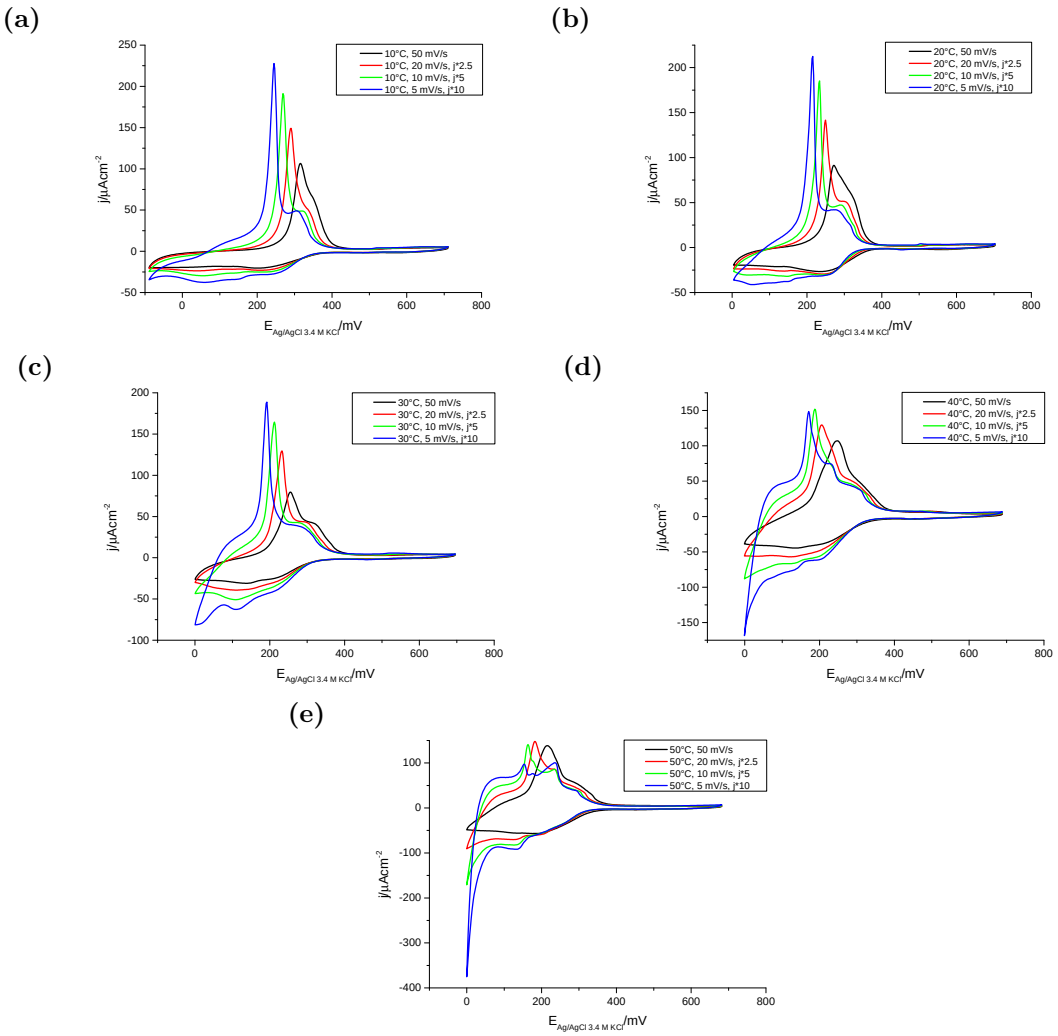

Figure 6.2.: CVs of Au(111) in 0.1 M perchloric acid 1 mM copper perchlorate at scan rates of 50 mV/s, 20 mV/s, 10 mV/s and 5 mV/s for (a) 10°C, (b) 20°C, (c) 30°C, (d) 40°C and (e) 50°C. The CVs for 20 mV/s, 10 mV/s and 5 mV/s have the current density j scaled for convenience by a factor of 2.5, 5 and 10, respectively.

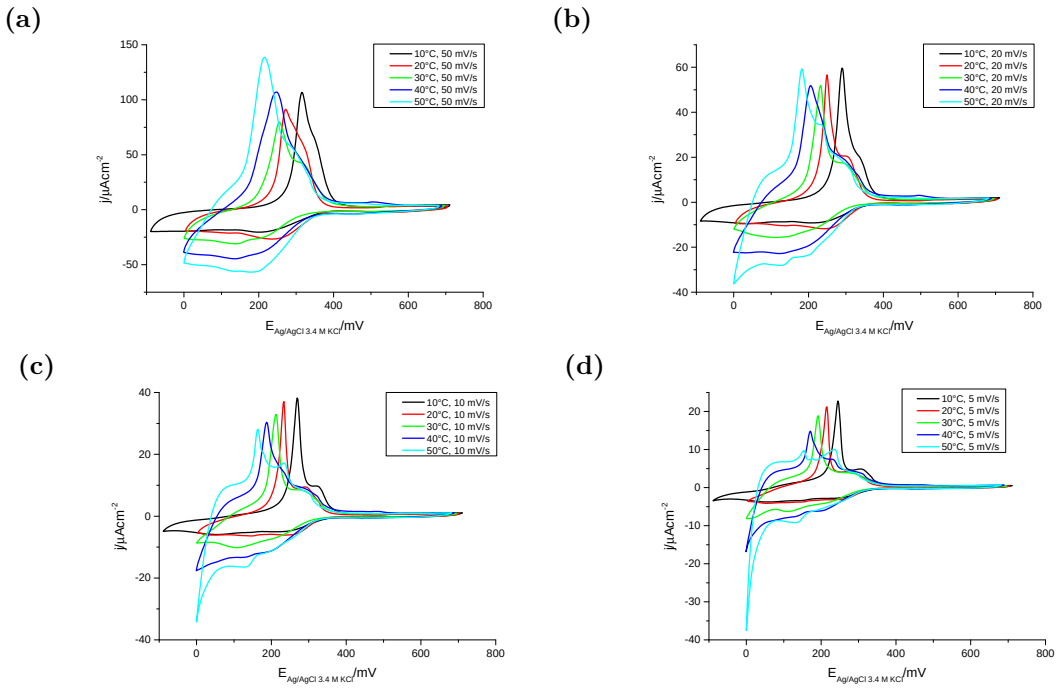

Figure 6.3.: CVs of Au(111) in 0.1 M perchloric acid 1 mM copper perchlorate at 10°C, 20°C, 30°C, 40°C and 50°C for (a) 50 mV/s, (b) 20 mV/s, (c) 10 mV/s and (d) 5 mV/s.

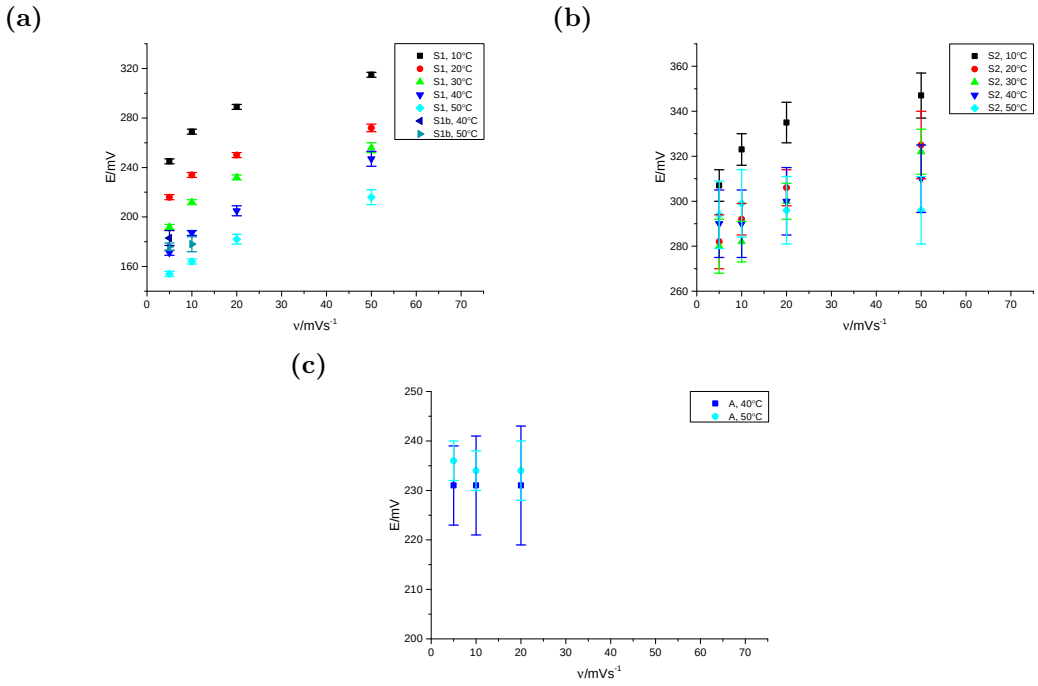

Figure 6.4.: Change of the peak positions with the scan rate ν at different temperatures for (a) peak S1 and S1b, (b) peak S2 and (c) peak A.

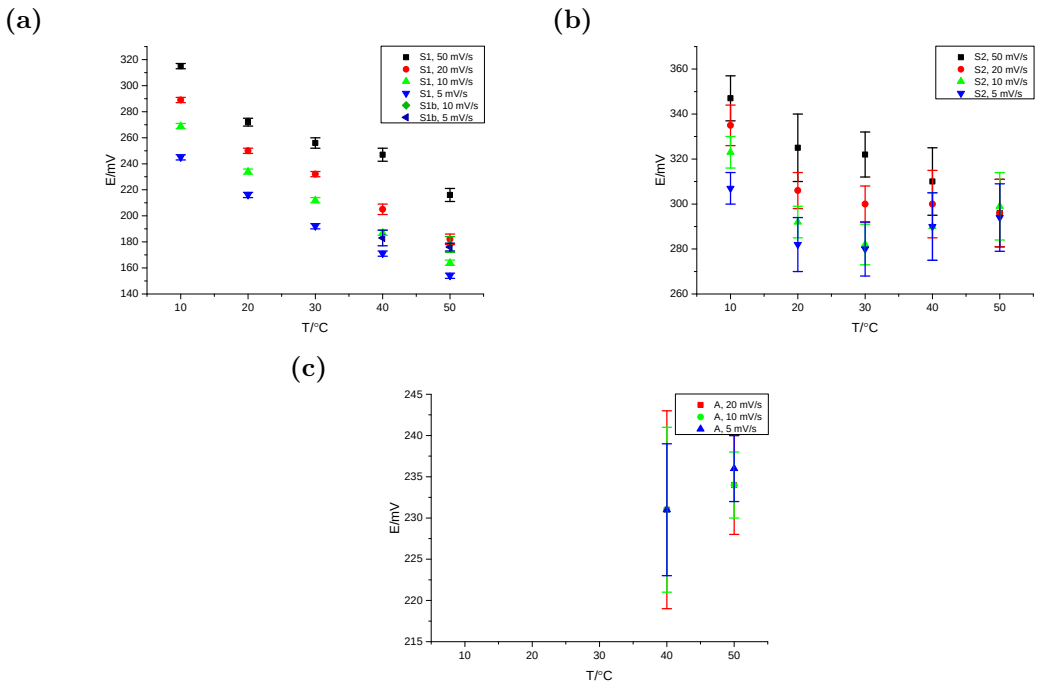

Figure 6.5.: Change of the peak positions with the temperatures at different scan rates for (a) peak S1 and S1b, (b) peak S2 and (c) peak A.

Peak S1 shows a decreasing peak potential as well as a sharpening of the peak with decreasing scan rate (see Fig. 6.4a). The peak potential also decreases with increasing temperature (see Fig. 6.5a). At low scan rates and high temperatures, a peak splitting can be observed, with the second peak labelled S1b. However, the trend of peak S1 in those instances is the same as at higher scan rates or lower temperatures. For peak S1b, not enough data points exist to extract a trend.
Peak S2 shows a strong scan rate dependence at lower temperatures, with 10°C and 20°C showing a decreasing peak potential with decreasing scan rate. However, at higher temperatures, the lower scan rates show little change in the peak potential, with 50°C showing no significant change of the peak potential with the scan rate (see Fig. 6.4b). For the temperature dependence of the peak potential (see Fig. 6.5b), only 50 mV/s shows a decreasing peak potential with increasing temperature, which could also be due to scan rate effects. For the other scan rates, there is a decrease of the peak potential between 10°C and 20°C, with the peak potential for the other temperatures showing no significant change when considering the error.
Peak A is only visible at 40°C and 50°C, and shows no significant dependence on the scan rate while there are not enough data points to establish a temperature dependence (see Fig. 6.4c and Fig. 6.5c).

6.1.2. Chronoamperometry

For the determination of the kinetics as well as the coverage, chronoamperometric transients were taken for each temperature. The starting potential for all transients was 0.6 V, with the end potentials between 0.3 V and 0 V in 50 mV steps. After each transient, the potential was returned to the starting potential. The transients are shown in Fig. 6.6. Generally, a falling current over time is observed. However, at lower end potentials and lower temperatures, two separate current peak were observed, which shift towards earlier times with increasing temperature. For 0 mV end potential and 50°C, there is an observed oscillation after 90 s. This was taken to be due to an external influence, but the data up to 80 s was used as no better dataset was available and further measurements were not possible.

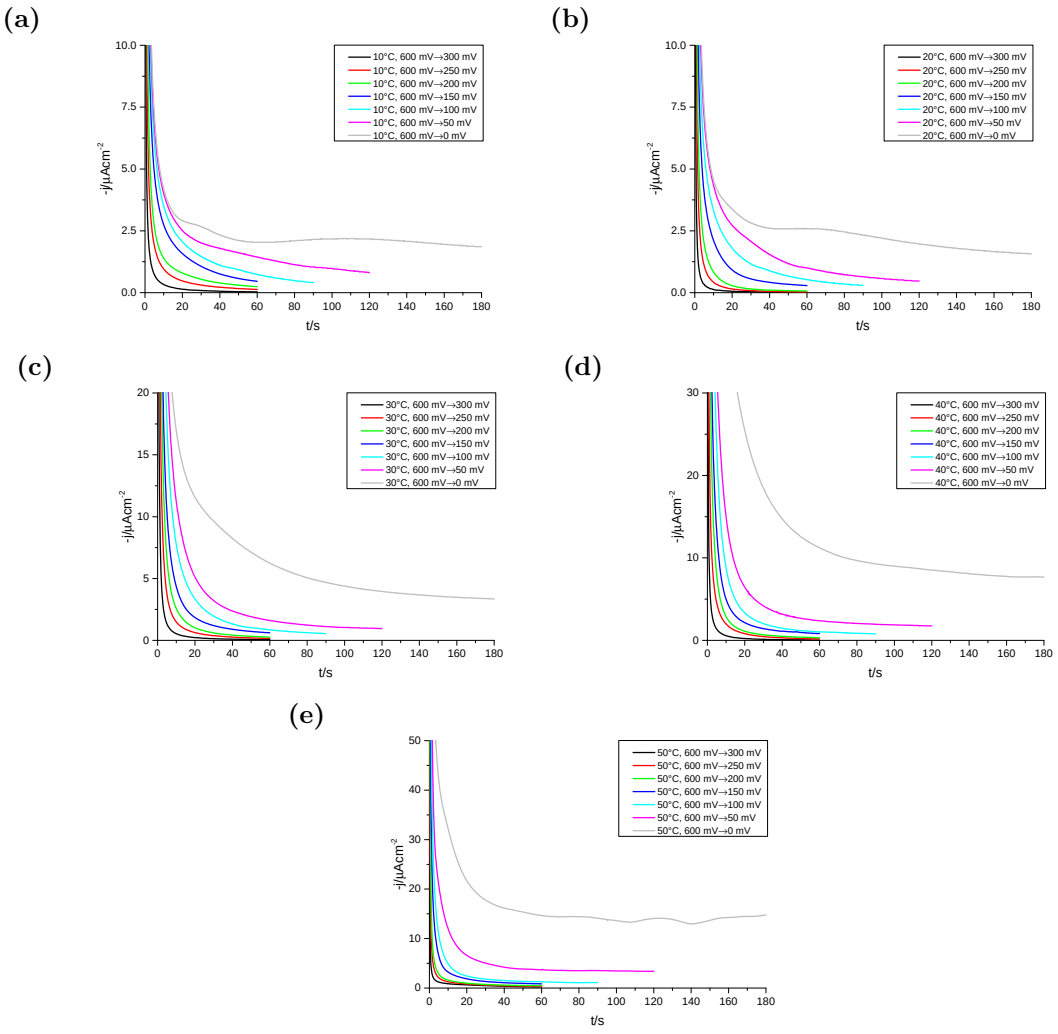

Figure 6.6.: Transients for Au(111) in 0.1 M perchloric acid 1 mM copper perchlorate with a fixed starting potential of 0.6 V at (a) 10°C, (b) 20°C, (c) 30°C, (d) 40°C and (e) 50°C.

Alloying

Since there was evidence of a possible copper-gold surface alloy forming, an experiment using chronoamperometric transients was designed to test this. Since the transient for fixed starting and end potential should not change unless the system changed, a transient for the dissolution of the adlayer with a starting potential before the alloying, in this case 180 mV to 600 mV, was chosen to be compared depending on the history of potential jumps before this transients. To validate the choice of transient, the potential was jumped from 600 mV to 180 mV and held there for 60 s, before returning to 600 mV. This was repeated to give the transients labelled baseline (1) and (2). Then, the potential was held at a lower potential thought to be in the alloying range (alloying potential) for either 60 s or 120 s before being held at 180 mV for 60 s, after which the transient from 180 mV to 600 mV was measured. The 60 s at 180 mV were to insure that the starting surface for the transient was consistent baring surface changes due to the history that were irreversible in that time frame. If the surface of the crystal was not changed, then the transients should show no significant change. The repeat of the baseline transient was to show that any change would be due to the jump to potentials lower than 180 mV. This was done representatively for 10°C and 50°C.

The transients for this experiment are shown in Fig. 6.7. The baseline transients are consistent, while there is a systematic change in the transient depending on the alloying potential and holding time at that potential. There is also a difference depending on the temperature. At 10°C, there is a change depending on the holding time at the alloying potential, with the transient for 120 s being similar to the one at 60 s for the next lower alloying potential. On the other hand, 50°C does not show significant change depending on the holding time at the alloying potential.

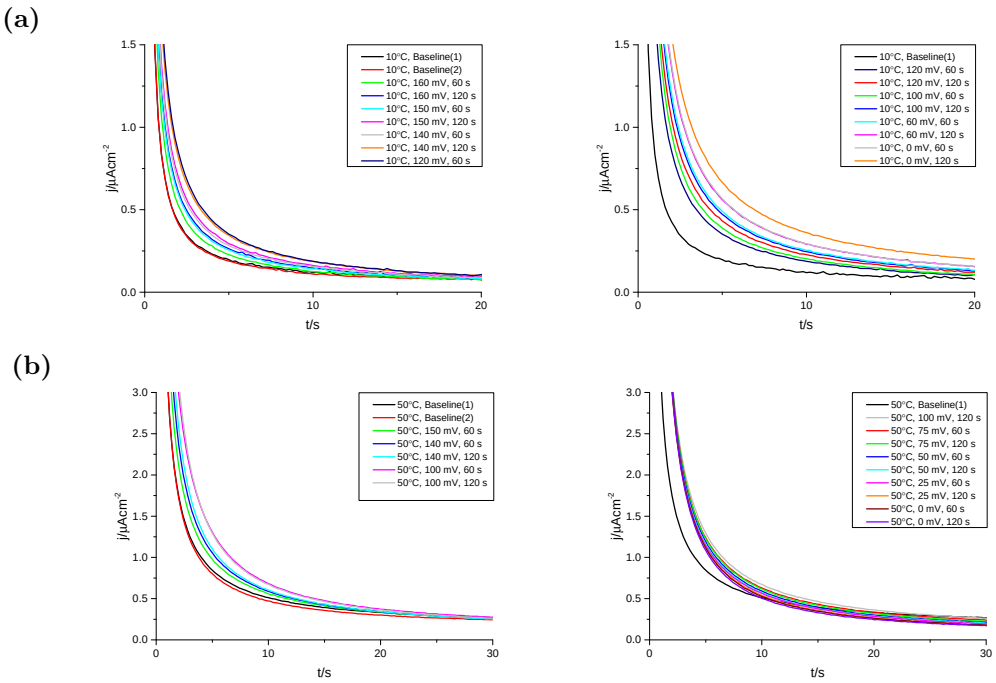

Figure 6.7.: Transients for Au(111) in 0.1 M perchloric acid 1 mM copper perchlorate for 180 mV→600 mV at (a) 10°C and (b) 50°C. The alloying potential as well as the holding time at that potential are indicated for each transient.

6.2. Analysis & discussion

6.2.1. Cyclic voltammetry

For the peaks of the CV (see Fig. 6.1), S1 and S2 are known from the literature. According to both Hotlos et al.[74] and Krznaric et al.,[73] S1 is the transition of a (2x2) adlayer with $\theta_{Cu} = 0.75ML$ to a structure with a lower copper coverage. While Hotlos et al.[74] attributes this structure to a coadsorption of copper and chloride, with $\theta_{Cl} = 0.25ML$, the results of Krznaric et al.[73] indicate a coadsorption of copper, chloride and perchlorate. For the structure that is formed due to the transition, Hotlos et al.[74] indicated that it is likely a "(5×5)" structure of coadsorbed copper and chloride, with $\theta_{Cu} = 0.64ML$, though a disordered, metastable phase was also found. Krznaric et al.[73] found that at low chloride concentrations, the formed structure should be different from the "(5×5)" adlayer, which would mean it could be the disordered, metastable adlayer. As the formed structure has a lower copper coverage and thus should have a higher chloride coverage, a kinetic limitation due to the diffusion limited transport of copper to the interface is possible.[74]

For S2, it would be the dissolution of the phase formed in the transition represented by peak S1, which could be either the disordered, metastable phase or the "(5×5)" adlayer.[73,74] This peak was also shown by Hotlos et al.[74] and Krznaric et al.[73] to be very sensitive to the chloride concentration, meaning it can be used as a way to approximate the amount of chloride in the electrolyte to establish the likely processes, as the Cu-UPD in perchloric acid is strongly influenced by the chloride concentration. While there is an inherent chloride concentration in perchloric acid, S2 in Fig. 6.3d does not show much change with the temperature, which would indicate that the chloride concentration does not significantly change at the different temperatures. Also, the rather low peak S2 coupled with the broad deposition peaks as well as the absence of anodic peaks beyond the labelled ones are indications of a chloride concentration below 10^{-6} M,[73,74] so any residual chloride is likely due to the inherent chloride in perchloric acid. Also, since there seems to be no change of the chloride concentration with the temperature, any changes in the CV with temperature are not due to a change in the chloride concentration.

Since the CVs indicate a very low chloride concentration, it is more likely that

peak S2 does not represent the dissolution of the "(5×5)" phase, but rather another structure, which was assumed to be the disordered, metastable adlayer, though not enough information exists to be able to confidently assign the structure. As already shown in Ch. 1.4.4, the results of Krznaric et al.[73] indicate a different structure for peak S2 at low chloride concentrations, which likely wasn't seen at those concentrations in the STM by Hotlos et al.[74] due to the tip influencing the local chloride concentration. As Hotlos et al.[74] also found the disordered, metastable adlayer at low chloride concentration using STM, it was seen as likely that this could be the structure at low chloride concentrations.
While the chronoamperometry will be discussed in more detail later, the transients in Fig. 6.7 indicate a change in the surface at potentials below 180 mV, which is assumed to be due to surface alloying of copper and gold, as already indicated by Hotlos et al.[74] The transients also indicate that the alloying is faster at higher temperatures. As a change in the surface would influence the resulting CV, it was seen as necessary to mention this for the discussion of the CVs. Peak A is only visible at high temperatures and scan rates below 50 mV/s. Its growth has also been found to coincide with changes in the cathodic part of the CV that were seen to likely be due to the surface alloying. The appearance at only high temperatures and lower scan rates is likely due to the kinetics of the alloying, which is indicated to be faster at higher temperatures. Likely, at low temperatures, the alloying is slow enough to not influence the CV in the time frame of the measurements, while at higher temperatures the alloying is fast enough to be seen at the lower scan rates. Furthermore, peak A increased if the potential was held in the alloying range during the CV. Thus, peak A was assigned to the dissolution of the surface gold-copper alloy.
The appearance of peak S1b coincides with the appearance of peak A. As it is an anodic peak at lower potentials than peak A, this would mean the surface is still alloyed for this peak. Since a surface alloy means the surface is not only gold, but both gold and copper, and peak S1 is the transition of the (2x2) phase on gold, this would mean it is likely that peak S1b is due to the process of S1 being influenced by the copper-gold surface alloy.
The scan rate dependence of peak S1 (see Fig. 6.4a) coupled with the slight sharpening of the peak with decreasing scan rate could indicate a kinetic limitation, which would likely be due to the diffusion-limited transport of chloride to the

interface according to Hotlos et al.[74] However, the scan rate dependence does not show a strong dependence on the temperature, which would be the case if it was diffusion-limited, as the increase in kinetic energy due to the increase in temperature would increase the speed of the diffusion. While chloride is a minority species, at least some dependence of the scan rate dependence on the temperature would be expected if it was due to diffusion-limitation. Hotlos et al.[74] postulated an island-growth from the STM images for the transition of the (2x2) phase of peak S1, which would mean a two-dimensional growth, possibly with nucleation. A two-dimensional nucleation and growth process would have a non-linear scan rate dependence at low scan rates, as shown by Bosco et al.[80] However, to test this dependence, at least the peak current density would be needed in addition to the peak potential, which is be hard to accurately determine for all temperatures and scan rates due to overlap and changes of the surface of the crystal due to surface alloying. Thus, while the scan rate dependence might be affected by diffusion-limitation, but likely not very strongly, it could also be due to the nature of the process.

The temperature dependence for peak S1 (see Fig. 6.5a) also shows a decreasing peak potential with increasing temperature. This could be due to the (2x2) phase being less stable at higher temperatures. An increase in temperature increases the thermal energy of the system, which increases the kinetic energy of the anions and cations. An increase in kinetic energy would mean an increase of the mobility of the ions. If the transition for peak S1 is from the (2x2) phase to a disordered phase, then the increasing mobility of the adspecies with increasing temperature would make the disordered phase energetically favourable at higher temperatures. Thus, a decrease of the stability of the (2x2) phase with increasing temperature would be expected. Looking at Fig. 6.3d, peak S1 also seems to have a lower charge density, especially at 50°C. As the strongest decrease of the charge density of peak S1 coincides with the appearance of peak A and thus a likely strong surface alloying also shows that peak S1 is affected by the surface alloying, as would be expected. Possibly, the changes in the surface also influence the peak potential of peak S1.

While not enough data points for most dependences of peak A and S1b are available, except that peak A does not show any dependence on the scan rate (see Fig. 6.4c), there is a strong connection between peak S1, S1b and A. It was said

before that the peaks of the CV are sensitive to surface changes, and a surface alloy would be such a change in the surface. As said previously, the appearance of peak S1b is likely due to the surface alloy, while peak A is the dissolution of the alloy and thus an indication of the amount of alloy formed. While peak S1 shows a decrease in the peak current density with temperature, it is much stronger at 40°C and especially 50°C, with peak A appearing at 40°C and increasing strongly at 50°C. As the charge density of a peak is an indicator of the amount of the correlated phase, it seems that the amount of the adlayer is decreased with increased surface alloying. One reason could be that part of the copper for the formation of the Cu-UPD adlayers is used for the formation of the surface alloy instead, or that the phases don't form on the alloyed surface. However, as there is no strong decrease of peak S2, which is the dissolution of the adlayer formed in the transition of peak S1, the amount of disordered adlayer in the surface after the dissolution of the alloy has to be similar to the ones with less or no significant amount of alloy. As such, if the amount of the adlayers is less while the surface is alloyed, then the dissolution of the alloy also leads to the formation of the rest of the disordered adlayer. In the work of Hotlos et al.,[74] the protrusions suspected to be due to alloying were shown to leave holes in the adlayers once they disappeared, with the holes annealing within minutes. This would support the hypothesis that the full adlayer does not form while the surface is alloyed, with the rest of the appropriate adlayer forming once the alloy is dissolved.

Peak S2 has a strong scan rate dependence of the peak potential which changes with the temperature (see Fig. 6.4b), though the strong overlap, especially at high scan rates, could also influence the dependence. However, the scan rate dependence as well as the peak potential not changing with the scan rate at low scan rates and high temperatures point towards a kinetic limitation. As the kinetic energy increases with increasing temperature, the speed of the process increases. Therefore, the process becomes fast enough at low scan rates and high temperatures to not be kinetically limited, which means that it is fast compared to the scan rate. Since S2 is an anodic peak, it would be the dissolution of the disordered coadsorbed adlayer of copper, perchlorate and chloride. Not enough is known about the process behind the dissolution to establish which step is kinetically limited and what form the kinetic limitation takes.

For the temperature dependence of peak S2 (see Fig. 6.5b), only 50 mV/s shows a

different trend, which is likely due to the scan rate dependence. The other scan rates show no significant change in peak potential except at 10°C, which has an increased peak potential compared to the higher temperatures. Since peak S2 is the dissolution of the disordered phase and the kinetic energy of the system, and thus the mobility of the adspecies, is lower at low temperatures, it is possible that the disordered layer is energetically favourable at more positive potentials at 10°C compared to the solvation of the adspecies due to the lower kinetic energy.
While there a no distinct enough peaks for the discussion of the cathodic part of the CV, there are some changes seen with the scan rate and the temperature (see Fig. 6.3d). There is a falling current at the lower potential limit that increases with increasing temperatures. It is only seen slightly at low scan rates for low temperatures but shows an increasing influence as well as being seen at increasing scan rates with increasing temperature. Also, the charge density of the cathodic part of the CV increases with increasing temperature, which is not mirrored in the anodic peaks and is partially due to the mentioned falling current. While the anodic peaks do not mirror the change in charge density, there is an increasing current with increasing temperature between 0 V and 0.1 V in the anodic part of the CV. This is likely an effect of the surface change which manifests in a change of the double-layer charging current. Since the anodic peaks do not show the same increase, it is likely that the increasing charge density of the cathodic part of the CV is due to processes other than the Cu-UPD, and might be at least partially due to the surface alloying. The falling current is likely due to an earlier onset of the hydrogen evolution, which was shown to be at higher potentials with increasing temperature by Hamelin et al.[72] on Au(111) in perchloric acid. While the work of Hamelin et al.[72] is not for the Cu-UPD, it does match the results found in this work. Also, it is possible that the surface alloy might influence the hydrogen evolution, though I am not aware of any studies on the subject.

6.2.2. Chronoamperometry

To extract the kinetics and coverages, the chronoamperometric transients were fitted with the Avrami equation (see Sec. 1.1.2 Eq. 1.3):[12]

$$j_i(t) = q_i \cdot m_i \cdot k_i \cdot t^{(m_i-1)} \cdot e^{(-k_i \cdot t^{m_i})}$$

With the current density j, the charge density q, the rate constant k and m representing the type of process.[12] The time constant is $\tau = k^{-\frac{1}{m_i}}$, which is useful to compare the kinetics of processes with different m, as the unit of k depends on m. Herein, m=1 represents either a surface diffusion-controlled two-dimensional instantaneous nucleation and growth process or a one-dimensional instantaneous nucleation and growth process,[11] m=2 is instantaneous nucleation and growth and m=3 is progressive nucleation and growth.[5,12] The transients were assumed to be a superposition of several processes that each could be described with the Avrami equation. This is only a rough estimate, since it has been shown that surface alloying is likely to take place, which is not described by the Avrami equation. However, to the best of our knowledge there is no mathematical equation which sufficiently describes the surface alloying for this purpose. As such, it was decided to use the Avrami equation to approximate the transients.
For the investigation of the surface alloying (see Fig. 6.7), selected transient were modelled with 3 functions that each had m=1. The starting potential of the transients was 180 mV, while the CVs show peak A, which is attributed to the dissolution of the alloy, around 230 mV. Thus, at the starting potential, the surface alloy, if it was formed, should still be present. As such, the transient would show the dissolution of the alloy. Even if the alloy was dissolved before the starting potential, the transient would still reflect the induced surface defects due to the previous alloying. Furthermore, at 10°C, the transient would also show the desorption of the (2x2) adlayer, while at 50°C, it would show the desorption of the disordered copper-perchlorate-chloride adlayer. As such, the exact kinetics of the dissolution of the alloy cannot be given with any degree of confidence. However, the goal of the experiment was not the extraction of the kinetics of the dissolution of the alloy but rather to show the change in the transients. This in turn shows a change in the surface, since the other factors influencing the transients are not supposed to change. The surface alloy was seen as the most likely source of the surface changes.
Tab. 6.1 and 6.2 show the χ^2_{red} for those fits, which show that the fit is good, if possibly slightly overparameterized. Generally, Fig. 6.8a and 6.9a show an increase of the charge when holding at potentials below 180 mV, which increases with both holding time at the alloying potential and with decreasing alloying potential. The deviation from the trend for 50°C and 0 mV might point towards another

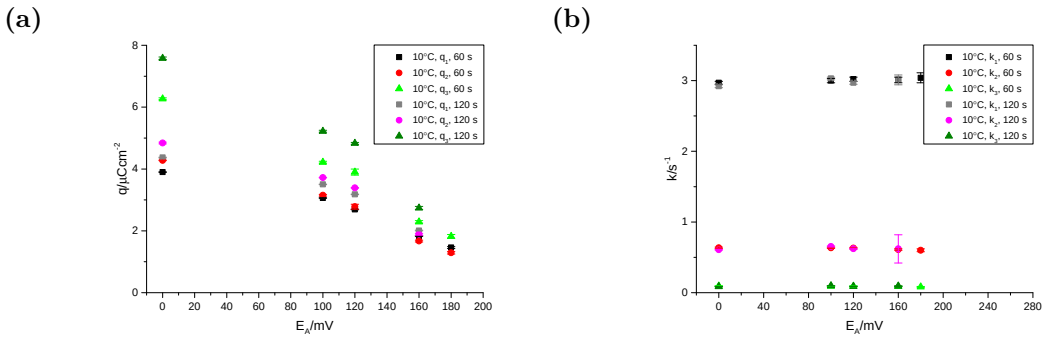

Figure 6.8.: Fit parameters for the transients of Au(111) in 0.1 M perchloric acid 1 mM copper perchlorate for 180 mV→600 mV at 10°C: (a) the charge density q and (b) the rate constant k against the alloying potential E_A for different holding times at the same. The baseline is at 180 mV.

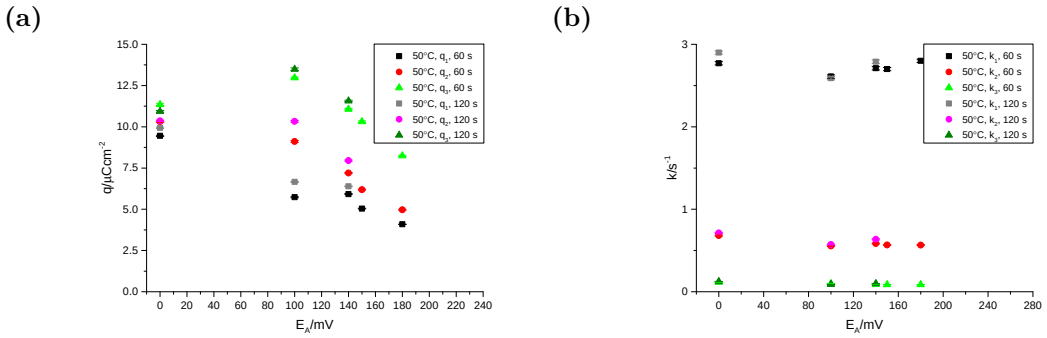

Figure 6.9.: Fit parameters for the transients of Au(111) in 0.1 M perchloric acid 1 mM copper perchlorate for 180 mV→600 mV at 50°C: (a) the charge density q and (b) the rate constant k against the alloying potential E_A for different holding times at the same. The baseline is at 180 mV.

Table 6.1.: χ^2_{red} for the fits of the alloying investigation transients at 10°C (Fig. 6.7a) ordered by previous potential history.

180 mV	160 mV		120 mV		100 mV		0 mV	
	60 s	120 s	60 s	120 s	60 s	120 s	60 s	120 s
0.0014	0.00098	0.0013	0.0013	0.0017	0.0016	0.0018	0.0025	0.0034

Table 6.2.: χ^2_{red} for the fits of the alloying investigation transients at 50°C (Fig. 6.7b) ordered by previous potential history.

180 mV	150 mV	140 mV		100 mV		0 mV	
	60 s	60 s	120 s	60 s	120 s	60 s	120 s
0.0040	0.0050	0.0060	0.0075	0.0082	0.0097	0.0101	0.0091

influence being added at this potential. For both temperatures k changes little (see Fig. 6.8b and 6.9b), though there is a slight increase at lower E_A. As said before, due to having several processes taking place as well as having no actual model for the alloying process, none of the processes can be assigned nor can the kinetics of the dissolution of the alloy be extracted. However, the presented fits do show a change in the transient depending on the alloying potential. Transients with the same start and end potential for the same system should be identical under the same conditions. The experiment was designed so that the only change in conditions would be a change in the crystal surface, thus the change in the transient depending on the alloying potential would indicate a surface change. As bulk deposition was found to start below -0.1 V for 10°C and below 0 V above that, the found change cannot be due to bulk deposition. The Cu-UPD itself should not change the Au(111) surface. Due to these considerations as well as the indications of alloying in the work of Hotlos et al.,[74] it was found to be likely that the surface change was due to the formation of a gold-copper surface alloy. However, further research would be needed to proof the existence of the surface alloy, as chronoamperometry cannot show the actual structure of the surface.
Furthermore, while the kinetics of the dissolution of the alloy cannot be extracted, and of course the applicability of the model is in question, having changes in the charge density instead of the kinetics is not unexpected. If the previous assumption of the 180 mV→600 mV transient showing the dissolution of the alloy is correct, then, except for maybe the baseline, no change in the kinetics is expected as the processes itself do not change. However, the amount of alloy would change based on the alloying potential as well as the time at the same. Thus, the charge density q, which correlates to the amount of alloy, would increase if the amount of alloy increases. Both a decrease in the alloying potential as well as an increase in the time at the alloying potential would be expected to increase the amount of alloy and thus the charge density q, which is seen in Fig. 6.8a and 6.9a. A decreased influence of the holding time, which might be seen at 50°C in Fig. 6.9a for at least function 3, would point towards faster alloying, since it would mean the alloy needs less time to be formed.
The evidence of alloying seen in the CVs is stronger at higher temperatures, so it is likely that the alloying becomes faster with increasing temperature. This would correlate with the possible lesser dependence on the holding time of the charge

density q in Fig. 6.9a compared to Fig. 6.8a. Furthermore, this also explains why little evidence of the alloying has been found previously with cyclic voltammetry, as the process is too slow to show a noticeable influence on the CV at room temperature. To our best knowledge, no other study of the system at increased temperature has been done, which would preclude evidence of the alloying.
The transients in Fig. 6.6 were also fitted with the Avrami equation. As they showed two current peaks at low potential and low temperature, two functions with m$\neq$ 1 (function 3 and 4) were included to describe them. It was found that m=2 gave a better fit for both of those current peaks. For the transients at higher potential, at least two functions with m=1 (function 1 and 2) were necessary to describe the transients. Function 3 and 4 were also included even at high potential to see when they would start contributing to the process, as they would give a negligible charge density otherwise. For elevated temperatures, an additional slow process with m=2 (function 5) was necessary to achieve a reasonable fit.
Instead of the coverage, the value for the number of electrons per surface atom $n_{e^-,a} = \frac{q_i}{-e \cdot n_A}$ was used, with e being the elementary charge and $n_A = 1.39 \cdot 10^{15} cm^{-2}$ [40] being the number of gold atoms on an ideal Au(111)-(1x1) surface. This was due to the fact that it was unlikely that all processes were due to the Cu-UPD, which would lead to misleading coverages. For the Cu-UPD, it is often assumed that 2 electrons are exchanged per deposited copper atom, which would mean that $\theta_{Cu} = \frac{n_{e^-,a}}{2}$ if $n_{e^-,a}$ is due to the Cu-UPD. As such, a value of $n_{e^-,a} = 2$ would correspond to 1 ML of deposited copper, assuming that the exchanged electrons are due to the Cu-UPD. The resulting values for the number of electrons per surface atom $n_{e^-,a}$ are shown in Fig. 6.10 and 6.12 and the time constants in Fig. 6.11 and 6.13 for respectively the temperature dependence and the overall parameters at one temperature. Tab. 6.3 shows the offset at each potential and temperature, while Tab. 6.4 shows the χ^2_{red} as a measure of the goodness of fit.

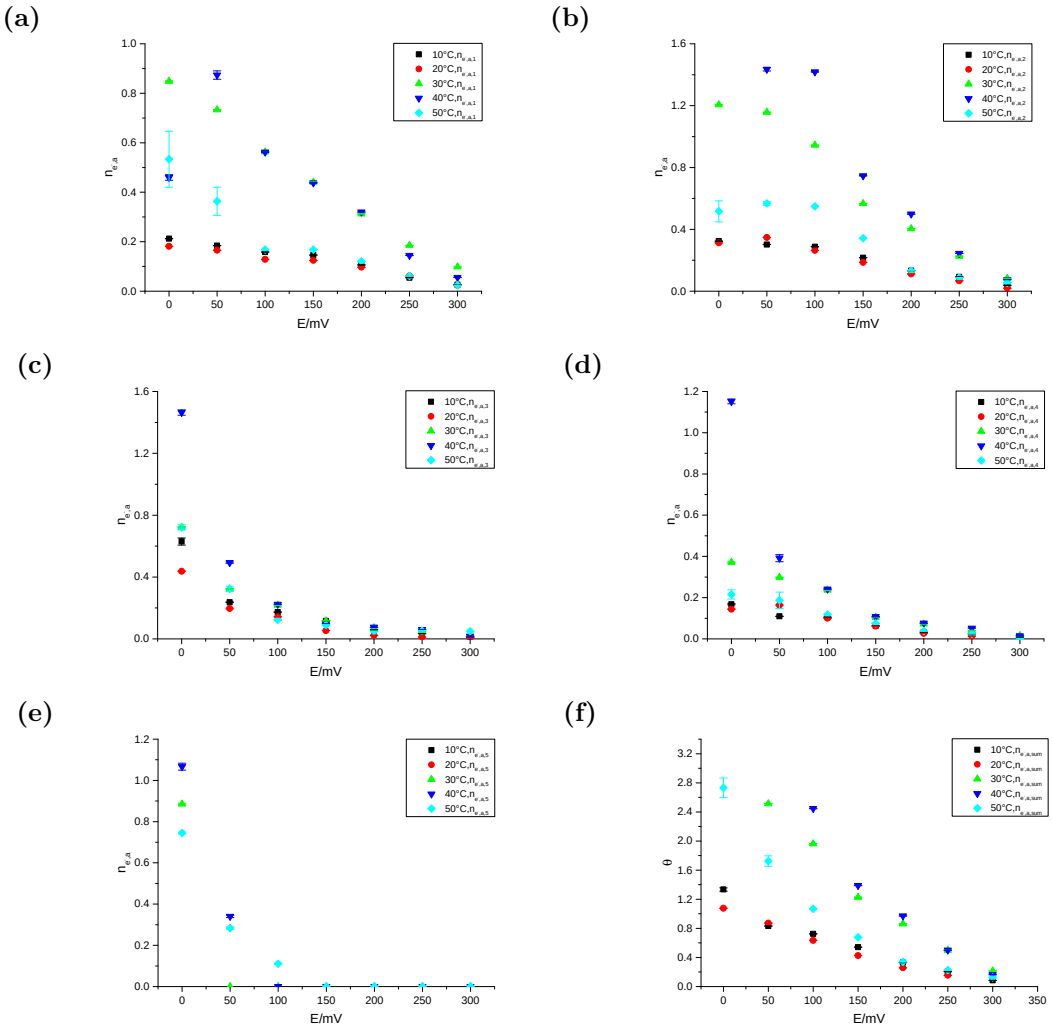

Figure 6.10.: Plot of the number of electrons per surface atom $n_{e^-,a}$ of (a) function 1, (b) function 2, (c) function 3, (d) function 4, (e) function 5 and (f) the overall number of electrons per surface atom over the potential at different temperatures for the fit of the transients in Fig. 6.6 of the Cu-UPD on Au(111) in 0.1 M perchloric acid.

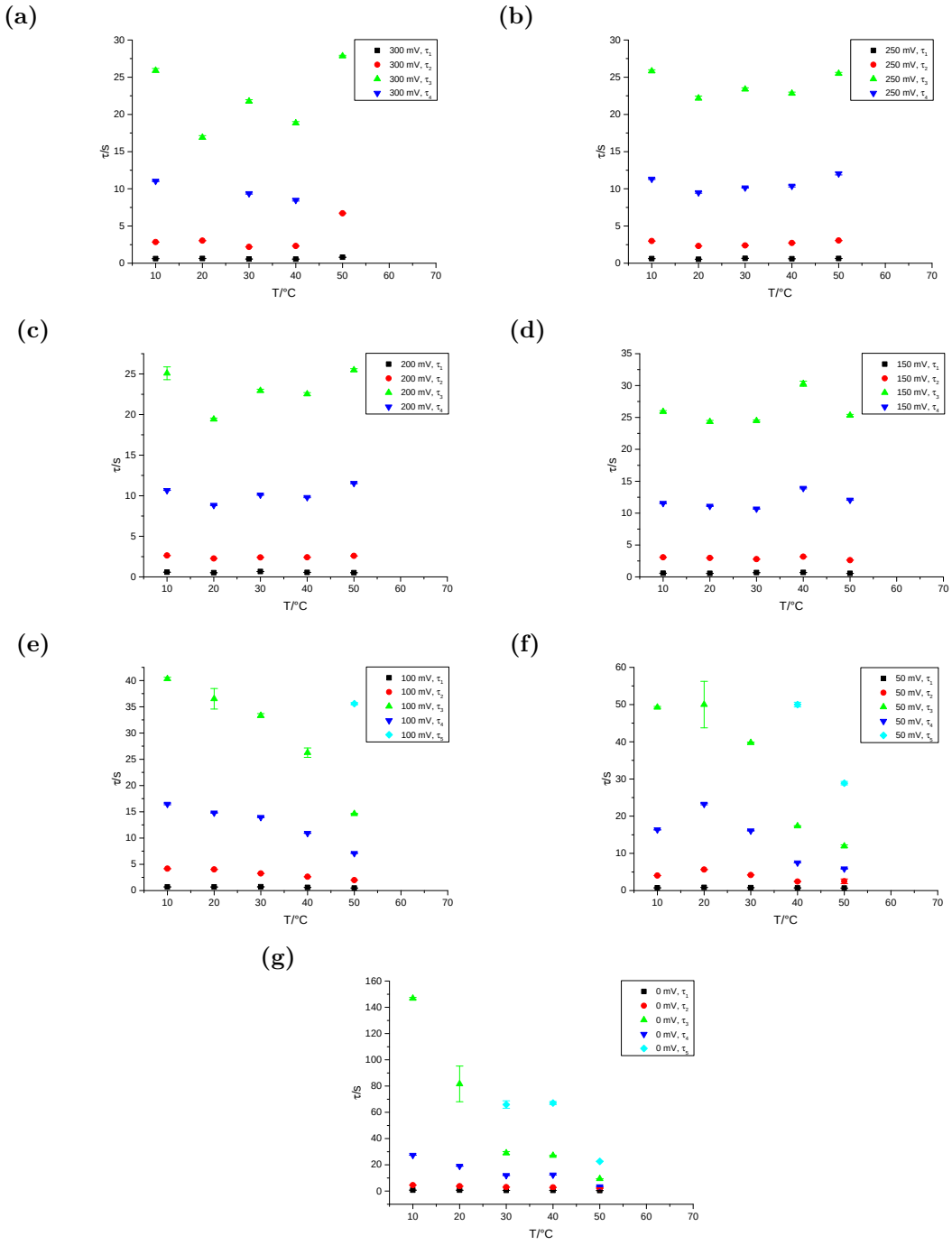

Figure 6.11.: Plot of the time constant τ at (a) 300 mV, (b) 250 mV, (c) 200 mV, (d) 150 mV, (e) 100 mV, (f) 50 mV and (g) 0 mV over the temperature at different end potentials for the fit of the transients in Fig. 6.6 of the Cu-UPD on Au(111) in 0.1 M perchloric acid.

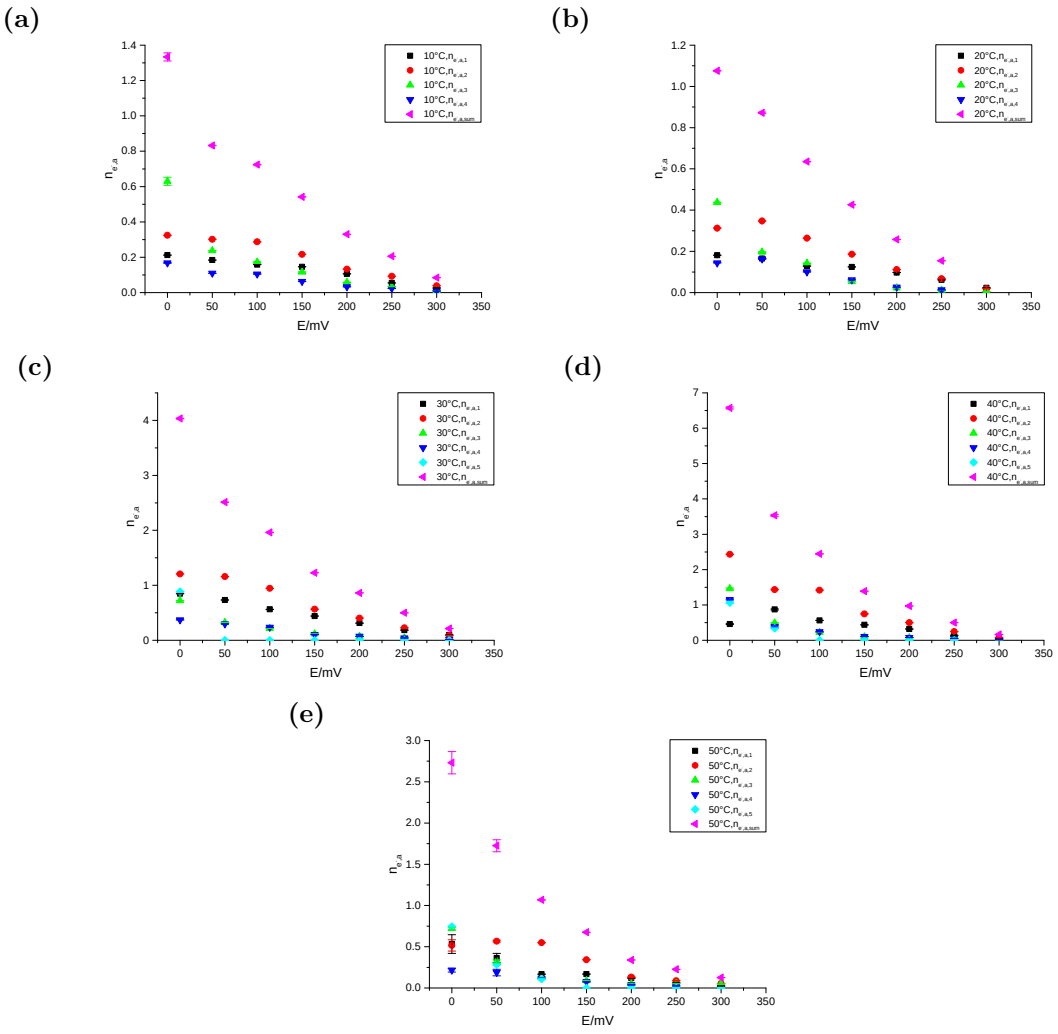

Figure 6.12.: Plot of the number of electrons per surface atom $n_{e^-,a}$ at (a) 10°C, (b) 20°C, (c) 30°C, (d) 40°C and (e) 50°C over the potential for the fit of the transients in Fig. 6.6 of the Cu-UPD on Au(111) in 0.1 M perchloric acid.

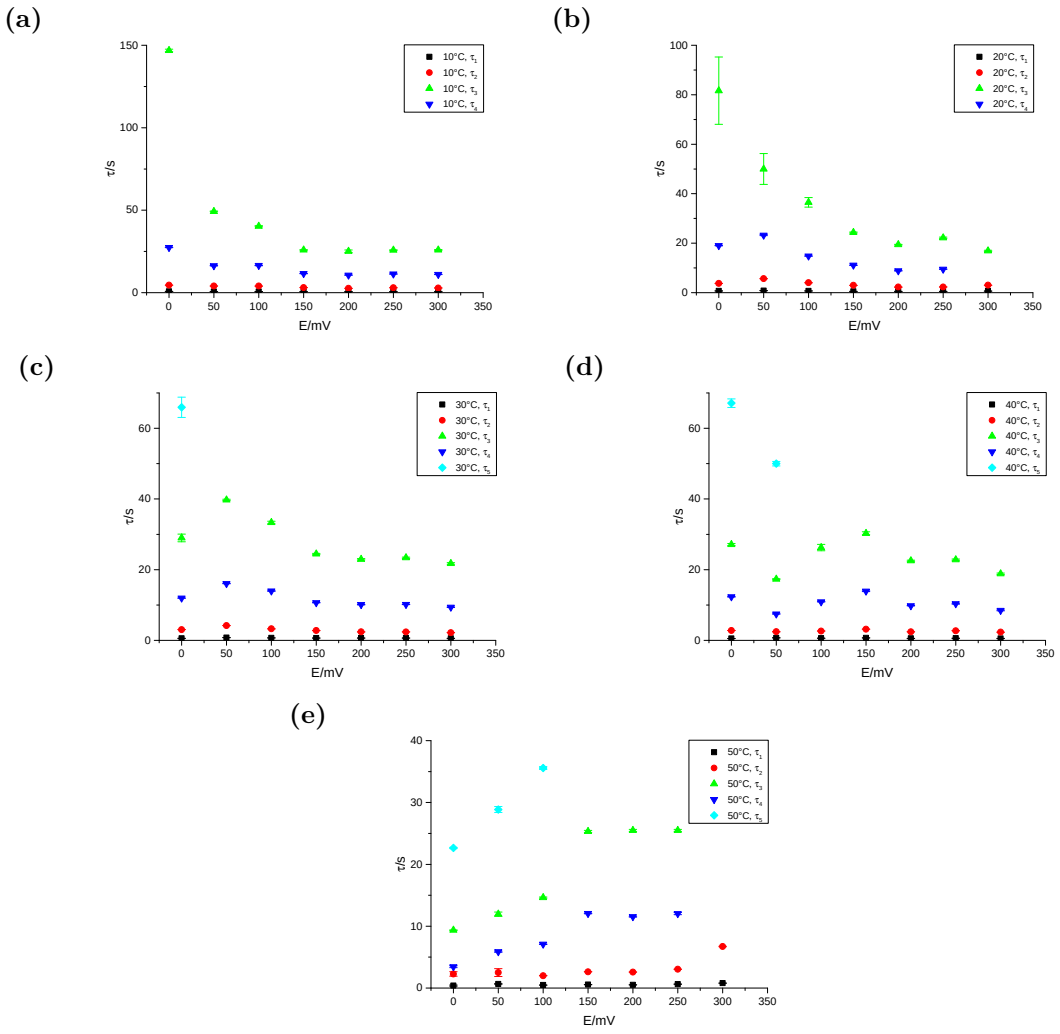

Figure 6.13.: Plot of the time constants τ at (a) 10°C, (b) 20°C, (c) 30°C, (d) 40°C and (e) 50°C over the potential for the fit of the transients in Fig. 6.6 of the Cu-UPD on Au(111) in 0.1 M perchloric acid.

Table 6.3.: Offset in µAcm^{-2} for the fit of the transients in Fig. 6.6 of the Cu-UPD on Au(111) in 0.1 M perchloric acid.

	10°C	20°C	30°C	40°C	50°C
300 mV	-0.0322±0.0005	-0.0222±0.0004	-0.0701±0.0006	-0.073±0.001	-0.219±0.001
250 mV	-0.136±0.001	-0.0336±0.0008	-0.176±0.001	-0.2±0.003	-0.332±0.001
200 mV	-0.256±0.001	-0.0786±0.0006	-0.29±0.001	-0.357±0.003	-0.479±0.001
150 mV	-0.466±0.003	-0.301±0.001	-0.638±0.003	-0.795±0.008	-0.866±0.003
100 mV	-0.41±0.005	-0.317±0.003	-0.57±0.01	-0.911±0.005	-1.089±0.003
50 mV	-0.865±0.003	-0.488±0.006	-1.043±0.004	-1.64±0.01	-3.45±0.01
0 mV	-1.34±0.03	-1.567±0.003	-3.47±0.005	-7.83±0.04	-14.78±-0.01

Table 6.4.: χ^2_{red} for the fit of the transients in Fig. 6.6 of the Cu-UPD on Au(111) in 0.1 M perchloric acid.

	10°C	20°C	30°C	40°C	50°C
300 mV	0.00034	0.0013	0.0023	0.0021	0.0038
250 mV	0.0024	0.0012	0.0092	0.016	0.004
200 mV	0.0075	0.0034	0.018	0.031	0.0056
150 mV	0.017	0.0086	0.034	0.027	0.011
100 mV	0.04	0.026	0.27	0.34	0.035
50 mV	0.063	0.056	0.22	1.23	0.58
0 mV	0.057	0.024	0.38	2.3	5.1

The χ^2_{red} in most instances show a good fit, although with a possible overparameterization. Only at higher temperature and low potentials, for 40°C at 50 mV and 0 mV and for 50°C at 0 mV, is the χ^2_{red} above one, which indicates that the model is not within the error range. However, the fits at 40°C are still near one, and, as already explained, the model is only an approximation due to not having a specific description for the surface alloying. As such, the fits are judged to be of reasonable goodness. For 0 mV at 50°C, the higher χ^2_{red} might be due to an external influence on the measurement. That particular transient had been noted to have an oscillation after 90 s, and only the first 80 s were used. That does reduce the available data as well as likely influencing the fit for function 5, which is a very slow process. As such, the higher χ^2_{red} for this transient is not unexpected, however the fit should still be usable.

Above 100 mV, the kinetics of the processes show no systematic change with the temperature (see Fig. 6.11a-6.11d). Then, the processes become faster with increasing temperature (see Fig. 6.11e-6.11g), though the influence of the temperature on τ_1 is less compared to the other processes. The increase of the speed of the reaction is expected, as the Cu-UPD is known to be kinetically hindered.[73–75] With increasing temperature the kinetic energy of the species increases, which counteracts the kinetic hindrance and increases the speed of the process. As for the change of the kinetics with the potential (see Fig. 6.13), no change is shown above 150 mV, while at or below 150 mV the processes become slower with decreasing potential. The calculated time constants are however influenced by the addition of function 5 at higher temperatures. This is likely to not reflect an actual change in the kinetics but rather is an artefact of the change of the model. However, for 50°C, all processes tend to become faster instead after the addition of function 5, contrary to the trend at other temperatures. The decrease in the reaction speed could be due to the formation of the surface alloy influencing the speed of the processes. Also, the deficiencies of the model could mean that more than one function shows influence of the alloying, with the alloying influence being stronger at lower potentials.

For the number of electrons per surface atom $n_{e^-,a}$, it has to be kept in mind that there is no correction for anion coadsorption, which has been shown to play a role in the Cu-UPD[73–75] and which would correspond to an opposite charge density compared to the Cu-UPD. Neglecting the anion adsorption would falsify

the total value of $n_{e^-,a}$. However, as even the actual composition of the UPD layer is still under debate, the influence of the anion adsorption cannot be estimated. Furthermore, it is likely that at least some of the processes are due to other phenomena that happen in the potential range of the Cu-UPD, f.e. alloying or hydrogen evolution. As such, the number of electrons per surface atom $n_{e^-,a}$ should be seen as a way to estimate the contribution of the processes as well as to show if the charge density strongly exceeds what is expected for the Cu-UPD, which would point towards other processes taking place.
Fig. 6.12 shows the values for $n_{e^-,a}$ at each temperature. The values for $n_{e^-,a}$ tend to increase with decreasing potential, which is expected. They do not show any strongly defined steps, which would also be expected due to the lack of sharp peaks in the CV which would indicate a sudden phase transition. While Hotlos et al.[74] and Krznaric et al.[73] found two different phases, the copper coverage of the first phase for low chloride concentrations is unknown. For higher chloride concentrations, the difference of the copper coverage is only 0.11 ML.[74] As such, it would not show a strong step in the values for $n_{e^-,a}$. Furthermore, the Cu-UPD is strongly kinetically hindered,[73–75] which means the processes are slow. Any steps in the values for $n_{e^-,a}$ over the potential tend to be less strongly expressed for slow processes compared to fast processes. As such, even if sudden changes in the values for $n_{e^-,a}$ with the potential would exist due to the structural transition, the slow kinetics of the process would strongly mask them.
At high temperatures, the overall number of electrons per surface atom $n_{e^-,a,sum}$ is also shown to be above two, which would mean that not all of the processes are due to the Cu-UPD. Faster alloying at higher temperatures might also mean that it influences the other processes earlier, which could lead to a change in the process and apparent charge density, and thus in $n_{e^-,a,sum}$.
Fig. 6.10 shows the number of electrons per surface atom $n_{e^-,a,i}$ from each process separately. It is noticeable that while there is a general increase of the coverage with the temperature, 50°C shows consistently lower values for $n_{e^-,a}$ than 40°C. At 0 mV and 50 mV this might be due to a strong increase in the offset for those fits compared to the lower temperatures (see Tab. 6.3), but the higher potentials also tend to show a lower values for $n_{e^-,a}$ for that temperature. So while an artificially high offset might play into the lower values for $n_{e^-,a}$, more likely the meniscus was smaller than expected. The area of the meniscus defines the area

of the interface between electrolyte and single crystal, which is needed for the calculation of $n_{e^-,a}$ as it defines the surface area of the crystal. Generally, it is assumed that the meniscus covers the whole surface of the crystal. However, if a meniscus covers less surface area than expected, the resulting values for $n_{e^-,a}$ would be artificially reduced due to the wrong assumption of the surface area. While care has been taken to produce reproducible menisci, this is a possibility especially at higher temperatures. Also noticeable in Fig. 6.10 is that for 10°C and 20°C, the values for $n_{e^-,a}$ tend to be very similar, with strong changes only at the elevated temperatures.

For the interpretation of the functions and their dependences, a knowledge of the processes they represent would be helpful. It has to be kept in mind, however, that due to the previous discussed shortcomings of the model, some functions might be due to more than one process, or that a process is described by more than one function.

Function 5 only appears at low potentials and high temperatures, while the potential range of the function increases with increasing temperature. It has already been said while discussing the CVs that at high temperatures the hydrogen evolution starts at higher potentials, with the starting potential increasing with the temperature, as shown by Hamelin et al.[72] for perchloric acid without copper. This fits with the behaviour of function 5. Furthermore, the falling current indicating the hydrogen evolution in the CV starts appearing at 30°C, which coincides with the appearance of function 5 in the chronoamperometry. As such, function 5 is assigned to the hydrogen evolution. This partially explains the increased values for $n_{e^-,a}$ at higher temperatures, which also mirrors the increased current density in the CVs at higher temperatures. Since a nucleation model is used, the model obviously doesn't fit the type of process. This wrong assumption of the model means the extracted kinetics do not reflect reality and thus the time constant should be discounted.

For function 1 as well as function 2, $n_{e^-,a}$ contributes even at the higher potentials, with little change below 200 mV below 30°C (see Fig. 6.10a and 6.10b). The change at higher temperature might be due to other processes influencing it. They are likely connected with the Cu-UPD, probably to the formation of the first structure, which is assumed to be the disordered adlayer of coadsorbed copper and chloride found by Hotlos et al.,[74] though it is likely to also have coadsorbed

perchlorate as shown by Krznaric et al.[73]
Functions 3 and 4 start to contribute to $n_{e^-,a}$ below 200 mV (see Fig. 6.10c and 6.10d), which would indicate either the formation of the (2×2) adlayer or the surface alloy. Looking at the temperature dependence of the time constant (see Fig. 6.11), τ_3 shows a much stronger decrease with the temperature compared to τ_4, as well being a much slower process. As the Cu-UPD can be seen at low temperatures in the CV, while the indications of the alloying only show up at high temperatures in the CV due to the alloying being too slow compared to the scan rate, function 4 is assigned to the formation of the (2×2) adlayer of the Cu-UPD, while function 3 is assigned to the formation of the surface alloy.
However, it has to be remembered that the form of the function assigned to the alloying does not necessarily indicate that the interpretation usually used for that function in the Avrami equation is valid. Therefore, while a tentative time constant for the alloying can be extracted, an appropriate theoretical model would be needed for any reliable interpretation. The amount of the surface alloy formed might slightly increase with the temperature, but it is more likely that the change in the calculated values for $n_{e^-,a}$ with the temperature (see Fig. 6.10c) is due to correlations between the different functions, as there is no uniform trend. The change in the amount of alloy seen in the CVs with the temperature should be due to the kinetics, especially as it also increases with decreasing scan rate, and thus not show in the calculated values for $n_{e^-,a}$ of the transients.
Since function 4 has m=2, the formation of the (2×2) adlayer seems to follow an instantaneous nucleation and two-dimensional growth. This correlates well with the STM images of Hotlos et al.,[74] in which they found an island-growth mechanism, which would be a two-dimensional growth. The slight difference in the values for $n_{e^-,a}$ as well as the outlier at 0 V and 40°C (see Fig. 6.10d) are more likely to be an artefact due to the superposition of several functions, which introduces correlations between the functions, rather than an actual change in the values for $n_{e^-,a}$, since it would represent the copper coverage, which should not increase. A decrease of the coverage with the temperature might be possible due to the formation of the surface alloy decreasing the surface area on which the phase forms, which would mirror the decrease of the charge density of peak S1 in the CVs. An increase of the coverage of the (2×2) phase with the temperature, especially considering the mentioned trend in the CVs, would be less plausible.

Possibly part of the copper might deposit on the surface alloy without forming the (2×2) phase, reducing the amount of coadsorbed anions and thus increasing the apparent coverage and thus the apparent values for $n_{e^-,a}$ due to the decrease in the charge density due to the anions, but not actual increasing the charge density due to the copper deposition.

6.3. Summary

An investigation of the temperature dependence of the Cu-UPD on Au(111) in perchloric acid using cyclic voltammetry and chronoamperometry was performed. A likely surface alloy formation during the Cu-UPD was observed, which strongly affects the CVs at higher temperatures. While some conclusions about the kinetics of the Cu-UPD can be drawn, the system is rather complicated due to the surface alloy formation.

The onset of the HER was found to occur at higher potentials with increasing temperature similar to the results in Ch. 5 as well as the work of Hamelin et al.[72] in copper-free perchloric acid. There are also some indications that the ordered copper-chloride-perchlorate phase is less stable than the disordered phase at higher temperatures, similar to what was found for sulphuric acid in Ch. 4.

The kinetics of the formation of the Cu-UPD layer become faster with increasing temperature at potentials below 150 mV. Since the Cu-UPD in perchloric acid is known to be kinetically limited, it is likely that the increase in kinetic energy with increasing temperature counteracts the limitation. Furthermore, the formation of the (2×2) adlayer shows an instantaneous nucleation with two-dimensional growth, which correlates well with the results of Hotlos et al.[74]

All in all, the influence of the temperature on the Cu-UPD on Au(111) in perchloric acid seems to be due to the increase in kinetic energy with increasing temperature, which mainly counteracts the kinetic limitation of the Cu-UPD process as well as increases the speed of the surface alloying.

7. Conclusion

The temperature dependence of Au(111) and the Cu-UPD on Au(111) in sulphuric acid and perchloric acid has been investigated via cyclic voltammetry as well as via chronoamperometry in the case of the Cu-UPD. Systematic changes with the temperature have been found, mostly due to the increasing kinetic energy with increasing temperature. An increase in the kinetic energy of the particles leads to a higher mobility as well as faster diffusion of said particles.
For order-disorder phase transition, this decreases the stability of the ordered phase with increasing temperature, since the disordered phase becomes energetically more favourable due to the increased mobility of the adspecies. This could be seen for Au(111) in sulphuric acid as well as for the Cu-UPD in sulphuric acid. The Cu-UPD in perchloric acid becomes faster at higher temperatures since the increased kinetic energy with increasing temperature counteracts the kinetic limitation of the Cu-UPD. Also, the increased kinetic energy leads to faster surface diffusion, which for example leads to faster electrochemical annealing as seen for Au(111) in perchloric acid. It could also be seen in the increased speed of the order-disorder phase transition of the Cu-UPD in sulphuric acid.
While the decreased stability of the ordered adlayer seems to be the only effect of the temperature for Au(111) in sulphuric acid, this is not applicable to perchloric acid. It has been shown that the peak potential for the perchlorate adsorption decreases with increasing temperature, which was attributed to the hydration shell becoming less strongly bound with increasing temperature. As Lucas et al.[16] found that the effect of temperature for bromide on Au(001) was only due to the increased surface mobility of the anion, the effect of the temperature on the anion seems to also be correlated to the strength of adsorption and thus the strength of solvation of the anion. The strength of adsorption would be $Br^- > SO_4^{2-} > ClO_4^-$.[19] The most strongly adsorbing anion, bromide, only has the kinetics of the ordering being temperature dependent. Sulphate, which is more strongly adsorbing than

perchlorate but less strongly adsorbing than bromide, shows an effect of the temperature on the order-disorder phase transition due to the increased mobility. For the most weakly adsorbing anion, perchlorate, an effect of the temperature on the perchlorate adsorption due to a decrease in the solvation strength has been found. Since there is no ordered perchlorate adlayer, no information about the influence of temperature on the order-disorder phase transition for perchlorate could be obtained. Nevertheless, this shows a trend of increasing influence of the temperature on the anion with decreasing strength of adsorption.

The Cu-UPD in sulphuric acid showed an effect of the temperature on the formation of the honeycomb phase, which became faster but less stable than the mobile adlayer with increasing temperature. However, the formation of the copper monolayer showed no influence of the temperature. Meanwhile, in perchloric acid a strong influence of the temperature on the speed of the Cu-UPD is seen. While there is some indication that the ordered phase is also less stable than the mobile phase at higher temperatures, not enough information was available to conclusively determine that. For the more strongly adsorbing bromide, Gründer et al. [15] found an improved ordering of the copper-bromide adlayer due to faster surface diffusion with increasing temperature. Similar to the copper-free electrolytes, the effect of the temperature seems to increase for less strongly adsorbed anions.

There was a limit on the investigated temperature range due to instrumental restraints. As the electrolyte is water-based, 10°C was chosen as the lowest temperature to avoid problems due to the freezing of the electrolyte or the heat-transfer fluid, which was water. The upper temperature limit was below 60°C. While the boiling point of water under standard conditions is at 100°C, temperatures above room temperature already have a faster evaporation of the water as well as the formation of bubbles in the electrolyte. This lead to experimental difficulties at and above 40°C, which increased with increasing temperature. However, a certain range of elevated temperatures was necessary for the study. An upper temperature limit below 60°C gave an acceptable range of elevated temperatures while still keeping the experimental difficulties at a reasonable level.

For the chronoamperometry, the Cu-UPD in sulphuric acid did not show the expected current peaks for nucleation and two-dimensional growth. In perchloric acid, current peaks for nucleation and two-dimensional growth were seen. However, the Cu-UPD in perchloric acid is known to be kinetically hindered, and as such a

much slower process than in sulphuric acid. Furthermore, the current peaks in perchloric acid were masked with increasing temperature, as the process became faster. Thus, it can be inferred that the current peaks in sulphuric acid at all temperatures were masked since it is a much faster process than in perchloric acid.
The Cu-UPD in perchloric acid also showed evidence of alloying in the chronoamperometry as well as in the cyclic voltammetry at elevated temperatures. It only showed in the CVs above room temperature because it is a slow process with the speed increasing with increasing temperature. Therefore, the measurement time at and below room temperature was too fast to show influence of the alloying.

7.1. Future Outlook

For the evaluation of the alloying, a numerical treatment of the process would be needed to model the chronoamperometric transients. Furthermore, while evidence of the alloying was presented, techniques that show the state and composition of the surface would be needed to further show the existence of the alloy. A general study of the temperature dependence with methods showing the surface structure, f.e. STM or XRD, would also be helpful to proof whether or not changes in the structures occur.
Additionally, a theoretical model for the copper-sulphate coadsorption in the chronoamperometric transients would be helpful to fully evaluate the Cu-UPD in sulphuric acid using chronoamperometry.
Last but not least, different electrolyte compositions with different ionic strength and concentrations of the anions are used in the literature. Therefore, a systematic study of the influence of the ionic strength as well as the anion concentration of the electrolyte on the CVs as well as the chronoamperometric transients would be helpful to confidently evaluate results for the Cu-UPD in regards to the existing literature.

Bibliography

[1] Dini, J.; Snyder, D. In *Modern Electroplating*, 5th ed.; Schlesinger, M., Paunovic, M., Eds.; John Wiley & Sons, 2010; Chapter 2, pp 33–78.

[2] Kolb, D. M. *Angewandte Chemie International Edition* **2001**, *40*, 1162–1181.

[3] Gileadi, E. *Physical Electrochemistry*; WILEY-VCH, 2011; p 394.

[4] Elgrishi, N.; Rountree, K. J.; McCarthy, B. D.; Rountree, E. S.; Eisenhart, T. T.; Dempsey, J. L. *Journal of Chemical Education* **2018**, *95*, 197–206.

[5] Pletscher, D.; Greef, R.; Peat, R.; Peter, L. M.; Robinson, J. *Instrumental Methods in Electrochemistry*; Horwood Publishing Limited, 2006; p 443.

[6] Schmickler, W.; Santos, E. *Interfacial Electrochemistry*; Springer Berlin Heidelberg, 2010; pp 1–272.

[7] Lucas, C. A.; Marković, N. M. In *Encyclopedia of Electrochemistry, Volume 2, Interfacial Kinetics and Mass Transport*; Bard, A. J., Stratmann, M., Calvo, E. J., Eds.; WILEY-VCH, 2003; Chapter 4.1 Struct.

[8] Avrami, M. *The Journal of Chemical Physics* **1939**, *7*, 1103.

[9] Avrami, M. *The Journal of Chemical Physics* **1940**, *8*, 212.

[10] Avrami, M. *The Journal of Chemical Physics* **1941**, *9*, 177.

[11] Fleischmann, M.; Thirsk, H. In *Advances in Electrochemistry and Electrochemical Engineering*; Delahay, P., Tobias, C., Eds.; Interscience: New York, NY, 1963; Vol. 3; Chapter 3, pp 123–210.

[12] Gründer, Y.; Drünkler, A.; Golks, F.; Wijts, G.; Stettner, J.; Zegenhagen, J.; Magnussen, O. *Journal of Electroanalytical Chemistry* **2014**, *712*, 74–81.

[13] Jerkiewicz, G.; Perreault, F.; Radovic-Hrapovic, Z. *The Journal of Physical Chemistry C* **2009**, *113*, 12309–12316.

[14] Radovic-Hrapovic, Z.; Jerkiewicz, G. *Thin Films: Preparation, Characterization, Applications*; Springer US: Boston, MA, 2002; pp 53–67.

[15] Gründer, Y.; Markovic, N. M.; Thompson, P.; Lucas, C. a. *Surface Science* **2015**, *631*, 123–129.

[16] Lucas, C. A.; Thompson, P.; Cormack, M.; Brownrigg, A.; Fowler, B.; Strmcnik, D.; Stamenkovic, V.; Greeley, J.; Menzel, A.; You, H.; Marković, N. M. *Journal of the American Chemical Society* **2009**, *131*, 7654–61.

[17] Herrero, E.; Buller, L. J.; Abruña, H. D. *Chemical Reviews* **2001**, *101*, 1897–1930.

[18] Shi, Z.; Wu, S.; Lipkowski, J. *Electrochimica Acta* **1995**, *40*, 9–15.

[19] Tripkovic, D. V.; Strmcnik, D.; van der Vliet, D.; Stamenkovic, V.; Markovic, N. M. *Faraday Discussions* **2008**, *140*, 25–40.

[20] Magnussen, O. M. *Chemical Reviews* **2002**, *102*, 679–726.

[21] Kolb, D. M. *Progress in Surface Science* **1996**, *51*, 109–173.

[22] Guo, Q.; Yin, F.; Palmer, R. E. *Small* **2005**, *1*, 76–79.

[23] Repain, V.; Berroir, J. M.; Rousset, S.; Lecoeur, J. *Europhysics Letters* **1999**, *47*, 435–441.

[24] Chauraud, D.; Durinck, J.; Drouet, M.; Vernisse, L.; Bonneville, J.; Coupeau, C. *Physical Review B* **2017**, *96*, 6–9.

[25] Sandy, A. R.; Mochrie, S. G. J.; Zehner, D. M.; Huang, K. G.; Gibbs, D. *Physical Review B* **1991**, *43*, 4667–4687.

[26] Barth, J. V.; Brune, H.; Ertl, G.; Behm, R. J. *Physical Review B* **1990**, *42*, 9307–9318.

[27] Hasegawa, Y.; Avouris, P. *Science (New York, N.Y.)* **1992**, *258*, 1763–1765.

[28] Silva, F.; Martins, A. *Electrochimica Acta* **1998**, *44*, 919–929.

[29] Dretschkow, T. H.; Wandlowski, T. H. *Berichte der Bunsengesellschaft für physikalische Chemie* **1997**, *101*, 749–757.

[30] Magnussen, O. M.; Hageböck, J.; Hotlos, J.; Behm, R. J. *Faraday Discuss.* **1992**, *94*, 329–338.

[31] Edens, G. J.; Gao, X.; Weaver, M. J. *Journal of Electroanalytical Chemistry* **1994**, *375*, 357–366.

[32] Shi, Z.; Lipkowski, J.; Mirwald, S.; Pettinger, B. *Journal of Electroanalytical Chemistry* **1995**, *396*.

[33] Kibler, L. *Preparation and Characterization of Noble Metal Single Crystal Electrode Surfaces*; International Society of Electrochemistry, 2003; pp 1–56.

[34] Kondo, T.; Morita, J.; Hanaoka, K.; Takakusagi, S.; Tamura, K.; Takahasi, M.; Mizuki, J. N.; Uosaki, K. *Journal of Physical Chemistry C* **2007**, *111*, 13197–13204.

[35] Giesen, M.; Kolb, D. M. *Surface Science* **2000**, *468*, 149–164.

[36] Shi, Z.; Lipkowski, J.; Gamboa, M.; Zelenay, P.; Wieckowski, A. *Journal of Electroanalytical Chemistry* **1994**, *366*, 317–326.

[37] Uchida, H.; Hiei, M.; Watanabe, M. *Journal of Electroanalytical Chemistry* **1998**, *452*, 97–106.

[38] de Moraes, I. R.; Nart, F. C. *Journal of Electroanalytical Chemistry* **1999**, *461*, 110–120.

[39] Ataka, K.; Osawa, M. *Langmuir* **1998**, *14*, 951–959.

[40] Shi, Z.; Lipkowski, J. *Journal of Electroanalytical Chemistry* **1994**, *365*, 303–309.

[41] Shi, Z.; Lipkowski, J. **1994**, *364*, 289–294.

[42] Hachiya, T.; Honbo, H.; Itaya, K. *Journal of Electroanalytical Chemistry and Interfacial Electrochemistry* **1991**, *315*, 275–291.

[43] Zhang, J.; Sung, Y.-E.; Rikvold, P. A.; Wieckowski, A. *The Journal of Chemical Physics* **1996**, *104*, 5699–5712.

[44] Madry, B.; Wandelt, K.; Nowicki, M. *Electrochimica Acta* **2016**, *217*, 249–261.

[45] Magnussen, O. M.; Hotlos, J.; Nichols, R. J.; Kolb, D. M.; Behm, R. J. *Physical Review Letters* **1990**, *64*, 2929–2932.

[46] Magnussen, O. M.; Hotlos, J.; Beitel, G.; Kolb, D. M.; Behm, R. J. *Journal of Vacuum Science & Technology B: Microelectronics and Nanometer Structures* **1991**, *9*, 969.

[47] Vasiljevic, N.; Viyannalage, L. T.; Dimitrov, N.; Sieradzki, K. *Journal of Electroanalytical Chemistry* **2008**, *613*, 118–124.

[48] Pobelov, I. V.; Nagy, G.; Wandlowski, T. *Journal of Chemical Sciences* **2009**, *121*, 745–756.

[49] Toney, M. F.; Howard, J. N.; Richer, J.; Borges, G. L.; Gordon, J. G.; Melroy, O. R.; Yee, D.; Sorensen, L. B. *Physical Review Letters* **1995**, *75*, 4472–4475.

[50] Chabala, E. D.; Cairns, J.; Rayment, T. *Journal of Electroanalytical Chemistry* **1996**, *412*, 77–84.

[51] Nakamura, M.; Endo, O.; Ohta, T.; Ito, M.; Yoda, Y. *Surface Science* **2002**, *514*, 227–233.

[52] Ataka, K.; Nishina, G.; Cai, W.; Sun, S.-G.; Osawa, M. *Electrochemistry Communications* **2000**, *2*, 417–421.

[53] Hölzle, M.; Retter, U.; Kolb, D. *Journal of Electroanalytical Chemistry* **1994**, *371*, 101–109.

[54] Hölzle, M.; Zwing, V.; Kolb, D. *Electrochimica Acta* **1995**, *40*, 1237–1247.

[55] Garfias-Garcia, E.; Palomar-Pardavé, M.; Romero-Romo, M.; Ramírez-Silva, M. T.; Batina, N. Kinetics Mechanism of Copper UPD Nucleation and Growth on Mono and Polycrystaline Gold. ECS Transactions. 2007; pp 35–43.

[56] Lee, J. R. I.; O'Malley, R. L.; O'Connell, T. J.; Vollmer, A.; Rayment, T. *The Journal of Physical Chemistry C* **2009**, *113*, 12260–12271.

[57] Frittmann, S.; Schuster, R. *The Journal of Physical Chemistry C* **2016**, *120*, 21522–21535.

[58] Blum, L.; Huckaby, D. A. *Journal of Electroanalytical Chemistry* **1994**, *375*, 69–77.

[59] Legault, M.; Blum, L.; Huckaby, D. A. *Journal of Electroanalytical Chemistry* **1996**, *409*, 79–86.

[60] Huckaby, D. A.; Blum, L. *Langmuir* **1995**, *11*, 4583–4587.

[61] Huckaby, D. A.; Legault, M. D.; Blum, L. *The Journal of Chemical Physics* **1998**, *109*, 3600–3606.

[62] Xu, J.; Wang, X. *Surface Science* **1998**, *408*, 317–325.

[63] Matsumoto, H.; Inukai, J.; Ito, M. *Journal of Electroanalytical Chemistry* **1994**, *379*, 223–231.

[64] Angerstein-Kozlowska, H.; Conway, B. E.; Hamelin, A.; Stoicoviciu, L. *Electrochimica Acta* **1986**, *31*, 1051–1061.

[65] Zhumaev, U.; Pobelov, I.; Rudnev, A.; Kuzume, A.; Wandlowski, T. *Electrochemistry Communications* **2014**, *44*, 31–33.

[66] Silva, F.; Martins, A. *Journal of Electroanalytical Chemistry* **1999**, *467*, 335–341.

[67] Zhumaev, U.; Lai, A.; Pobelov, I.; Kuzume, A.; Rudnev, A.; Wandlowski, T. *Electrochimica Acta* **2014**, *146*, 112–118.

[68] Ataka, K.; Yotsuyanagi, T.; Osawa, M. *The Journal of Physical Chemistry* **1996**, *100*, 10664–10672.

[69] Hamelin, A. *Journal of electroanalytical chemistry and interfacial ...* **1986**, *210*, 303–309.

[70] Uchida, H.; Ikeda, N.; Watanabe, M. *Journal of Electroanalytical Chemistry* **1997**, *424*, 5–12.

[71] Cahan, B. D.; Villullas, H. M.; Yeager, E. B. *Journal of Electroanalytical Chemistry* **1991**, *306*, 213–238.

[72] Hamelin, A.; Stoicoviciu, L.; Chang, S. C.; Weaver, M. J. *Journal of Electroanalytical Chemistry* **1991**, *307*, 183–194.

[73] Krznarić, D.; Goričnik, T. *Langmuir* **2001**, *17*, 4347–4351.

[74] Hotlos, J.; Magnussen, O. M.; Behm, R. J. *Surface Science* **1995**, *335*, 129–144.

[75] Zei, M. S.; Qiao, G.; Lehmpfuhl, G.; Kolb, D. M. *Berichte der Bunsengesellschaft für physikalische Chemie* **1987**, *91*, 349–353.

[76] Ishikawa, R. M.; Hubbard, A. T. *Journal of Electroanalytical Chemistry and Interfacial Electrochemistry* **1976**, *69*, 317–338.

[77] Manne, S.; Hansma, P. K.; Massie, J.; Elings, V. B.; Gewith, A. A. *Science* **1991**, *251*, 183–186.

[78] Sawyer, D. T.; Sobkowiak, A.; Roberts, J. L. *Electrochemistry for chemists*, 2nd ed.; Wiley: New York, NY, 1995; p 528.

[79] Xia, X. H.; Nagle, L.; Schuster, R.; Magnussen, O. M.; Behm, R. J. *Physical Chemistry Chemical Physics* **2000**, *2*, 4387–4392.

[80] Bosco, E.; Rangarajan, S. K. *Journal of Electroanalytical Chemistry* **1981**, *129*, 25–51.

[81] Schultze, J. W.; Dickertmann, D. *Surface Science* **1976**, *54*, 489–505.

[82] Donets, A.; Chizhik, V. *Structural Chemistry* **2011**, *22*, 465–470.

A. Appendix

A.1. Python script for fitting with Avrami equation

Script used for fitting the chronoamperometric transients with the Avrami equation. The used script was developed by Yvonne Gründer, with minor modifications by Lena Reichenbach.

```
1
2
3  import lmfit as lf
4  import numpy as np
5  import sys
6  import scipy
7  import os
8  import time
9  import scipy.optimize as optimization
10
11 #This function just returns True or False depending on the input
12 def TF(tocheck):
13         if tocheck == "T":
14                 return True
15         if tocheck == "t":
16                 return True
17         if tocheck == "F":
18                 return False
19         if tocheck == "f":
20                 return False
21         else:
22
23                 print "Unrecognised Vary Flag, should be T/F"
24                 quit()
25
26 #Function to read the parameters file
```

```
27 def read_parameters(filename):
28
29         params = lf.Parameters()
30         line = []
31         raw = 1
32
33         f = open(filename, 'r')
34
35         #skip first two lines
36         [f.readline() for i in xrange(2)]
37
38         #read parameters from file
39         while raw:
40                 raw = f.readline()
41                 line = raw.split()
42                 if len(line) >1 and line[0] == "P":
43                         params.add(line[1],    value= float(line[2]),
       min=float(line[3]), max=float(line[4]),vary=TF(line[5]))
44                 if len(line) >1 and line[0] == "M":
45                         method = line[1]
46                 if len(line) >1 and line[0] == "T":
47                         tol = float(line[1])
48
49         return params, method, tol
50
51 #function to read in a list of HKL values, structure factors, and
       errors
52 #since this program only treats the specular rod H and K should be
       zero
53 def read_data(filename):
54
55         f = open(filename, 'r')
56         line = []
57         data = []
58         raw = 1
59
60         #skip first line
61         f.readline()
62
63         #read parameters from file
64         while raw:
```

```
65                  raw = f.readline()
66                  if len(raw.split()) > 1:
67                          data.append(raw.split())
68          return data
69
70
71  def model1(t,params):
72      S1=params['S1'].value
73      k1=params['k1'].value
74      m1=params['m1'].value
75      off=params['offset'].value
76      current1=S1*m1*k1*np.power(t,(m1-1))*np.exp(-np.power(t,m1)*k1)
77      return current1
78
79  def model2(t,params):
80      S2=params['S2'].value
81      k2=params['k2'].value
82      m2=params['m2'].value
83      off=params['offset'].value
84      current2=S2*m2*k2*np.power(t,(m2-1))*np.exp(-np.power(t,m2)*k2)
85      return current2
86
87  def model3(t,params):
88      S3=params['S3'].value
89      k3=params['k3'].value
90      m3=params['m3'].value
91      off=params['offset'].value
92      current3=(S3*m3*k3*np.power(t,(m3-1))*np.exp(-np.power(t,m3)*k3)
        )
93      return current3
94
95  def model4(t,params):
96      S4=params['S4'].value
97      k4=params['k4'].value
98      m4=params['m4'].value
99      t4=params['t4'].value
100     off=params['offset'].value
101     current4=(S4*m4*k4*np.power((t-t4),(m4-1))*np.exp(-np.power((t-
        t4),m4)*k4)
102     return current4
103
```

```
104 def model5(t,params):
105     S5=params['S5'].value
106     k5=params['k5'].value
107     m5=params['m5'].value
108     t5=params['t5'].value
109     off=params['offset'].value
110     current5=(S5*m5*k5*np.power((t-t5),(m5-1))*np.exp(-np.power((t-
        t5),m5)*k5))
111     return current5
112 
113 def model(t,params):
114     S1=params['S1'].value
115     k1=params['k1'].value
116     m1=params['m1'].value
117     S2=params['S2'].value
118     k2=params['k2'].value
119     m2=params['m2'].value
120     S3=params['S3'].value
121     k3=params['k3'].value
122     m3=params['m3'].value
123     S4=params['S4'].value
124     k4=params['k4'].value
125     m4=params['m4'].value
126     t4=params['t4'].value
127     S5=params['S5'].value
128     k5=params['k5'].value
129     m5=params['m5'].value
130     t5=params['t5'].value
131     off=params['offset'].value
132     current=((S1*m1*k1*np.power(t,(m1-1))*np.exp(-np.power(t,m1)*k1)
        +S2*m2*k2*np.power(t,(m2-1))*np.exp(-np.power(t,m2)*k2)+S3*k3*m3*
        np.power(t,(m3-1))*np.exp(-np.power(t,m3)*k3))+(S4*m4*k4*np.power
        ((t-t4),(m4-1))*np.exp(-np.power((t-t4),m4)*k4))+(S5*m5*k5*np.
        power((t-t5),(m5-1))*np.exp(-np.power((t-t5),m5)*k5))+params['
        offset'].value)
133 
134     return current
135 
136 
137 import numdifftools as ndt
138 
```

```
139
140
141
142 def residual(params, t, expA,experror):
143
144         points = len(t)
145
146         mod = np.zeros(points)
147         for i in range(points):
148                 mod[i] = model(t[i],params)
149
150         return (expE - mod)**2#./np.power(experror,2)#/np.power(expE
    ,0.8)
151         #fitting criteria -> if later part activated, weighted by
    value of
152         #data (lower values give lower discrepance which means fit
    more weighted towards fitting those well)
153
154 params,fmethod,tol = read_parameters('params.py')
155 data = read_data('data.txt')
156 data = np.asarray(data)
157 data = data.astype(np.float64)
158 texp = data[2:len(data[:,0]),0]
159 expE = data[2:len(data[:,0]),1]
160 experror=abs(0.1)
161
162 #preform the fit
163 result = lf.Minimizer(residual, params,  fcn_args=(texp,expE,
    experror))
164 result.prepare_fit()
165
166 if fmethod == "leastsq":
167         result.leastsq(xtol = tol, ftol = tol, maxfev = 999999999)
168 if fmethod == "lbfgsb":
169         result.lbfgsb()
170 if fmethod == "nelder":
171         result.fmin(ftol = tol, xtol = tol, maxfun=999999999)
172 if fmethod == "anneal":
173         result.anneal(xtol = tol, ftol = tol, maxfev = 999999999)
174 if fmethod == "bent":
```

```
175         result.leastsq(xtol = tol, ftol = tol, maxfev = 999999999,
    full_output=1)
176
177
178 #calculate chi squared
179 theory = np.zeros(len(texp))
180 theory1 = np.zeros(len(texp))
181 theory2 = np.zeros(len(texp))
182 theory3 = np.zeros(len(texp))
183 theory4 = np.zeros(len(texp))
184 theory5 = np.zeros(len(texp))
185 final = np.zeros(len(texp))
186 chisq = 0
187 res=np.zeros(len(texp))
188
189 for i in range(len(texp)):
190
191         theory[i] = model(texp[i],params)
192         theory1[i] = model1(texp[i],params)+params['offset'].value
193         theory2[i] = model2(texp[i],params)+params['offset'].value
194         theory3[i] = model3(texp[i],params)+params['offset'].value
195         theory4[i] = model4(texp[i],params)+params['offset'].value
196         theory5[i] = model5(texp[i],params)+params['offset'].value
197         final[i] = model(texp[i],params)
198         res[i]=final[i]-expE[i]
199         chisq = chisq + ((expE[i] - final[i])/experror)**2
200 #         chisq = chisq + ((expE[i] - final[i])/experror[i])**2 #USE
    if error as funktion of i
201
202 #for i in range(len(texp)):
203 #         theory[i]=model[texp[i],params]
204 # write error report
205 lf.report_fit(params)
206
207
208 # plot results!
209 #convert y to log scale and seperate the different rods
210
211 print
212 print "Fit Succeeded"
213 print "----------------------"
```

```
214 print    "Chi Squared:", chisq
215 if fmethod == "leastsq":
216                 print    "Degrees of Freedom:", result.nfree
217                 print    "Reduced Chi Squared:", chisq/result.nfree
218
219 import pylab
220 from matplotlib.ticker import NullFormatter,MultipleLocator,
        FormatStrFormatter
221 import math
222
223 myxlim=[1,5]
224 pylab.figure()
225 pylab.plot(texp, (expE), "bo", label='Experiment', markersize=4)
226 pylab.plot(texp, theory, "r-", label='Theory')
227 pylab.xlim(myxlim)
228 pylab.show()
229
230 myxlim=[1,5]
231 pylab.figure()
232 pylab.plot(texp, np.log(expE), "bo", label='Experiment', markersize
        =4)
233 pylab.plot(texp, np.log(theory), "r-", label='Theory')
234 pylab.plot(texp, np.log(theory1), "b-", label='1')
235 pylab.plot(texp, np.log(theory2), "c-", label='2')
236 pylab.plot(texp, np.log(theory3), "g-", label='3')
237 pylab.plot(texp, np.log(theory4), "y-", label='4')
238 pylab.plot(texp, np.log(theory5), "m-", label='5')
239 pylab.xlim(myxlim)
240 pylab.show()
241
242
243
244 pylab.figure()
245 pylab.plot(texp, np.log(expE), "bo", label='Experiment', markersize
        =2)
246 pylab.plot(texp, np.log(theory), "r-", label='Theory', linewidth=2)
247 pylab.show()
248
249
250 pylab.figure()
```

```
pylab.plot(texp, np.log(expE), "bo", label='Experiment', markersize=4)
pylab.plot(texp, np.log(theory), "r-", label='Theory', linewidth=2)
pylab.plot(texp, np.log(theory1), "b-", label='1')
pylab.plot(texp, np.log(theory2), "c-", label='2')
pylab.plot(texp, np.log(theory3), "g-", label='3')
pylab.plot(texp, np.log(theory4), "y-", label='4')
pylab.plot(texp, np.log(theory5), "m-", label='5')
pylab.show()


myxlim=[1,5]
pylab.figure()
pylab.plot(texp, (expE), "bo", label='Experiment', markersize=4)
pylab.plot(texp, theory, "r-", label='Theory')
pylab.plot(texp, theory1, "b-", label='1')
pylab.plot(texp, theory2, "c-", label='2')
pylab.plot(texp, theory3, "g-", label='3')
pylab.plot(texp, theory4, "y-", label='4')
pylab.plot(texp, theory5, "m-", label='5')
pylab.xlim(myxlim)
pylab.show()

myxlim=[0,60]
pylab.figure()
pylab.plot(texp, (expE), "bo", label='Experiment', markersize=4)
pylab.plot(texp, theory, "r-", label='Theory')
pylab.plot(texp, theory1, "b-", label='1')
pylab.plot(texp, theory2, "c-", label='2')
pylab.plot(texp, theory3, "g-", label='3')
pylab.plot(texp, theory4, "y-", label='4')
pylab.plot(texp, theory5, "m-", label='5')
pylab.xlim(myxlim)
pylab.show()

myxlim=[0,20]
myylim=[-20,0.2]
pylab.figure()
pylab.plot(texp, (expE), "bo", label='Experiment', markersize=4)
pylab.plot(texp, theory, "r-", label='Theory')
pylab.xlim(myxlim)
```

```
pylab.ylim(myylim)
pylab.show()

myxlim=[0,5]
myylim=[-20,0.2]
pylab.figure()
pylab.plot(texp, (expE), "bo", label='Experiment', markersize=4)
pylab.plot(texp, theory, "r-", label='Theory')
pylab.xlim(myxlim)
pylab.ylim(myylim)
pylab.show()

#res is normal residuals (exp.value-theo.value)
pylab.figure()
myxlim=[-0.1,5]
pylab.plot(texp, res, "ro", label='Residuals', markersize=3)
pylab.xlim(myxlim)
pylab.show()

y0=0*texp
pylab.figure()
pylab.plot(texp, res, "ro", label='Residuals', markersize=3)
pylab.plot(texp, y0 , "b-")
pylab.show()

myylim=[-0.3,0.3]
pylab.figure()
pylab.plot(texp, res, "ro", label='Residuals', markersize=3)
pylab.plot(texp, y0 , "b-")
pylab.ylim(myylim)
pylab.show()


#Save to fit to a log
def writelog(filename, paramw, chisq,rchi):
        localtime = time.asctime( time.localtime(time.time()) )
        FILE = open(filename,"a") #Open the file in write mode
        FILE.write("
    ------------------------------------------------------------------\n")
        FILE.write("FIT LOG:"+localtime+"\nCHISQ: "+str(chisq)+"\
    nRed-CHISQ: "+str(rchi)+"\n")
```

```
330         FILE.write("
    ----------------------------------------------------------------------\n")
331         FILE.write(str(params))
332         FILE.close
333
334 writelog('fit_20C.log', params, chisq, chisq/result.nfree)
335
336
337
338 #output the results
339 def writecal(t, y,e):
340
341
342         FILE = open('avrami.cal',"a")
343
344         FILE.write(str(t)+"\t"+str(y)+"\t"+str(e)+"\n")
345         FILE.close
346
347
348 #rewrite files with headers
349 FILE = open('avrami.cal',"w") #Open the file in write mode
350 FILE.write("")
351 FILE.close
352
353 for i in range(len(texp)):
354         writecal(texp[i], theory[i],expE[i])
```

A.1.1. params.py

```
1 C PARAMETER FILE
2 C ------------------------
3 C SYSTEM:    Cu(II) in 0.1M HClO4 (N2)
4 C
5 C Minimisation method [leastsq/nelder] (least squares or downhill
    simplex)
6 C lbfgsb (L-BFGS-B algorithm), anneal (simulated annealing, not
    woking)
7 M leastsq
8 C Roughness method (BETA/POISSON/GAUSS/LINEAR/COSINE)
9 R BETA
```

```
C PARAMETER VALUE    MIN MAX VARY(T/F)
C ---------------------------------------------------------------
P S1          1    1e-12   30 T
P k1      1.5   1e-12   4   T
P m1      1     1   3 F
P S2          2 1e-12    20 T
P k2          0.2   1e-12   1 T
P m2        1    1 3 F
P S3          5 1e-12    50 T
P k3          0.006 0.00005   0.9 T
P m3      1         1 3 F
P S4        0   1e-12       40 F
P k4        0.003 0.00001    0.002 F
P m4       2    1     3 F
P t4      0       1e-12    30   F
P S5          0         1e-12     30 F
P k5          0.00001         1e-12    0.0001   F
P m5      2           0 3 F
P t5      0       0 20   f
P offset       0.1 1e-12 0.5 T
C Fitting Settings
C ---------------------------------------------------------------
C Minimisation method [leastsq/nelder] (least squares or downhill
    simplex)
C [lbfgsb/anneal] (L-BFGS-B algorithm or simulated annealing) are
    possible also
C but not reliable in the current implentation of lmfit-py.
M leastsq
C Fitting Tolerence (lower the more accurate the fit)
T 1.e-16
```